BEHAVIOUR OF RECTANGULAR RC COLUMNS CONFINED WITH BI-DIRECTIONAL GFRP UNDER COMBINED AXIAL AND BENDING LOADINGS

By

ABDURRA'UF MUKHTAR GORA, B.Eng., MSc.
Department of Civil Engineering
University of Nottingham

Thesis submitted to the University of Nottingham for the degree of Doctor of Philosophy

October 2021

Dedicated to my mother and father for their prayers and endless love……

ABSTRACT

Concrete structural members, such as columns, can deteriorate owing to a variety of circumstances, including concrete cracks, steel reinforcement corrosion, poor structural design, excessive loading, natural disasters, and harsh weather conditions. Various corrective actions may be necessary to rehabilitate the structural members depending on the nature and severity of the deterioration or defect. Advanced fibre reinforced polymer (FRP) composites have been increasingly used over the last two decades for strengthening, upgrading, and restoring degraded civil engineering infrastructure. Substantial experimental investigations have been conducted in recent years to understand the compressive behaviour of FRP-confined concrete columns. It is very evident that only a few studies have investigated the behaviour of eccentrically loaded noncircular RC columns wrapped with FRP composites. This study presents the experimental investigation on the behaviour and performance of rectangular reinforced concrete (RC) columns with full bi-directional glass fibre reinforced polymer (GFRP) wrapping under combined axial and bending loading conditions.

To achieve the objectives of this research, small rectangular RC columns with a scale of 1:3 the prototype column's size and lower concrete compressive strength were used. A total of sixteen rectangular RC specimens with cross-sections of 100 × 150mm and 800mm in height were constructed and tested under axial, eccentric, and flexural loading conditions. The corners of columns were rounded with a radius of 20mm to prevent the FRP rupture failures. The effect of bi-directional GFRP reinforcement on rectangular RC columns with different number of layers (i.e. zero, one, two and three) and eccentricities (i.e. 0, 25mm,

and 50mm) were investigated. Among the 16 rectangular RC specimens, 12 specimens were tested under axial and eccentric loading, and four specimens were tested under flexural loading condition. Moreover, a numerical study using finite element (FE) method was performed on 16 GFRP-confined rectangular RC specimens under concentric, eccentric and flexural loads, to determine the load-displacement behaviour and ductility.

The experimental results reveal that the rectangular RC columns with bi-directional GFRP confinement under axial loading achieved a substantial improvement in ultimate axial load capacity and ductility. Also, the ultimate axial capacity of GFRP confined rectangular columns increased with increasing number of bi-directional GFRP layers to a maximum of 187%. Similarly, the GFRP confined specimens under flexural loading achieved a significant enhancement in flexural load capacity of 51% in addition to ductility enhancement. Furthermore, subjecting the specimens to eccentric loading led to a loss in the ultimate capacity and ductility of the specimens. On the other hand, the loss in ultimate load carrying capacity and ductility increases with increased in eccentricity.

The results of finite element analysis (FEA) revealed a significant enhancement in the load carrying capacity and ductility of GFRP confined rectangular RC columns over the control columns (i.e. without GFRP wrapping). For columns governed by eccentric loading, the ductility significantly increases with increased in GFRP layers, and remarkably decreases when the eccentricity was increased. The comparison between the experimental and finite element analysis results of GFRP confined columns showed a reasonably close agreement, except in columns subjected to concentric loading. For specimens subjected to flexural loading, the FE results of the control beam agrees quite well with the load-deflection plot of the actual beam in both linear and nonlinear range, whereas the load-deflection curves of the FE GFRP wrapped beams are much stiffer than that of the experimental beams in both linear and nonlinear range of the curves.

The theoretical axial load-bending moment interaction diagram showed that specimens wrapped with three layers of GFRP reinforcement outperformed specimens with one and two layers of GFRP reinforcement. The axial load-bending moment interaction diagrams demonstrated that, with the exception of the control and three layers GFRP wrapped column, the FEA provided axial load values that were extremely close to the experimental values under concentric loading. When eccentric loading was applied, the FEA produced ultimate bending moment values that were higher than the experimental results. For specimens under flexural loading, the FEA gave bending moment values that were significantly greater than the experimental results.

LIST OF PUBLICATIONS

Journal publications:

A.M. Gora, J. Jaganathan, M.P. Anwar, and H.Y. Leung, "Experimental studies and theoretical models for concrete columns confined with FRP composites: a review", World Journal of Engineering. 16 (2019) 509–525. doi:10.1108/WJE-01-2018-0026.

Conference papers:

Gora, A.M., Jaganathan, J., Anwar, M.P. and Alengaram, U.J. (2018), 'Finite element analysis of rectangular reinforced concrete columns wrapped with FRP composites', IOP Conference Series: Materials Science and Engineering, Vol. 431

ACKNOWLEDGMENTS

All thanks, glory, praise and admiration be to God almighty, the most exalted in greatness and nobility, the most gracious the most merciful. O Allah you offered me the fortitude and strength to tackle with the hardships I have faced and guided me to complete this study.

Firstly, I would like to express my deepest gratitude to my supervisors: Dr. Mohammad Anwar Parvez, Dr. Jayaprakash Jaganathan and Dr. U. Johnson Alengaram for their motivation, encouragement, patience, guidance and support from the beginning to completion of this research work. I would like to acknowledge with much recognition the Civil Engineering Laboratory technician Mr. Adzarudin Abu Zarim for his technical assistance in fabricating the test specimens.

I would like to express my profound appreciation to my dear parents Alhaji Mukhtar A. Gora and Hajiya Rabi'atu for the love, scarifies and support they have rendered to me from birth up to this stage. I would also like to thank my lovely wife and my children for their patience, understanding and continuous support in the completion of my study.

I would like to acknowledge anyone who helped me throughout this process especially, my uncle Alhaji Ali Balarabe for his continuous support both financially and from the heart.

Finally, I acknowledge the financial support from the Nigerian government and Bayero University Kano, for the partial funding of my PhD through the needs assessment grant.

TABLE OF CONTENTS

LIST OF FIGURES

Chapter 5

Chapter 6

Appendix

LIST OF TABLES

Chapter 6

LIST OF ABBREVIATIONS

3D	:	Three-Dimensional
AFRP	:	Aramid Fibre Reinforced Polymer
ASTM	:	American Society for Testing and Materials
CDPM	:	Concrete Damage-Plastic Model
CFRP	:	Carbon Fibre Reinforced Polymer
FE	:	Finite Element
FEA	:	Finite Element Analysis
FEM	:	Finite Element Method
FRP	:	Fibre Reinforced Polymer
GFRP	:	Glass Fibre Reinforced Polymer
HFRP	:	Hybrid Fibre Reinforced Polymer
HSC	:	High Strength Concrete
LVDT	:	Linear Variable Differential Transformer
MCR	:	Modified Confinement Ratio
NSC	:	Normal Strength Concrete
PCS	:	Prefabricated Cage System
P-M	:	Axial Load versus Bending Moment Interaction diagram
RC	:	Reinforced Concrete

LIST OF SYMBOLS

A_1	:	area under the axial load-displacement curve up to the ultimate axial displacement
A_2	:	area under the curve up to the yield axial displacement
d	:	diameter of circular concrete section
D	:	diagonal length of square/rectangular concrete section
e	:	*eccentricity*
E_{co}	:	tangent modulus of concrete
E_{frp}	:	elastic modulus of FRP
E_{se}	:	elastic modulus of steel bars
E_{sec}	:	secant modulus of concrete
E_{sp}	:	plastic modulus of steel bars
E_x	:	elastic modulus of FRP in the x direction
E_y	:	elastic modulus of FRP in the y direction
E_z	:	elastic modulus of FRP in the z direction
f_c	:	concrete compressive stress at a given strain ε_c
f_c'	:	unconfined concrete stress corresponding to the strain ε_c'
f_{co}'	:	compressive strength of unconfined concrete
f_{frp}	:	ultimate tensile strength of the FRP jacket
f_l	:	maximum confining pressure in FRP
f_t	:	ultimate uniaxial tensile strength (modulus of rupture) of concrete
f_y	:	yield strength of steel bars
G_{xy}	:	shear modulus of FRP in the x-y plane

G_{xz}	:	shear modulus of FRP in the x-z plane
G_{yz}	:	shear modulus of FRP in the y-z plane
L	:	shear span length
M_u	:	bending moment
P_{ult}	:	ultimate axial load
P_y	:	yield axial load
$\mathrm{R_c}$	:	corner radius of square/rectangular concrete section
t_{frp}	:	thickness of FRP wrap
v	:	Poison's ratio
v_{xy}	:	major Poison's ratio for the xy plane
v_{xz}	:	major Poison's ratio for the xz plane
v_{yz}	:	major Poison's ratio for the yz plane
β_t	:	shear transfer coefficient
δ	:	lateral displacement
δ_u	:	maximum axial displacement at ultimate load
δ_y	:	axial displacement at yield load
λ	:	ductility index
ρ_{frp}	:	volumetric ratio of FRP for the fully wrapped circular concrete cross-section
ε_c	:	compressive strain of concrete at a given stress f_c
ε_c'	:	unconfined concrete strain corresponding to the stress f_c'
ε_{fu}	:	ultimate tensile strain of FRP composites

CHAPTER 1: INTRODUCTION

1.1 Background

The number of Civil Engineering infrastructures in the world continues to increase, as does their average age. Most of these structures are deteriorated or deficient and are perhaps required to be upgraded due to various environmental factors like variations in usage, excessive loading, and natural disasters or aggressive environmental conditions. The demand for increased sustenance is unavoidable. Entire replacement is likely to become an increasing financial liability, and is of course a waste of natural resources if upgrading is a potential alternative. Depending on the nature and severity of the deterioration or deficiency, various corrective measures may be required to rehabilitate the structure. Conventional rehabilitating techniques, including concrete and steel jacketing, have been used extensively for the repair and rehabilitation of reinforced concrete (RC) structures (Wu and Eamon, 2017). Several researchers have investigated the influence of these jacketing methods on the compressive behaviour of RC columns and found that they are useful in enhancing the performance of these columns (Xiao and Wu, 2003; Bousias et al., 2006; Vandoros and Dritsos, 2006; Bousias et al., 2007; Julio and Branco, 2008; Vandoros and Dritsos, 2008; Garzón-Roca et al., 2011; Campione, 2012; Kaish et al., 2012; Choi et al., 2013; Kaish et al., 2013; Lai and Ho, 2015). Regardless of their significant advantages in regard to strength and ductility enhancement, these jacketing systems also have some inherent shortcomings, including that they are labour intensive and time-consuming and can possibly increase the cross-sectional area of structural members.

Advanced fibre reinforced polymer (FRP) composites have been increasingly used over the last two decades for strengthening, upgrading, and restoring degraded civil engineering infrastructures. FRP composites potentially imparts important characteristics that include excellent corrosion resistance, good strength-to-weight ratio, high stiffness-to-weight ratio, and ease of construction, making them the most suitable alternative for external strengthening and upgrading RC members to improve their ultimate capacity and structural integrity (Teng et al., 2002; Hollaway, 2010; Rasheed, 2014). Several experimental studies have proven that FRP wrapping of RC columns is an effective means of enhancing their strength and ductility as it provides confinement to the concrete core (Mirmiran et al., 1998; Chaallal et al., 2000, Matthys, 2000; 2003; Pessiki et al., 2001; Ilki and Kumbasar, 2003; Lam and Teng, 2004; Masia et al., 2004; Silva and Rodrigues, 2006; Sheikh et al., 2007; Ilki et al., 2008; Ozbakkaloglu and Oehlers, 2008; Cui and Sheikh, 2010; Sezen and Miller, 2011; Alecci et al., 2014; Moshiri et al., 2015; Vincent and Ozbakkaloglu, 2015; Wang et al., 2017; Parghi and Alam, 2018). Moreover, the efficiency of FRP is primarily affected by the cross-section of the column specimen. Past studies have shown that FRP confinement in non-circular columns is non-uniform and hence provides insufficient confinement to concrete in the core; in contrast, there is uniform confinement in columns with circular cross-sections. However, variations in the FRP confinement pressure could lead to disproportionate losses in the effectiveness of the confining FRP.

This research work presents experimental and numerical investigations of rectangular RC columns confined with bi-directional GFRP under axial, eccentric and flexural loadings conditions. The main test variables considered in this study include the number of FRP layers and the intensity of load eccentricities.

1.2 Research Significance

Considerable experimental investigations have been undertaken in the past to evaluate the behaviour of concentrically loaded circular and non-circular concrete columns with FRP wrapping (Toutanji, 1999; Chaallal et al., 2003; Matthys et al., 2006; Al-Salloum, 2007; Almusallam, 2007; Wang and Wu, 2008 Ozbakkaloglu and Oehlers, 2008; Cui and Sheikh, 2010; Hosseinpour and Abbasnia, 2014; Triantafyllou et al., 2015; Vincent and Ozbakkaloglu, 2015). In a real-scenario, concentrically loaded columns with zero eccentricity are perhaps non-existent, and even columns with a combination of concentric and small eccentric loadings are relatively rare (Limbrunner, 2013). However, unavoidable imperfections of construction could introduce eccentricities and consequent bending in the structural member. Therefore, structural members under simultaneous compression and bending are very common in almost all type of concrete structures (Nilson et al., 2010).

Scholars have previously performed experimental investigations on eccentrically loaded concrete columns with FRP wrapping. Most of these investigations were focused on circular columns (Fam et al., 2003; Li and Hadi, 2003; Hadi and Li, 2004; Tao et al., 2004; Hadi, 2007b, 2007a, 2009; Wu and Jiang, 2013; Siddiqui et al., 2014; Hadi et al., 2018; Xing et al., 2020), with only a few studies dealing with non-circular concrete columns (Hadi and Widiarsa, 2012; Hassan et al., 2017; Lin et al., 2020; Mai et al., 2018; Siddiqui et al., 2020). It is apparent from the literature review that research contributions towards FRP-confined non-circular RC sections under eccentric loadings are lacking.

Consequently, additional experimental investigations on eccentrically loaded FRP strengthen concrete columns in non-circular sections needs to be undertaken to realise their behaviour and performance. Besides experimental investigations, some Scholars have performed numerical investigations to understand the behaviour of FRP-confined concrete columns using finite element method (FEM) (Mirmiran et al., 2000; Chakrabarti et al., 2008; Wu et al., 2009; Mostofinejad and Saadatmand, 2010; Chakrabarti, 2011; Hajsadeghi et al., 2011; Hu et al., 2011). The studies have proved that finite element numerical simulation is a very efficient method to effectively simulate the behaviour of FRP-confined concrete columns. In the present study, a three-dimensional nonlinear finite element model for FRP confined rectangular RC columns was developed and validated with experimental findings. The nonlinear finite element analysis was aimed at contributing to the understanding of the behaviour of rectangular RC beams and columns wrapped with FRP under three loading conditions (i.e. concentric, eccentric, and bending loadings). The primary effort focused on the influence of number of GFRP layers and load eccentricity on the load carrying capacity and ductility of small rectangular RC columns, scaled up to 1:3 the size of the prototype column. In addition, theoretical axial load-bending moment interaction diagrams of experimentally tested specimens and finite element analysis specimens were developed and compared.

1.3 Aims and Objectives

The aim of this study is to investigate the structural behaviour of rectangular reinforced concrete (RC) columns confined with bi-directional glass fibre reinforced polymer (GFRP) composites subjected to three different loading conditions (concentric, eccentric and flexural loadings).

The following specific objectives are set to achieve the above aim.

a. To investigate experimentally the effects of bi-directional GFRP confinement on the behaviour of RC columns under axial, eccentric and flexural loading conditions.
b. Perform a finite element analysis to examine the behaviour of GFRP wrapped rectangular RC columns under concentric, eccentric and flexural loading conditions. The results obtained from the FE analysis are than validated with the experimental results.
c. To assess the influence of load eccentricity on the axial capacity of rectangular RC columns wrapped with bi-directional GFRP reinforcement.

d. Develop theoretical axial load-bending moment interaction diagrams for the experimentally tested specimens and compare them with the results of the finite element analysis.

1.4 Scope of the Study

The scope of this research work is limited to twelve RC columns and four RC beams considering the resource constraints. This work focusses on rectangular RC columns with a characteristic concrete cylinder strength of 20MPa and a target mean concrete cylinder compressive strength of 30MPa. A series of 16 rectangular RC specimens were fabricated in Civil Engineering Laboratory located at the University of Nottingham, Malaysia. The end corbels in each of the rectangular RC columns with eccentric loading had a cross-section measuring 100mm × 300mm and a length of 150mm. Each specimen had a length of 800mm and a cross-section of 100mm × 150mm. Due to the limitations in the capacity of the testing facility available in the Engineering research building, small rectangular RC columns with a scale of 1:3 times size of prototype column and a lower concrete compressive strength are employed in this study. The scale (1:3) for the specimens was selected based on Buckingham Π theorem (Altunışı et al., 2018). Detailed calculations for the scale selection are presented in appendix B. All specimens had a sectional corner radius of 20mm. All these rectangular RC specimens are reinforced with 4-12mm longitudinal reinforcement and transverse steel stirrups of 6mm diameter. The variables in this investigation are the amount of GFRP wrap layers (i.e. 0, 1, 2 and 3 layers) and three axial eccentricities (i.e. 0, 25mm and 50mm), respectively. Among the

16 specimens, four specimens were tested under concentric loading, eight specimens were subjected to 25mm and 50mm load eccentricities and the remaining four specimens were tested as beams under pure bending load. The finite element analysis results performed in ANSYS software were compared with the experimental results.

1.5 Thesis Overview

The outline of the thesis is briefly described in this section. This thesis constitutes seven chapters. The detailed background and description of the problem statement, objectives, and scope of this study are presented in this chapter.

Chapter 2 presents a comprehensive review of the available experimental research studies on FRP-confined concrete columns with circular and non-circular cross-sections subjected to concentric and eccentric loadings. It also described the behaviour and mechanics of FRP confinement in circular and non-circular concrete sections. Eventually, a detailed review of previous finite element studies conducted to simulate the behaviour of FRP-confined concrete columns is presented.

Chapter 3 describes the detailed of the experimental investigations conducted in the laboratory, including a description of constituent materials (concrete, FRP and steel reinforcement), detail design of column specimens, casting and curing of columns, FRP wrapping of column specimens, and testing setup and instrumentation of test specimens. The results of materials testing that was carried out to evaluate the mechanical properties of the relevant constituent materials are also discussed.

In chapter 4, the outcomes of the experimental program described in chapter 3 are presented and discussed.

Chapter 5 presents the detailed formulation of the finite element analysis that was implemented in this study. This includes the description of the FE software used in performing the analysis, selection of element types and material models, modelling and meshing, a description of boundary conditions, loading and simulation.

The results obtained from the finite element analysis are clearly reported and discussed in Chapter 6. Moreover, the finite element results are validated with the experimental results.

The conclusions drawn from this research work and the recommendations for future research are summarised in chapter 7.

CHAPTER 2: LITERATURE REVIEW

2.1 General

This chapter presents a comprehensive review of previous experimental investigations of FRP-confined concrete columns in both circular and non-circular cross-sections subjected to a concentric and eccentric loads. The chapter begins by reviewing the existing experimental research studies on such columns and then highlights the behaviour and mechanics of FRP confinement in circular and non-circular concrete columns. The chapter also reviews the performed numerical investigations on FRP-confined concrete columns using finite element method to have an in-depth understanding of their overall behaviour and performance. Finally, various test parameters that influenced the behaviour and performance of FRP-confined concrete columns subjected to concentric and eccentric loadings are discussed.

2.2 Experimental Investigations

2.2.1 Axially Loaded FRP-Confined Circular Concrete Columns

Researchers have conducted numerous empirical studies to assess the performance of circular concrete columns confined by FRP composites under axial loads. Mirmiran et al. (1998) investigated the influence of different test parameters on the behaviour of FRP-confined concrete columns subjected to axial loading. These test parameters included the type of concrete cross-section, length-to-diameter ratio, and adhesive bond. To examine the influence of concrete cross-sectional shape, the researchers tested a series of 12 square concrete columns with a 152.5mm × 152.5mm cross-section and height of 305mm, and thirty 152.5mm × 305mm cylindrical specimens. The square columns had a corner radius of 6.35mm. Unidirectional E-glass fibre tubes and polyester resin were used to confine all the concrete column specimens. The FRP tubes had a varying thickness of 1.45, 2.21, and 2.97mm. The results showed that the glass fibre reinforced polymer (GFRP) confinement in the non-circular section was insufficient in restraining the concrete in the core compared to the uniformly confined circular concrete columns. Concerning the effect of GFRP confinement in non-circular concrete columns, the authors introduced a modified confinement ratio (MCR) given by:

$$MCR = \left(\frac{2R}{D}\right)\frac{f_l}{f'_{co}} \tag{2.1}$$

$$f_l = \frac{2f_{frp}t_{frp}}{D} \tag{2.2}$$

where D is the internal dimension of the tube, R is the corner radius, f_l is the confinement pressure, f_{frp} and t_{frp} are the hoop strength of FRP tube and jacket thickness, and $\frac{f_l}{f'_{co}}$ is the confinement ratio for the equivalent circular section. Moreover, the results confirmed that no strengthening is expected for an *MCR<15%* because of the insufficient FRP confinement of the concrete core in non-circular sections. The authors suggested that rounding sharp corners could improve the effectiveness of the GFRP jacket and concluded that the gain in axial stress and strain of the strengthened columns depends on FRP jacket strength and stiffness.

Saafi et al. (1999) investigated the behaviour of uniaxially loaded short concrete columns confined by FRP tubes. The test specimens consisted of 18 FRP-confined concrete cylinders and 12 plain circular concrete columns without FRP jacketing. The tested columns had a diameter of 152.4mm and a height of 432mm. All the concrete cylinders had compressive strength of 38MPa and modulus of elasticity of 30GPa. The selected FRP tubes were prepared from CFRP (i.e. thickness of 0.8, 1.6 and 2.4mm) and GFRP (i.e. thickness of 0.11, 0.23 and 0.55mm). Based on experimental results, Saafi et al. (1999) reported that CFRP and GFRP-confined concrete cylinders demonstrated a significant increase in strength, ductility, and energy absorption. The failure of concrete cylinders confined with FRP tubes was rupture of the FRP tubes, which commence with a cracking noise during the early and middle stage of loading. They also confirmed that the confinement coefficient is a function of confining pressure.

Toutanji (1999) tested 18 plain concrete cylindrical specimens, in which, 12 were wrapped with CFRP and GFRP sheets and subjected to uniaxial loading. All the cylindrical concrete columns are measuring 76mm in diameter and 305mm in height. The results show that FRP wrapping can improve the strength and ductility of the concrete columns to about 200% as well as enhancing energy absorption.

Xiao and Wu (2003) tested 243 standard circular concrete columns wrapped with CFRP and GFRP jackets, and measuring 152mm in diameter and 300mm in height under uniaxial compressive loading. The results of the work show that initial part of the stress-strain curve (Figure 2.1) for CFRP-confined concrete resembled that of unconfined concrete before reaching maximum stress. After exceeding maximum stress, the stress-strain curves of the strengthened columns showed a linear behaviour until rupture of the CFRP.

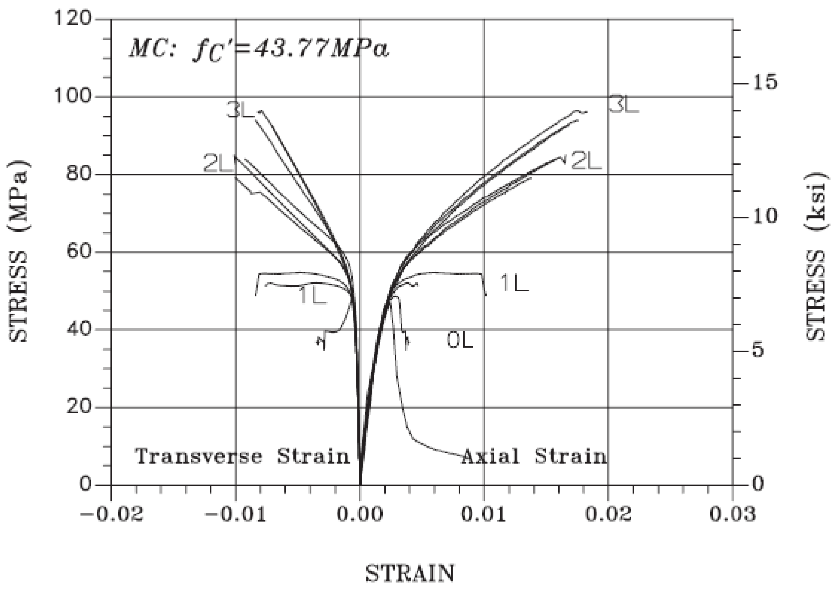

Figure 2.1 Axial stress-strain relationships for concrete with carbon fibre composite jackets (Xiao and Wu, 2003)

Berthet et al. (2005) investigated the compressive behaviour of axially loaded short cylindrical concrete columns confined with carbon and glass fabrics. The investigated parameters include compressive strength of concrete, number of FRP layers, and type of FRP reinforcement. In this study, five grades of concrete were used to prepare the concrete cylinders (20MPa, 40MPa, 50MPa, 100MPa, and 200MPa). Three concrete grade specimens were 160mm in diameter and 320mm in height, and two were 70mm in diameter and 140mm in height. The cylindrical concrete columns were wrapped with high tensile strength carbon fibre reinforced polymer (CFRP) and GFRP reinforcements. The results demonstrated a significant increase in ultimate axial strength and strain due to an increased number of FRP layers. The ultimate capacity of strengthened concrete cylinders was also found to be dependent on confinement pressure and concrete strength. Furthermore, the study concluded that the mechanical confinement efficiency of FRP wraps decreased to about 15% and 25% due to the increase in the strength of the concrete core.

Matthys et al. (2006) studied the behaviour of large-scale FRP-confined cylindrical concrete columns subjected to axial loads. They prepared a series of six large-scale RC cylinders with a diameter of 400mm, height of 2000mm, and a concrete compressive strength of 36.1MPa. The RC columns were strengthened with CFRP sheets, GFRP fabrics, and hybrid fibre reinforced polymer (HFRP) fabrics. The results showed that FRP confinement is an efficient means of enhancing the strength and ductility of RC columns. However, strength and ductility gain depend on the stiffness and tensile strength of the FRP fabric material. The authors also reported that the tensile strain of FRP reinforcement was much higher than the effective hoop failure strain considering the linear elastic behaviour of the FRP composites. Figure 2.2 illustrates the mechanism of FRP rupture experienced by the strengthened columns.

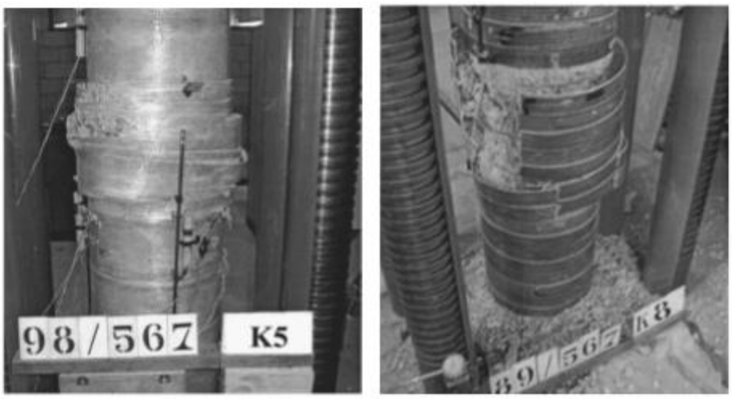

Figure 2.2 Failure of GFRP and HFRP fully wrapped column (Matthys et al., 2006)

Almusallam (2007) studied the performance of axially loaded concrete cylinders confined with E-glass fabrics material having a tensile strength of 540MPa and elastic modulus of 27GPa. The plain concrete columns had a dimension of 150mm × 300mm and concrete strength ranging from 40 to 100MPa. The findings show that GFRP laminates, when used as external reinforcement to concrete cylinders, can enhance the axial and lateral strength of concrete cylinders up to 110% and provide ductility enhancement. Moreover, the author confirmed that the strengthened cylindrical columns with normal concrete strength experienced a significant percentage gain in ultimate strength compared to the wrapped cylinders with high-strength concrete, as shown in Figure 2.3.

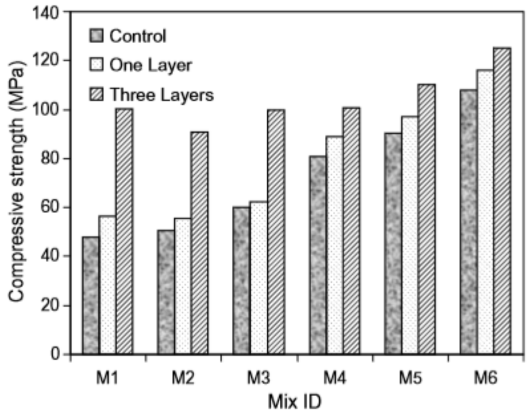

Figure 2.3 Variation of compressive strength gain with number of FRP layers (Almusallam, 2007)

Sheikh et al. (2007) investigated the behaviour of large-scale concrete-filled prefabricated glass FRP shells subjected to a concentric load. A series of 17 cylindrical concrete columns with a diameter of 356mm and height of 1524mm were fabricated and tested. The column specimens were prepared with concrete cured for 28 days and compressive strength of 30MPa. The effect of test variables, including number of GFRP layers, fibre orientation, and amount of longitudinal and lateral steel hoops, was examined. It was found that the prefabricated GFRP shells could be used as permanent formwork as well as an effective confinement reinforcement for concrete columns. Moreover, the results also revealed that the cylindrical columns with inclined GFRP shells experienced more ductile behaviour compared to columns with longitudinal or lateral GFRP shells.

Sezen and Miller (2011) investigated the effects of jacketing systems, including FRP wrap, steel jackets, concrete jackets with welded wire fabric, concrete jackets strengthened with rebar, and concrete jackets with prefabricated cage system (PCS) reinforcement (see Figures 2.4 and 2.5), on the behaviour of RC circular columns. They cast a series of 15 RC columns with a height of 762mm and a diameter of 152mm and subjected to axial loading. The results demonstrate that RC columns confined by concrete jackets reinforced with rebar sustained significant axial load before failure and experienced a sudden decline in load-carrying capacity after the collapse. The results of the investigation also confirm that FRP wrapping was very efficient, improving the axial strength of the RC cylinders by 140% without an increase in section size as with other jacketing systems.

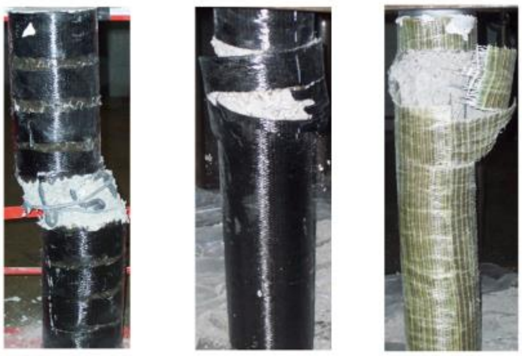

(a) **(b)** **(c)**

Figure 2.4 Columns strengthened using (a) CFRP strips (b) CFRP sheet (c) GFRP sheet (Sezen and Miller, 2011)

(a) **(b)**

Figure 2.5 (a) Specimen jacketed with PCS reinforcement (b) PCS used for reinforcing concrete jackets (Sezen and Miller, 2011)

Toutanji and Balaguru (1998) conducted durability tests to investigate the behaviour of FRP-wrapped concrete cylinders exposed to wet-dry and freeze-thaw conditions and subjected to uniaxial compressive loading to failure. The parameters studied include type of FRP and environmental exposure conditions. The specimens consisted of 24 concrete cylinders measuring 76mm in diameter and 305mm in height and grouped into three groups with six specimens each, with two specimens confined with CFRP reinforcement, two confined with GFRP reinforcement, and two samples used as control specimens. Prior to compression testing, the specimens in the first group were subjected to room temperature, specimens in the second group were subjected to wet-dry cycling, and the remaining specimens were subjected to freeze-thaw cycling. The results show that exposure to wet-dry cycling had no significant effect on strength and ductility gains of the CFRP-confined columns but led to an up to 10% decrease in the strength and ductility of GFRP-confined concrete cylinders without influencing the stiffness. The experimental investigation also indicated that freeze-thaw exposure could result in a significant decrease in both strength and ductility of CFRP and GFRP strengthened columns. Moreover, the results show that the stiffness of concrete cylinders wrapped with CFRP and GFRP reinforcements is not affected by freeze-thaw environmental conditions.

El-Hacha et al. (2010) studied the influence of extreme temperature variations on the behaviour of axially loaded plain concrete cylinders confined with FRP reinforcement. The authors tested 36 plain concrete cylinders measuring 150mm in diameter and 300mm in height. Nine of the concrete cylinders were used as control specimens, and the remaining columns were strengthened with two layers of CFRP wrap. The strengthened concrete columns were exposed to three different temperature conditions, namely elevated temperatures (45°C), heating and cooling cycles (23-45˚C) and prolong heating (45°C). However, the strengthened concrete columns exposed to heating and cooling cycles were further exposed to freezing and thawing cycles, and the remaining columns were immersed in pure or salt water for 23 days. It was found that the strength of the CFRP-confined concrete columns is not affected by extreme exposure to elevated temperatures of about 45˚C.

Cui and Sheikh (2010b) conducted an experimental investigation to evaluate the influence of various parameters, including concrete strength, type of FRP, number of FRP layers, and concrete condition before FRP bonding, on the behaviour of axially loaded normal, medium, and high-strength concrete confined with FRP reinforcement. The authors tested 112 cylindrical columns of which 88 were wrapped with FRP and the remaining 24 were unwrapped. The cylindrical specimens had a diameter of 152mm and a height of 305mm with carbon and glass fabrics as the externally bonded reinforcement. The results of the findings show that the strength enhancement provided by the confining FRP is independent of the amount of FRP when high-modulus FRP is used. However, a minimum number of FRP layers is required to achieve strength enhancement when FRP with a low modulus is used. This minimum requirement increases with increasing unconfined concrete strength and decreases with FRP stiffness. The increase in the load-carrying capacity of the strengthened columns increases proportionally with the number of FRP layers and is more prominent in columns with low-grade concrete.

Other investigations include Vincent and Ozbakkaloglu (2014), who studied the behaviour of high-strength concrete (HSC) circular columns confined by prestressed aramid FRP tubes under axial loading. The researchers concluded that prestressed AFRP confinement could improve the toughness of strengthened concrete cylinders, leading to a significant enhancement in ductility and energy absorption. Silva and Rodrigues (2006) studied the influence of size and relative stiffness on the compressive failure of cylindrical concrete columns wrapped with GFRP reinforcement. The authors concluded that increasing the section diameter of the concrete cylinders resulted in a significant reduction in the compressive strength of the GFRP-wrapped columns if the thickness of the GFRP shell is not increased.

2.2.2 Axially Loaded FRP-Confined Non-Circular Concrete Columns

Shehata et al. (2001) tested 54 plain concrete short columns wrapped with CFRP reinforcements under axial compression. The parameters of the study were the type of cross-section (i.e. circular, square and rectangular) and amount of FRP sheets (one and two layers). The specimens were grouped into three, with each group having 18 specimens according to the cross-section shape. All the three groups were subdivided into three subgroups with six samples in each subgroup according to the degree of FRP confinement (i.e. unconfined and confined with one or two layers of the FRP). All the concrete columns have an unconfined concrete strength of around 25-30MPa. The circular concrete columns are measuring 150mm in diameter, the square concrete columns had a cross-section of 150mm × 150mm, and the rectangular specimens had a cross-section of 94mm × 188mm. All the specimens maintained the same height of 300mm and sharp corners of the square and rectangular specimens were rounded with a corner radius of 10mm. The results indicate that the efficiency of FRP confinement was sensitive to the geometry of cross-section and the degree of confinement. The authors also reported that the confinement coefficient depends on level of FRP confinement and concrete strength.

Chaallal et al. (2003) studied the behaviour of small rectangular and square concrete columns confined with CFRP wraps under axial loads and found a significant increase in the strength and ductility of the strengthened columns. However, the strength and ductility enhancement depends on stiffness of the FRP reinforcement and is more significant in columns with lower unconfined concrete compressive strength.

Al-Salloum (2007) conducted an experimental investigation on the performance of CFRP-jacketed square concrete columns under axial loading. The concrete section was varied from square to circular to determine the effect of the corner radius of a section. The specimens consisted of 16 unreinforced square concrete columns having a cross-section of 150mm × 150mm and a height of 500mm. The column specimens were divided into four groups according to the size of corner radius (i.e. 5mm, 25mm, 38mm and 50mm). Two specimens from each group were wrapped with one layer of CFRP jacket, while the remaining specimens were taken as control. Four plain concrete cylinders measuring 150mm in diameter and 300mm in height were also prepared, in which, two specimens were wrapped with one layer of CFRP sheet. The results show that concrete cylinders confined with CFRP exhibited better performance, followed by CFRP-confined concrete columns with a square cross-section and corner radius of 50mm, 38mm, 25mm, and 5mm. The strengthened square concrete columns failed at or near section corners. Other researchers (Wang and Wu, 2008; Hosseinpour and Abbasnia, 2014; Triantafyllou et al., 2015) have also reported a similar failure mechanism.

Kumutha et al. (2007) performed an experimental study on behaviour of 9 rectangular RC columns confined with GFRP wraps under axial compressive loading. The parameters investigated include aspect ratio of the cross-section and number of GFRP layers (i.e. zero, one, and two layers). The specimens had a cross-sectional area of 15625mm^2 and a height of 750mm, with a concrete compressive strength of approximately 27.45MPa. The failure pattern of GFRP-confined concrete columns was concrete crushing at or near the column ends followed by rupture of FRP in the circumferential direction. Because of high-stress concentration at sharp edges, the failure initiates at or near the edges of columns. The authors concluded that strength gain in all the GFRP-confined columns is directly related to aspect ratio of the cross-section because it decreases with increase in aspect ratio.

Ozbakkaloglu and Oehlers (2008) investigated the behaviour of square and rectangular concrete columns confined by CFRP tubes under concentric loading. The results show that CFRP confinement substantially improved the strength and ductility of both square and rectangular concrete columns, with higher performance in square columns. The results also confirm that the effectiveness of CFRP jackets decreased with increasing unconfined concrete strength.

Wang and Wu (2008) investigated the performance of normal and HSC columns confined with CFRP reinforcement under axial loading. The concrete columns had a concrete compressive strength of 30MPa and 50MPa. The tested specimens include 108 short square concrete columns with a 150mm × 150mm cross-section and height of 300mm. The columns had varying corner radii of 0, 15, 30, 45, 60, and 75mm and were wrapped with zero, one and two layers of CFRP wrap. The parameters investigated included the corner radius of specimens, thickness of the CFRP jacket, and strength of concrete. It was found that strength enhancement in CFRP-confined square concrete columns depends on the corner radius of the cross-section. The results also indicate that CFRP confinement in square columns with sharp corners is insignificant in improving column strength but significant in enhancing ductility. Similarly, Benzaid and Mesbah (2014) investigated the behaviour of short CFRP-wrapped circular and square RC columns under axial loading. The column specimens had different degrees of CFRP wrapping and concrete strength of 26MPa (normal strength), 50MPa (medium strength), or 62MPa (high strength). The researchers observed that the strengthened columns experienced a decline in confinement effectiveness due to increased unconfined concrete strength. Furthermore, it was found that CFRP confinement in circular concrete columns resulted in better efficiency compared to that of square concrete columns.

Toutanji et al. (2010) studied the behaviour of large-scale rectangular RC columns confined with CFRP under axial loading. The rectangular RC columns had a concrete compressive strength of 38.2MPa, with a cross-sectional area of 125000mm^2 and a height of 2000mm. The study was part of previous study conducted by Matthys et al. (2005). The results indicate that the overall performance of the CFRP-confined concrete columns decreases with increase in the aspect ratio, and the efficiency of FRP confinement directly depends on corner radius of the cross-section.

2.2.3 Eccentrically Loaded FRP-Confined Circular Columns

Some researchers have investigated the behaviour of concrete columns confined by FRP reinforcement under eccentric loading. However, most of these investigations have focused predominantly on circular concrete columns (Ghali et al., 2003; Li and Hadi, 2003; Hadi and Li, 2004; Hadi, 2009; Wu and Jiang, 2013; Siddiqui et al., 2014), with only limited studies available on eccentrically loaded FRP-confined non-circular concrete columns. Li and Hadi (2003) studied the behaviour of eccentrically loaded CFRP- and GFRP-wrapped circular concrete columns. To achieve a load eccentricity of 42.5mm and prevent premature failure, the authors introduced large end corbels in the column specimens. The results show that FRP wrapping slightly improves the performance of eccentrically loaded strengthened columns because eccentric loading results in axial and bending effects. Subsequently, Ghali et al. (2003) conducted a comprehensive experimental study on small-scale CFRP-confined cylindrical concrete columns subjected to eccentric loading. The circular concrete columns had a cross-sectional diameter of 150mm with heights of 610mm, 915mm, and 1220mm. The column specimens were tested with load eccentricities of 0, 7.5, and 15mm. The results show that an increase in load eccentricity resulted in a significant decrease in the ultimate load-carrying capacity of the strengthened concrete columns, namely 26% and 70% for CFRP-confined concrete columns with height to diameter (H/D) ratios of 4 and 8. From Figure 2.6, it is evident that the load-carrying capacity of the strengthened columns is very sensitive to the magnitude of the load eccentricity.

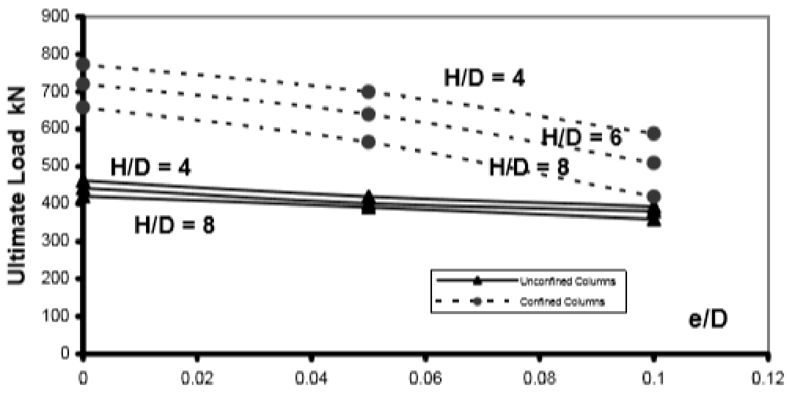

Figure 2.6 Influence of load eccentricity on ultimate load for confined and unconfined concrete cylinders (Ghali et al., 2003)

Fam et al., (2003) investigated the behaviour of concrete-filled GFRP circular tubes subjected to concentric and eccentric axial loads as well as pure bending. The results of the study demonstrate that increasing the load eccentricity can significantly reduce the level of confinement in FRP tubes due the strain gradient that subjects large part of the cross-section to tensile strains.

Hadi and Li (2004) investigated the effect of galvanised steel straps and FRP wrapping on the performance of concentrically and eccentrically loaded circular concrete columns. The tested columns had concrete compressive strength of 73.62MPa for columns subjected to concentric loading and 51MPa for columns subjected to eccentric loading. The authors concluded that external strengthening of columns by FRP composites provides the highest amount of confinement and that benefits can be enhanced by applying multiple layers of FRP composite. Hadi (2009) continued the investigation on 12 RC columns with circular cross-sections strengthened with different degrees of CFRP confinement (zero, one, or three layers). The strengthened columns were tested under varying load eccentricities of 0mm, 25mm, and 50mm and assigned to one of four groups according to the strengthening scheme. The first group consisted of RC columns without CFRP confinement. The second group had three layers of CFRP reinforcement used to confine the columns. The third group columns were made of RC incorporated with steel fibres with no CFRP wrapping. Lastly, the fourth group specimens were similar to the specimens in the third group but were confined with three layers of CFRP reinforcement. The results show that the eccentrically loaded RC columns experienced a decrease in ultimate capacity due to the increased load eccentricity. The results also confirm that the presence of steel fibre in concrete did not significantly strengthen the columns confined with CFRP jackets. Furthermore, according to the author, both steel fibre and CFRP confinement were effective in improving the ductility of the CFRP-confined RC columns. Figure 2.7 shows typical loading caps for applying eccentric loads.

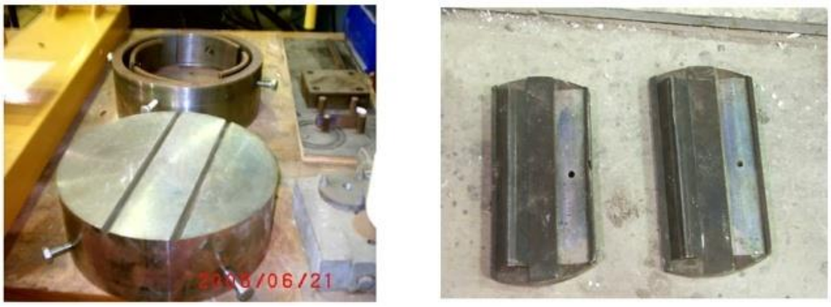

Figure 2.7 Loading caps for eccentric loads (Hadi, 2009)

Wu and Jiang (2013) investigated the stress-strain behaviour of eccentrically loaded cylindrical concrete columns confined by CFRP jackets. A total of 36 circular concrete columns measuring 150mm in diameter and 300mm in height were cast. The circular columns were wrapped with CFRP jackets using zero, one, and two layers. The strengthened columns were subjected to load eccentricities of 0, 10, 20, 30, 40, and 50mm. An increase in load eccentricity led to a decrease in the ultimate strength of the strengthened columns. It was also found that the stress distribution across the section was non-uniform due to the presence of eccentric loading. Consequently, the authors argue that it is inappropriate to use the stress-strain relationship for axially loaded columns for developing this relationship for eccentrically loaded columns because it underestimates the stiffness and strength of columns under eccentric loading. They also found that the strain at failure of the strengthened columns was higher in columns under eccentric load than in axially loaded columns of the same level of confinement.

Siddiqui et al. (2014) investigated the influence of hoop and longitudinal FRP confinement on the performance of circular RC columns under eccentric loading. Samples were a series of 12 cylindrical RC columns measuring 150mm in diameter with varying heights of 600mm, 900mm, and 1200mm. Each group consisted of four circular RC columns; one was considered a control specimen and the remaining three had different degrees of FRP confinement. One layer of hoop CFRP sheet was used to confine one column specimen, and the remaining two columns were confined with two and four layers of longitudinal CFRP reinforcements, respectively, and one layer of hoop CFRP sheet. All the columns were subjected to eccentric loadings using 25mm load eccentricity. The experimental results show that the hoop CFRP wraps substantially increased the strength and ductility of the strengthened RC columns because they confined the concrete and provided lateral support to the longitudinal fibres.

2.2.4 Eccentrically Loaded FRP-Confined Non-Circular Concrete Columns

Chaallal and Shahawy (2000) mainly focused on rectangular RC columns with bi-directional carbon fibre reinforced polymer (CFRP) wrapping subjected to eccentric loadings. The columns had cross-sections measuring 200 × 350mm and an overall height of 3600mm. Eccentric loading was achieved through large corbels at both ends of the rectangular columns. The outcomes demonstrated that the combined action of fibres in bi-directional CFRP composites led to a substantial gain in performance for rectangular RC columns.

Parvin and Wang (2001) conducted experimental and numerical studies on the influence of strain gradient in small-scale eccentrically loaded FRP-wrapped square concrete columns. The square concrete columns had a concrete cube strength of approximately 21.4MPa and rounded corners at the sharp edges with a radius of 8.26mm. A unidirectional CFRP was used to wrap the concrete columns using zero, one, and two layers. The study also investigated the influence of three different load eccentricities (0, 7.50, and 15.20mm). The authors report that CFRP wrapping can substantially improve the strength and ductility of strengthened columns under eccentric loading. However, axial strain gradient due to the presence of load eccentricity resulted in a 20% decrease in CFRP retrofitting capability.

Other work include a study by Maaddawy (2009), who studied the behaviour of square RC columns with full and partial CFRP wrapping under various eccentric loadings. The parameters investigated include wrapping conditions (i.e. no-FRP-wrapping, partial FRP-wrapping and full FRP-wrapping) and eccentricity to height ratio *e/h* (i.e. 0.3, 0.43, 0.57 and 0.86). The results show that the ultimate compressive strain enhancement caused by CFRP confinement was inversely proportional to the load eccentricity ratio, indicating that the level of FRP confinement has gradually reduced due to the increased load eccentricity ratio.

Sadeghian et al. (2010) conducted an experimental investigation of CFRP-confined rectangular RC columns subjected to eccentric loading. A series of seven large-scale RC rectangular columns with a cross-section of 200mm × 300mm, height of 1500mm, and end corbels 600mm in height were cast. The rectangular concrete columns had an overall height of 2700mm, and corners of the sections had a radius of 15mm. The various test parameters investigated include the number of FRP layers (i.e. two, three, or five layers), fibre orientation (i.e. 0°, 90°, $+45^{\circ}$ and -45°), and magnitude of load eccentricities of 200mm and 300mm. The results show that the strengthened columns exhibited a significant improvement in performance compared with the unconfined columns. The application of longitudinal CFRP wrap led to bending stiffness and moment capacity enhancement but no significant improvement in curvature capabilities. Moreover, the study found that strengthened specimens with angle orientation exhibited a significant increase in bending stiffness, moment capacity, and deflection capacity.

Similarly, Hadi and Widiarsa (2012) investigated the influence of CFRP wrapping and different load eccentricities on the behaviour of square RC columns. They cast 16 square RC columns with a section corner radius of 34mm. The columns had a cross-section measuring 200mm × 200mm and a height of 800mm. Twelve columns were tested under compressive loading using 0, 25, and 50mm load eccentricities, and the remaining four columns were tested as beams. The columns were divided into four groups according to the wrapping scheme. The first group consisted of unwrapped RC columns, and the second group had one layer of CFRP wrap to strengthen columns. The columns in the third group were confined with three layers of CFRP reinforcement, and the columns in the fourth group had one CFRP strap in the vertical direction and two CFRP wraps in the horizontal direction. The experimental results indicate that CFRP wraps significantly improved the strength and ductility of the strengthened RC columns. Moreover, the presence of vertical CFRP straps in the strengthened RC columns significantly improved the performance of the columns.

Following Hadi and Widiarsa, (2012), other similar investigations include Daugevičius et al. (2013), who studied the effects of load eccentricity on CFRP-confined rectangular RC columns. The authors tested a series of 14 rectangular RC columns, with six of the column specimens strengthened with one CFRP wrap. The rectangular RC columns had a cross-section of 150mm × 150mm and height of 625mm. The specimens were tested eccentrically to failure using eccentricities of 0, 30mm, and 45mm and with eccentricity/height ratios of 0.2 and 0.3. The results show that the ultimate capacity of the strengthened columns directly depends on the load eccentricity because an increase in load eccentricity from 0mm to 45mm led to an approximately 64% decrease in the ultimate capacity of the strengthened columns, as shown in Figure 2.8.

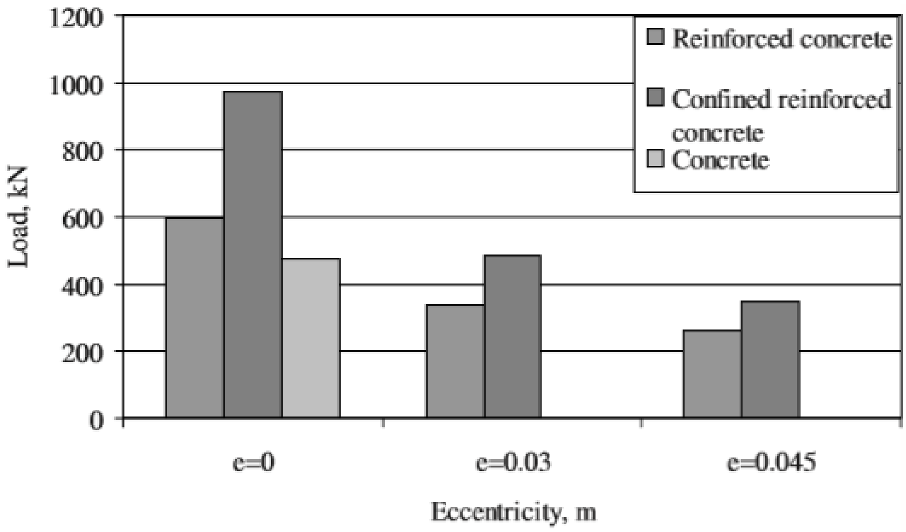

Figure 2.8 Variation of load carrying capacity with eccentricity (Daugevičius et al., 2013)

More recently, Hassan et al. (2017) and Mai et al. (2018) focused their attention on full and partial FRP wrapping of square RC columns under various loadings. Hassan et al. (2017) reported that GFRP wrapping of uniaxially loaded square RC columns resulted in a significant enhancement in strength and ductility by increasing the flexural capacity of the columns to up to 59%. On the other hand, Mai et al. (2018) found that the significant gains in strength and ductility of sqaure RC columns was higher in columns with full CFRP confinement compared to columns with partial CFRP confinement. They also reported that the increase in eccentricity resulted in a remarkable loss in the axial load capacity of CFRP wrapped square RC columns, with higher strength decrease in columns with full CFRP wrapping.

2.3 Mechanics of FRP Confinement

2.3.1 FRP Confinement in Circular Concrete Columns

In FRP-confined concrete, the externally bonded FRP reinforcement provides a passive type of confinement to the concrete core. This usually occurs due to the lateral dilation of the concrete when subjected to concentric loadings. FRP reinforcement produces tensile hoop stress because of the increasing axial stress and lateral strain. However, this tensile hoop stress is counterbalanced by a similar radial pressure, which resists the lateral dilation of the concrete (Lorenzis and Tepfers, 2003). External FRP reinforcement resists the lateral dilation of the concrete core in FRP-confined circular columns due to axial compressive stress. Figure 2.9 shows a typical confining action by FRP confinement in circular concrete columns.

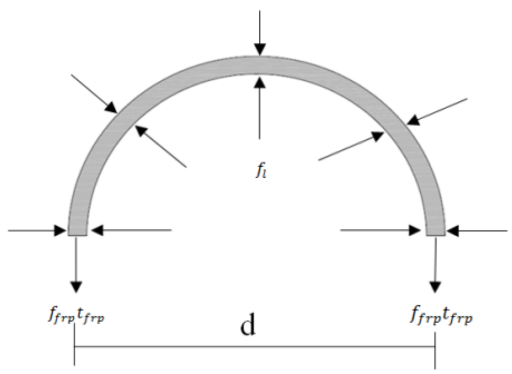

Figure 2.9 Confining action of FRP composites in circular concrete section

Furthermore, the circular concrete columns confined with FRP reinforcement under axial compression achieved uniform confinement over the concrete cross-section. The maximum confining pressure f_l in FRP is given by:

$$f_l = \frac{2E_{frp}t_{frp}\varepsilon_{fu}}{d} = \frac{\rho_{frp}f_{frp}}{2} \tag{2.3}$$

where E_{frp} is the elastic modulus of FRP, ε_{fu} is the ultimate tensile strain of FRP composites, f_{frp} is the ultimate tensile strength of the FRP jacket, t_{frp} is the thickness of FRP wrap, *'d'* is the diameter of circular concrete section, and ρ_{frp} is the volumetric ratio of FRP for the fully wrapped circular concrete cross-section, which can be evaluated as:

$$\rho_{frp} = \frac{\pi d t_{frp}}{\pi d^2/4} = \frac{4t_{frp}}{d} \tag{2.4}$$

2.3.2 FRP Confinement in Non-Circular Concrete Columns

In non-circular FRP-confined concrete columns, the FRP confining stress varies over the column cross-section, and only a portion of the concrete is adequately confined. These variations in confining pressure result in an excessive decrease in confinement efficiency (Mirmiran et al., 1998). Moreover, failure of FRP-confined rectangular and square concrete columns always commences at or near one of the corners and generally occurs by rupture of the FRP jacket (Al-Salloum, 2007; Youssef et al., 2007; Benzaid and Mesbah, 2014). The efficiency of FRP reinforcement can be enhanced by rounding the sharp edges of the concrete column. However, the rounded corners of the concrete cross-section are limited to small values due to the presence of inner steel rebar. Prior investigations of steel-confined concrete columns (Park and Paulay, 1975; Mander et al., 1988; Cusson and Paultre, 1995) have led to the simple suggestion that the transverse reinforcement encloses the concrete in a rectangular section by arching effects. From Figure 2.10(a), it is evident that only the concrete enclosed by the four second-degree parabolas is sufficiently restrained while the remaining concrete has negligible confinement. Though there are discrepancies among steel and FRP in confining concrete, it has been observed that only part of the section is adequately confined. This has also been confirmed for FRP confinement (Lam and Teng, 2003b).

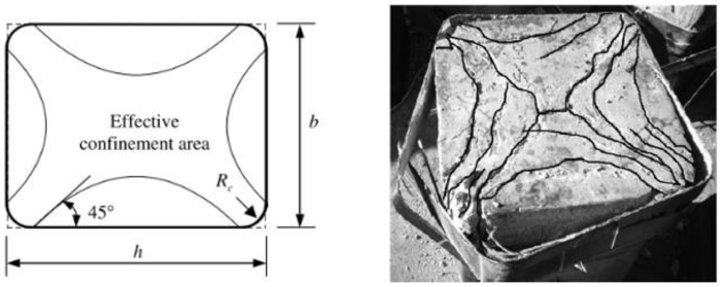

(a) **(b)**

Figure 2.10 Confinement of concrete column with FRP jacket (a) Effectively confined concrete in rectangular column (Lam and Teng 2003b) (b) Dilated square column confined with carbon/epoxy jacket (Youssef et al., 2007)

The adequacy of the confinement provided by FRP in square or rectangular concrete columns depends on the radius of the rounded corners. Al-Salloum (2007) reported that the behaviour of the FRP-confined square concrete columns gradually becomes similar to that of FRP-confined circular concrete columns with increasing corner radius, as illustrated in Figure 2.11. In Equation (2.3), the diagonal length of the non-circular section of the concrete is substituted for the diameter of circular concrete section *d*. However, for a non-circular concrete section with rounded corner radius R_c, the diagonal length of the section *'D'* is given by:

$$D = \sqrt{2b} - 2R_c(\sqrt{2} - 1) \quad (2.5)$$

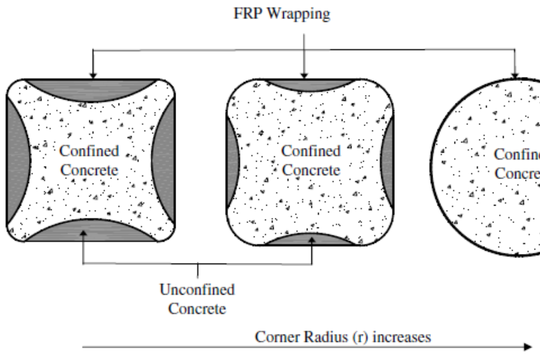

Figure 2.11 Effect of corner radius on confined concrete in square and cylindrical columns (Al-Salloum, 2007)

2.4 Finite Element Analysis Investigations

In addition to experimental studies and confinement models, some researchers (Mirmiran et al., 2000; Feng et al., 2002; Malvar et al., 2004; Chakrabarti et al., 2008; Karabinis et al., 2008; Wu *et al.*, 2009; Yu *et al.*, 2010; Mostofinejad and Saadatmand, 2010; Hajsadeghi et al., 2011; Hu et al., 2011; Parghi and Alam, 2016, 2017; Lin and Teng, 2017; Chellapandian et al., 2018; Zeng et al., 2018) have also performed numerical investigations to understand the overall behaviour of FRP-confined concrete columns using the finite element method (FEM). The FEM is a numerical method that solves the governing ordinary and partial differential equations of a system through the discretisation process. The method is gaining increasing popularity as a tool in the modelling of both uniformly and non-uniformly confined concrete columns, as it is capable of capturing complex stress distribution in concrete section planes. Previous studies have revealed that finite element analysis (FEA) can efficiently simulate the behaviour of FRP-confined concrete columns when an accurate numerical model is used (Feng et al., 2002; Yu et al., 2010).

Mirmiran et al. (2000) used a non-linear FEM to simulate the cyclic response of circular and square concrete columns confined by FRP composites using ANSYS software. They adopted a non-associative Drucker-Prager plasticity model, which accounts for the pressure sensitivity of concrete. The predicted stress-strain response of the columns indicates a positive correlation with the results obtained by the researchers in their experimental study (Figure 2.12). Nevertheless, the FEA results also reveal a similar stress concentration around the corners of the square concrete section, as determined in the experimental study. However, Feng et al. (2002) reported a similar observation.

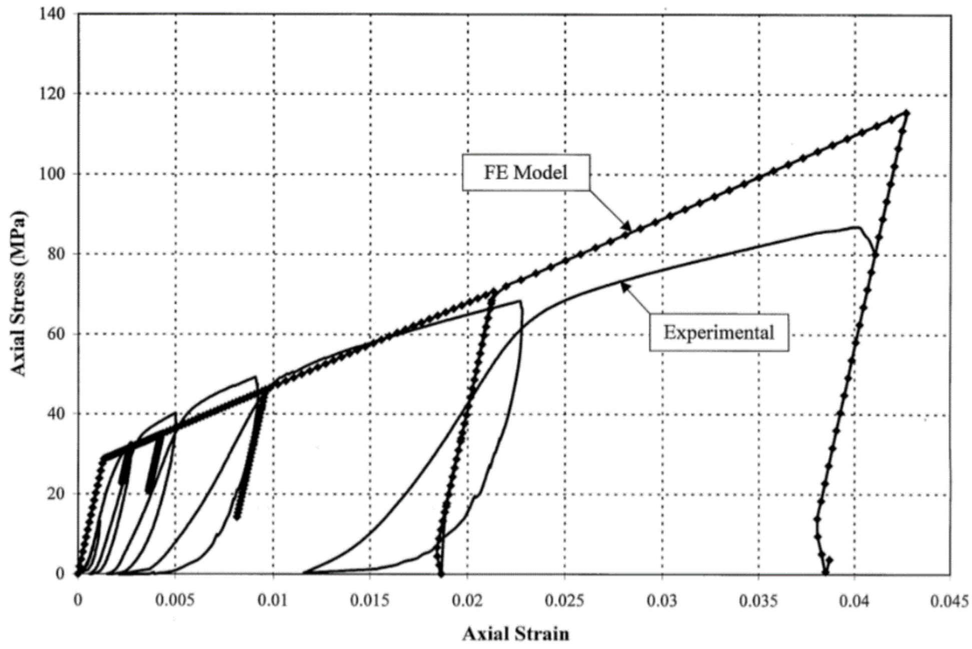

Figure 2.12 Comparison of predicted and experimental cyclic response of the columns (Mirmiran et al., 2000)

Malvar et al. (2004) performed a numerical analysis on concrete cylinders and prisms confined with different FRP materials (aramid, carbon, and glass). The model was developed using an explicit finite element (FE) code from DYNA3D with a concrete material model initially developed for blast analysis. The FEA results agree favourably with the experimental test results regarding strength enhancement for specimens with various degrees of FRP confinement. The authors confirm that FRP wrapping is an effective measure to improve the structural integrity of columns subjected to seismic and blast loadings.

Karabinis et al. (2008) performed 3D-FEA to evaluate the influence of FRP sheet confinement on the elastic buckling of longitudinal steel bars in old-type square

RC columns with deficient concrete strength and stirrup spacing subjected to compressive loading. The square RC columns had cross-sections measuring 200mm × 200mm with a rounded corner radius of 30mm. The specimens were reinforced with 14mm-diameter bars as longitudinal reinforcement and 6mm-diameter steel stirrups spaced at 200mm with CFRP as the external confining material. The 3D non-linear FEA was carried out in the ABAQUS (HKS 1997) FE program, and concrete behaviour was modelled with a Drucker-Prager-type material and non-associative flow rule. External CFRP confinement was found to be effective in enhancing the mechanical behaviour of the RC columns by providing adequate lateral confinement and hence preventing buckling of the longitudinal steel bars.

Chakrabarti et al. (2008) developed an efficient non-linear FE model for the analysis of plain and RC columns in circular and square sections confined by FRP sheets under axial loading. The model was carried out in the ANSYS FE program. They used SOLID65, SOLID46, and LINK8 elements to model concrete, FRP composites, and steel reinforcements. Considering the symmetry and loading, only a quarter-section of the circular columns was modelled. The FEA results reveal that externally bonded FRP significantly enhances the strength and ductility of the columns, with greater enhancement as the number of FRP layers increases. The study also found that the efficiency of the FRP confinement was more effective for columns with low concrete grades.

Wu et al. (2009) performed a 3D non-linear FEA to simulate the behaviour of aramid FRP (AFRP)-confined HSC columns using ANSYS FE code. The specimens are 100mm in diameter and 300mm in height and were made with three concrete grades of 46.43, 78.50, and 101.18MPa. The concrete core was modelled with an eight-node SOLID65 element, which is capable of cracking under tension and crushing under compression and has excellent resistance to plastic deformation. A four-node SHELL41 element was used to model the AFRP sheets. The results of the non-linear analysis show that columns with continuous AFRP wrapping experienced a significant increase in strength and ductility, whereas an increase in strength only was observed in columns with partial AFRP wrapping.

Hu et al., (2011) used the ANSYS FEA program to develop two non-linear FE models (FEM1 and FEM2) that can simulate the behaviour of FRP-wrapped RC columns under eccentric loading. In these two models, the failure behaviour of confined concrete was simulated using the William-Warnke failure criterion (William and Warnke, 1974). Two methods were employed to simulate the interfaces between concrete and the confining FRP composite for strength prediction. In the first method (FEM1), the contact elements TARGET170 and CONTA174 were used to connect concrete and FRP composite elements, whereas a perfect bond was assumed between concrete and FRP composite in the second method (FEM2). The numerical FEA results agreed with the experimental results for both FE models. The FEA results indicate that a perfect bond could efficiently simulate the interface between concrete and FRP as well as the interface elements. The authors concluded that the maximum concrete compressive stress and strain of the eccentrically loaded columns depends on the unconfined concrete strength as well as the level of confinement provided by external FRP composites.

Parghi and Alam (2016) performed a non-linear static pushover analysis on seven parameters that influenced the seismic behaviour of deficient circular RC bridge piers confined with CFRP composites using a three-level fractional factorial design method. These factors included the compressive strength of concrete, yield strength of steel, longitudinal steel reinforcement ratios, spacing of stirrups, axial load, shear span-depth ratio, and number of FRP layers, as depicted in Table 2.1. The authors used Seismostruct, a non-linear analysis program (SeismoStruct, 2015) to model the geometry of the bridge piers as a 2D FE frame. The results of the findings reveal that lateral load-carrying capacity, ductility, and the failure mechanism of the strengthened columns are significantly influenced by the shear span-depth ratio, yield strength of steel, longitudinal reinforcement ratio, axial load, and confining FRP reinforcement. Subsequently, Parghi and Alam (2017) reported similar results in their vulnerability study of non-seismically designed circular RC bridge piers retrofitted with CFRP composites.

Table 2.1 Level of factors for nonlinear pushover analysis (Parghi and Alam, 2016)

S/N	**Factors/parameters**	**Level**		
		Low (-1)	**Medium (0)**	**High (+1)**
1.	Compressive strength of concrete, f_c' (MPa)	25	30	35
2.	Yield strength of steel, f_y (MPa)	250	300	350
3.	Longitudinal steel reinforcement ratio, ρ_l (%)	1.5	2	2.5
4.	Spacing of stirrups, *s* (mm)	300	250	200
5.	Axial load, *P* (%)	5	10	15
6.	Shear span-depth ratio *(H/d)*	3	5	7
7.	CFRP layers *(n)*	1	2	3

Chellapandian et al. (2018) carried out numerical and analytical investigations to evaluate the influence of hybrid strengthening on initial post-cracking stiffness, peak and post-peak behaviour, and the failure mechanism of square RC columns subjected to axial and eccentric loadings. The numerical model was developed in ABAQUS, an FE program, and was compared with the experimental test results. The results reveal that the non-linear FE model was able to capture the overall behaviour of the strengthened and unstrengthened RC columns under axial and eccentric loadings. The authors concluded that the hybrid FRP strengthening is effective in enhancing initial post-cracking stiffness, strength, and ductility of the strengthened RC columns under both loading conditions.

Zeng et al. (2018) studied the behaviour of cylindrical concrete columns partially wrapped with CFRP strips under concentric loading. They also proposed a three-dimensional FE approach for modelling circular concrete columns partially wrapped with FRP reinforcement. The model was developed in ABAQUS based on a constitutive concrete damage-plastic model (CDPM). The authors reported that trends of axial and hoop strain distributions observed in the FE approach are in accordance with the experimental observations. It was also revealed that axial and hoop strain are larger at the mid-plane of the two adjacent FRP strips than at the mid-plane of each FRP strip.

2.5 Discussion of Previous Experimental Studies

This review presents a significant number of empirical investigations to understand the influence of various test parameters on the behaviour and performance of axially and eccentrically loaded FRP-confined circular and non-circular concrete columns. These parameters include the number of FRP layers (FRP thickness), concrete compressive strength, presence of a corner radius, and magnitude of load eccentricity.

The review shows that the rate at which the strength and ductility of the FRP-confined concrete columns increase primarily depends on the number of FRP layers (i.e., FRP stiffness), regardless of whether the column section is circular or non-circular and under axial or eccentric loading. Chaallal et al. (2003) confined rectangular concrete columns with between zero and four layers of CFRP. A strength enhancement of 90% was observed in rectangular concrete columns confined with four layers of CFRP. Berthet et al. (2005) used between two and 12 layers of CFRP and GFRP wraps to strengthen concrete cylinders. The researchers observed a substantial enhancement in load-carrying capacity, and structural ductility of the FRP-confined concrete cylinders as the level of confinement increased. In their investigation, Wang and Wu (2008) and Parvin and Wang (2001) used similar confinement levels of one and two layers of CFRP to wrap square concrete column specimens. The authors observed a significant improvement in strength and ductility of the strengthened columns with an increase in the number of CFRP layers. The CFRP-confined concrete columns with two layers demonstrated a strength enhancement double that of CFRP-confined concrete columns with one layer. Furthermore, Almusallam (2007) wrapped concrete cylinders with one and three layers of GFRP laminates and observed a compressive strength gain of up to 110% in GFRP-confined concrete cylinders with three layers. Other researchers (Li and Hadi, 2003; Hadi and Li, 2004; Matthys et al., 2006; Kumutha et al., 2007; Sadeghian et al., 2010) have also confirmed that the efficiency of FRP confinement can be improved by increasing the stiffness (layers) of FRP jackets.

The compressive strength of concrete is one of the fundamental parameters investigated by previous studies on FRP-confined concrete. Most of the studies reported in this review confirm that the effectiveness of confining FRP is essentially influenced by the compressive strength of concrete in the inner core. However, this phenomenon is yet to be investigated in detail by researchers. For both circular and non-circular concrete sections, the efficiency of the confining FRP decreases with an increase in concrete compressive strength. Chaallal et al. (2003) observed a 90% gain in strength and ductility for wrapped columns with concrete compressive strength of 20.7MPa compared to a 30% increase in performance for FRP-wrapped columns with concrete compressive strength of 41.4MPa. Furthermore, Almusallam (2007) reported a strength and ductility enhancement of 78.7% for wrapped columns with three layers and concrete compressive strength of 50.8MPa while a 16.1% gain was recorded for columns with a similar level of confinement but concrete compressive strength of 107.8MPa. The experimental investigation conducted by Berthet et al. (2005) shows that the efficiency of FRP confinement tends to diminish with an increase in concrete core strength. The authors observed a 15% decrease in confinement efficiency for FRP-confined concrete with 100MPa compressive strength and a 25% decrease for FRP-confined concrete with compressive strength of 200MPa. Furthermore, Benzaid and Mesbah (2014) observed 46% and 24% enhancement in the ultimate strength of normal and HSC wrapped columns with three layers of CFRP.

Regarding the influence of corner radius in non-circular concrete sections, research (Mirmiran et al., 1998; Al-Salloum, 2007; Ozbakkaloglu and Oehlers, 2008; Wang and Wu, 2008) has shown that the presence of sharp edges can lead to the variation in the confining pressure produced by FRP to the concrete core from a maximum at the corners to a minimum along the edges of a section. These variations in confining pressure result in premature failure of the confining FRP, which mostly commences at or near the corners of a section due to the concentration of stress in the region. Consequently, FRP confining pressure is insufficient to improve the strength and ductility of columns. However, to improve strength and ductility and prevent premature failure of FRP, researchers have recommended that the sharp edges should be rounded. Accordingly, further investigation should be conducted to better understand the significance of rounded corners on the performance of eccentrically loaded FRP-confined concrete columns.

In regard to the effect of load eccentricity, the behaviour of eccentrically loaded FRP-confined concrete columns is different from that of axially loaded columns because eccentricity of loading causes variation across a section in the confining pressure provided by the FRP. Further, significant experimental results involving eccentrically loaded FRP-confined concrete columns are also reported in the review (Parvin and Wei, 2001; Fam et al., 2003; Ghali et al., 2003; Hadi, 2009; Maaddawy, 2009; Hadi and Widiarsa, 2012; Widiarsa and Hadi, 2013; Wu and Jiang, 2013). The results show that eccentricity of loading can lead to a decrease in the strength of FRP-confined concrete columns in both circular and non-circular concrete sections. Jiang and Wu (2020) conducted an experiment in which they loaded 78 FRP confined short concrete columns eccentrically. The effect of load eccentricity on the axial strength of FRP-confined short concrete columns was examined. When the load eccentricity is minimal (e.g., 10 mm or 2e/b = 0.13), the axial strength reduction degree is limited and occasionally close to zero, according to the authors. When the load eccentricity increases, however, the axial strength decreases more substantially. Xing et al. (2020) reported that FRP confinement can improve both the ultimate load and deformability of eccentrically loaded circular RC columns. The researchers also confirmed that as the load eccentricity or column slenderness increases the ultimate axial load of an eccentrically loaded FRP confined circular RC column reduces rapidly. More recently, Jin et al. (2021) found a considerable size influence for nominal axial strength and lateral displacement in eccentrically loaded FRP confined RC columns. Because the nominal axial strength of RC columns with eccentricity to effective cross-sectional width ratios of 0.1 and 0.3 decreased by 28.9% and 23.2%, respectively, when the cross-sectional height of the column was increased from 200mm to 400mm. Generally, the accessible literature contains a limited number of experiments on eccentrically loaded FRP-confined concrete columns, particularly for square/rectangular cross-sections. Because the confinement mechanism for square and rectangular columns differs from that of circular columns, the correlation between column section size and confinement efficiency under eccentric loading should be fully understood.

2.6 Concluding Remarks

This chapter presents a general review of experimental studies on the behaviour and performance of FRP-confined concrete columns in both circular and non-circular cross-sections subjected to concentric and eccentric loadings. First, the behaviour and mechanics of FRP confinement in circular and non-circular concrete sections are reviewed. Then, existing numerical studies conducted by various researchers using finite element method to examine the compressive behaviour of FRP confined RC columns in both circular and non-circular sections under concentric and eccentric loading are reviewed. The review demonstrates that the performance and effectiveness of FRP confinement in concrete columns have been extensively investigated and the technique has been proven effective in enhancing the structural performance and ductility of strengthened column structures, as it provides confinement to the concrete core. The following conclusions can be drawn from the review.

- The review shows that the failure of FRP-confined concrete columns occurs suddenly and violently, resulting in the rupture of FRP composites. The rupture of FRP in cylindrical column sections usually commences at or near mid-height and then propagates towards the other ends of the column. However, unlike circular concrete columns, FRP rupture in non-circular column sections initiates at or near the corners of the section. This is attributed to the concentration of strain at the corners of the section.
- FRP confinement effectiveness is uniform in circular columns subjected to axial loads. However, in non-circular (square/rectangular) columns, the

confining pressure provided by the FRP jacket varies over the cross-section, and only part of the concrete is adequately confined. This variation in confining pressure results in excessive reduction in confinement efficiency.

- The confinement effectiveness provided by FRP depends on the number of FRP layers and concrete compressive strength. The higher the number of FRP layers, the greater the increase in confinement effectiveness. Likewise, the confinement efficiency is greater in columns with lower or normal concrete compressive strength.
- For eccentrically loaded FRP-confined concrete columns, the ultimate load-carrying capacity depends on the magnitude of load eccentricity. An increase in the load eccentricity results in a decrease in the ultimate capacity of the column.
- The reviewed experimental studies show that the confining FRP in FRP-confined concrete ruptures at tensile strain lower than the original FRP material tensile strain. By this observation, the effective confining pressure in confinement models should be preferably based on the hoop rupture strain of FRP than the FRP material tensile strain.

CHAPTER 3: EXPERIMENTAL PROGRAM

3.1 Introduction

The experimental program has been designed to investigate the effect of FRP confinement on the behaviour and performance of eccentrically loaded rectangular reinforced concrete (RC) columns. A total of 16 rectangular RC specimens were prepared and tested in this study. Among the 16 specimens, four were tested under axial loadings, eight specimens were tested under eccentric loadings while the remaining four specimens were tested under flexural load. The experimental works including casting and FRP strengthening of specimens were conducted in the Civil Engineering Laboratory at the University of Nottingham Malaysia campus, while static compression testing of RC specimens was undertaken in heavy structures Laboratory located at University of Malaya. The following sections provide detailed descriptions of the experimental programme.

3.2 Materials

The materials used in this research work to fabricate the tested columns are concrete, longitudinal and transverse steel bars, and bi-directional GFRP composites. Detailed descriptions of the materials are discussed below.

3.2.1 Concrete

A concrete mix was designed based on the recommendation of the BS 1881 part 125 (1986) design guideline was used to prepare the test specimens. The mix consists of ordinary Portland cement, fine natural sand, crushed coarse aggregates of 20mm maximum size and clean water. A series of 33 standard concrete cubes of 100mm × 100mm × 100mm in dimensions and 22 standard concrete cylinders of diameter 150mm and height of 300mm were tested to obtain the 28days concrete compressive strength. The modulus of rupture (tensile strength) (f_r) and Young's modulus (E_c) of concrete are calculated using the following equations (McCormac, Brown, 2013);

$$f_r = 7.5\lambda\sqrt{f_c'} \tag{3.1}$$

$$E_c = 4700\sqrt{f_c'} \tag{3.2}$$

Where, f_c' is the compressive strength of concrete and λ is a reduction factor which assumed a value of 1 for a normal weight concrete.

3.2.2 Steel Reinforcement

High yield deformed rebar of 12mm diameter were used as the longitudinal reinforcement, and mild steel rebar of 6mm diameter were used as transverse reinforcement (ties), respectively. The steel reinforcement bars were tested under tensile strength test to determine the yield strength and ultimate tensile strength.

3.2.3 FRP Composites

A bi-directional (EWR 600-100) glass FRP (GFRP) sheet was used as the external wrapping material. To gain insight into the mechanical properties of bi-directional GFRP composites, tensile strength test was carried out on FRP coupons for one, two, and three layers.

3.3 Details of Test Specimens

A series of 16 small-scale RC columns were prepared and subjected to axial, eccentric and flexural loading conditions until failure. The specimens were rectangular in cross-section, with end corbels for specimens with eccentric loading. Considering the limitations in the capacity of the static compression testing machine available in the engineering research building, small size rectangular RC columns were used in this research work. A scale of 1:3 size of a prototype rectangular RC column was used in selecting the section size and height of the column specimens. The scaling of all the column specimens in this study was based on Buckingham Π theorem. Detailed calculation of the column scaling is presented in appendix B. All specimens had a cross-section of 100mm × 150mm and a height of 800mm, with a concrete cover of 20mm. The cross-section of brackets at end of each column was 100mm × 300mm and was 150mm in height. To ensure sufficient confinement of the columns and to prevent variation of FRP confining pressure, the sharp edges of columns were chamfered to a radius of 20mm. All specimens were reinforced with longitudinal reinforcement of four 12-mm diameter steel bars and transverse reinforcement of 6-mm diameter steel spaced at 120mm centre to centre at the mid-height region of the test specimen and 65mm centre to centre at the upper and lower end regions. Considering the materials cost and resource constraints, only one rectangular RC column specimen was chosen for each case of testing. Figure 3.1 illustrates the specimen geometry and reinforcement details.

The test variables in this study were number of GFRP layers (zero, one, two, and three layers) and load eccentricities (0, 25mm, and 50mm). Table 3.1 presents the configuration of test specimens. The 16 test specimens were divided into four distinct groups: unwrapped and fully wrapped with one, two, and three layers of GFRP. Each group comprised four specimens in which one specimen was loaded axially, two specimens were tested under 25mm and 50mm eccentric loadings, and the last specimen was subjected to flexural loading.

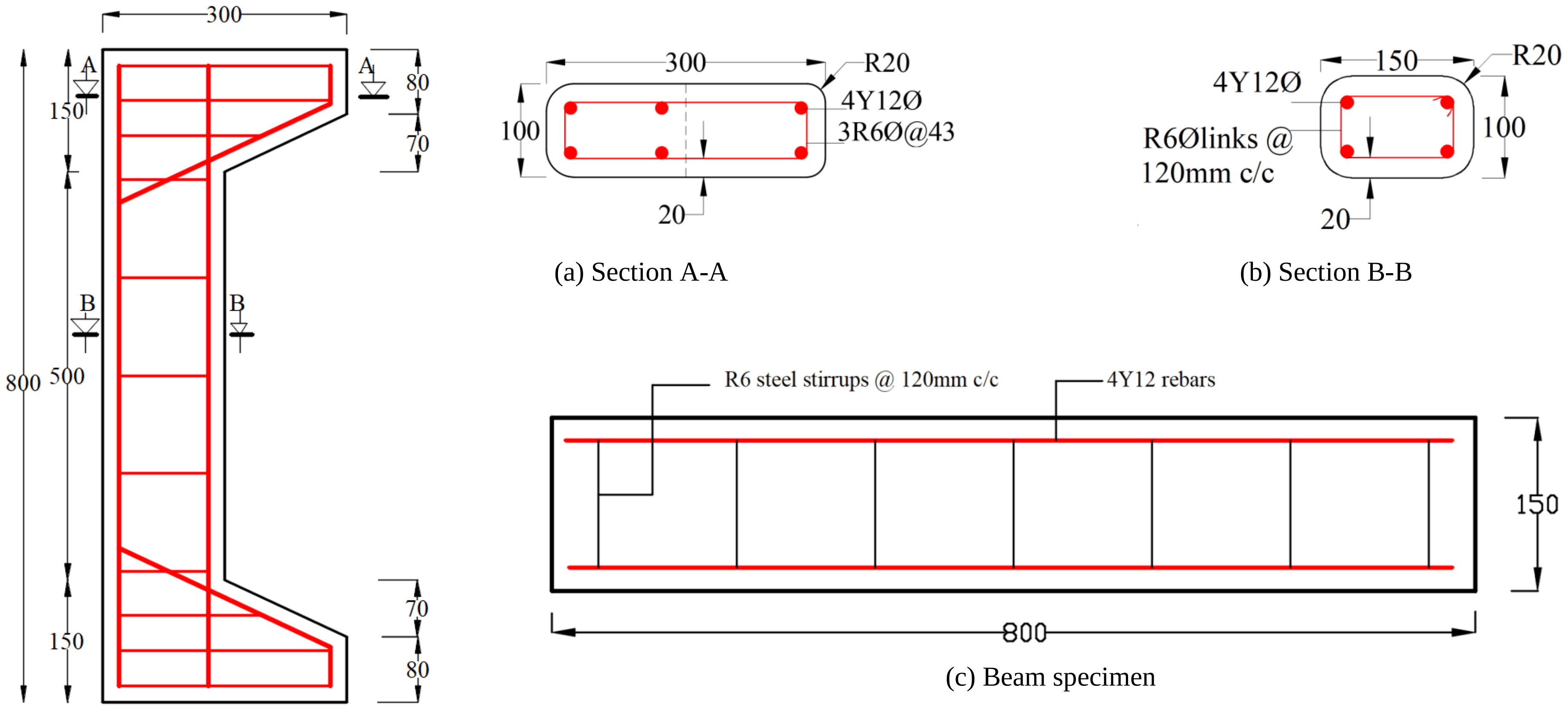

Figure 3.1 Specimen geometry and reinforcement details

Table 3.1 Configuration of test specimens

Test Specimen*	Width 'b' (mm)	Length 'L' (mm)	Height 'H' (mm)	Internal Reinforcement	Test eccentricity 'e' (mm)	Number of GFRP layers
0UC	100	150	800	4-12mm and R6mm	0	0
0UC-25e					25	0
0UC-50e					50	0
0UB					Bending	0
1FWC	100	150	800	4-12mm and R6mm	0	1
1FWC-25e					25	1
1FWC-50e					50	1
1FWB					Bending	1
2FWC	100	150	800	4-12mm and R6mm	0	2
2FWC-25e					25	2
2FWC-50e					50	2
2FWB					Bending	2
3FWC	100	150	800	4-12mm and R6mm	0	3
3FWC-25e					25	3
3FWC-50e					50	3
3FWB					Bending	3

*0, 1, 2 and 3 denote the number of GFRP layers, UC, UB, FWC, and FWB refer to unwrapped column, unwrapped beam, fully wrapped column, and fully wrapped beam, whereas 25e and 50e denote the eccentricity of loading, respectively.

3.4 Specimen Preparation

The tested columns were prepared in Civil Engineering laboratory located at University of Nottingham Malaysia. The Detailed descriptions of the procedures involved in fabricating the test specimens are discussed below.

3.4.1 Installation of Strain Gauges

Prior to pouring of concrete, the internal steel reinforcements of specimens were instrumented with electrical strain gauges to monitor strains induced in the steel reinforcement. However, the externally bonded GFRP reinforcement was also instrumented with electrical strain gauges of 10mm gauge length, in order to measure strains developed in the GFRP reinforcement. The strain gauges were attached to the longitudinal and lateral steel reinforcements, as well as the external GFRP reinforcement at the mid-height of the column specimens, as shown in Figure 3.2. Each specimen had four electrical strain gauges: one bonded to longitudinal steel, one bonded to transverse steel, while the remaining two were bonded to GFRP in longitudinal and transverse directions, respectively. For simplicity, the electrical strain gauges were placed in compression sides of all the columns tested under axial and eccentric loadings, as well as specimens subjected to four-point bending. It is worth mentioning that the electrical strain gauges were bonded on to steel reinforcement after constructing the steel bars cages (Figure 3.3). However, a sealant was applied on the surface of the electrical strain gauges to protect the strain gauges from environment.

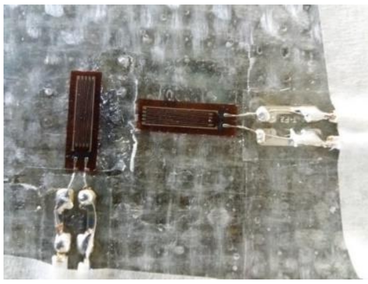

(a) Steel reinforcement **(b)** External GFRP composite

Figure 3.2 Steel reinforcement and GFRP instrumented with Strain gauges

(a) **(b)**

Figure 3.3 Steel Reinforcement Cages (a) Concentrically loaded columns (b) Eccentrically loaded columns

3.4.2 Casting of concrete Specimens

In this study, a wooden formwork with specific dimensions was used to cast the specimens. The formwork was prepared using plywood sheets of 3.6mm thickness and designed to be sufficiently stiff to prevent concrete leakage during vibration. The concrete was prepared using pan mixer. The column specimens were prepared at Civil Engineering Laboratory, University of Nottingham Malaysia. The concrete had a slump of 50mm, which is acceptable for RC placed with vibration. The reinforcement cage was placed in the prepared wooden formwork. The prepared concrete was poured in the formwork and compacted using vibrating table. A total of 3 concrete cubes and 2 concrete cylinders were cast for each batch in order to determine the compressive strength of concrete. All the concrete cubes, cylinders and RC specimens were cured for 28 days.

3.4.3 GFRP Wrapping

Prior to the application of GFRP reinforcement, the surface of concrete was grinded using a diamond grinder to expose the aggregates. A high-pressure air jet was then used to remove dust and loose particles from the prepared concrete surface. The bi-directional GFRP was applied on the surface of the columns in the test region with one, two, or three layers. The wet layup was employed to wrap the rectangular RC column specimens. The mixed resin was uniformly applied on the prepared concrete surface, and the GFRP sheet was gently placed at marked section. A hand held ribbed roller was used to release any trapped air and to squeeze out the epoxy resin. Subsequently, a second layer of epoxy resin was applied on the GFRP reinforcement. The successive layers of GFRP were applied over the first layer of GFRP reinforcement. It should be noted that an overlap of 60mm was used when applying the final layer of GFRP in the transverse direction of columns. All specimens of confined and unconfined columns had an additional GFRP strip of 100mm in width applied at both ends to avoid premature failure. The wrapped columns were kept in the laboratory at room temperature for approximately seven days to ensure adequate curing of the epoxy resin before testing. The GFRP strengthening process of rectangular RC specimens is depicted in Figure 3.4 below.

Figure 3.4 GFRP strengthening process of RC specimens

3.5 Materials Properties

Material testing was conducted to determine the mechanical properties of the constituent materials used in this study. The obtained results for the material properties of concrete, steel reinforcement and FRP composites are discussed in the following sections.

3.5.1 Concrete Testing

In this study, a preliminary test was conducted on concrete cubes with dimensions of 100 × 100 × 100mm and concrete cylinders with a diameter of

150mm and height of 300mm, to determine the 28-day concrete compressive strength. The test specimens were prepared according to the BS 8500-1 (2006) and tested based on the BS EN 12390-3 (2009). The specimens were removed from the curing tank and allowed to dry before testing. The compressive strength test was conducted using a calibrated 30 tonnes compression machine with rate of application of load of 0.6N/mm^2/s (BS EN 12390-3 2009) until failure. Illustrated in Figure 3.5 is the experimental set-up for the compression testing of concrete cubes and cylinders.

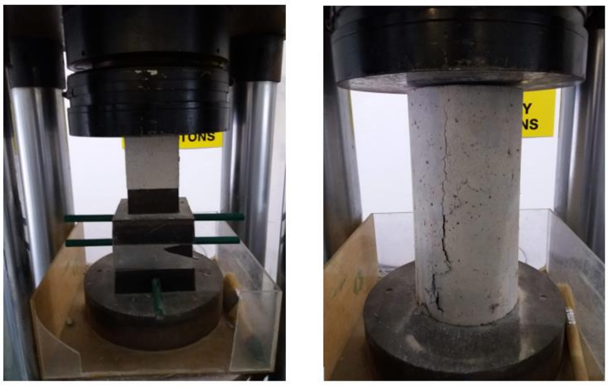

Figure 3.5 Compression testing of concrete cubes and cylinders

The results of the compressive strength test of concrete cubes and cylinders are summarised in Tables 3.2 and 3.3. The average 28days compressive strength for concrete cubes and cylinders were found to be 41.26MPa and 29.21MPa, with the corresponding tensile strength of 40.53MPa and Young's modulus of 25401.75MPa, respectively. It is obvious from Tables 3.2 and 3.3 that the concrete cubes generally have higher compressive strength values over the concrete cylinders.

Table 3.2 Results of compressive strength test of concrete cubes

Batch	Sample no.	Width (mm)	Length (mm)	Height (mm)	Maximum load (kN)	Compressive Strength (MPa)	Average Compressive strength (MPa)
1	1	100	100	100	432.40	43.24	43.22
	2	100	100	100	447.50	44.75	
	3	100	100	100	416.70	41.67	
2	1	100	100	100	418.70	41.87	39.84
	2	100	100	100	380.30	38.03	
	3	100	100	100	396.10	39.61	
3	1	100	100	100	407.70	40.77	40.63
	2	100	100	100	413.10	41.31	
	3	100	100	100	398.30	39.83	
4	1	100	100	100	398.10	39.81	40.50
	2	100	100	100	406.70	40.67	
	3	100	100	100	410.10	41.01	
5	1	100	100	100	389.40	38.94	39.82
	2	100	100	100	396.90	39.69	
	3	100	100	100	408.30	40.83	
6	1	100	100	100	413.10	41.31	41.02
	2	100	100	100	406.60	40.66	
	3	100	100	100	410.80	41.08	
7	1	100	100	100	430.40	43.04	42.32
	2	100	100	100	408.00	40.80	
	3	100	100	100	430.20	43.02	
8	1	100	100	100	431.10	43.11	43.95
	2	100	100	100	429.70	42.97	
	3	100	100	100	457.80	45.78	
9	1	100	100	100	403.80	40.38	39.41
	2	100	100	100	381.60	38.16	
	3	100	100	100	396.80	39.68	
10	1	100	100	100	410.80	41.08	40.43
	2	100	100	100	405.30	40.53	
	3	100	100	100	396.80	39.68	
11	1	100	100	100	420.00	42.00	42.76
	2	100	100	100	440.70	44.07	
	3	100	100	100	422.20	42.22	
Overall average							41.26

Table 3.3 Results of compressive strength test of concrete cylinders

Batch	Sample no.	Diameter (mm)	Height (mm)	Maximum load P (kN)	Compressive strength (MPa)	Average compressive strength (MPa)
1	1	150	300	527.30	29.84	29.98
	2	150	300	532.07	30.11	
2	1	150	300	501.15	28.36	29.73
	2	150	300	549.39	31.09	
3	1	150	300	543.80	30.77	28.99
	2	150	300	480.80	27.21	
4	1	150	300	546.50	30.92	28.58
	2	150	300	463.50	26.23	
5	1	150	300	567.24	32.10	28.54
	2	150	300	441.20	24.97	
6	1	150	300	515.46	29.17	29.06
	2	150	300	511.38	28.94	
7	1	150	300	535.45	30.30	28.01
	2	150	300	455.40	25.71	
8	1	150	300	510.20	28.87	28.31
	2	150	300	490.30	27.75	
9	1	150	300	494.61	27.99	27.38
	2	150	300	473.10	26.77	
10	1	150	300	561.94	31.80	30.93
	2	150	300	531.20	30.06	
11	1	150	300	609.50	34.49	31.75
	2	150	300	512.70	29.01	
Overall average						29.21

3.5.2 Steel Reinforcement Testing

The tensile test was conducted in accordance to ASTM A370-8a (2008) to determine the yield and tensile strength of steel reinforcement. The longitudinal steel rebar of three samples of 12mm diameter bar of 500mm in length was used. The tensile test was conducted using a 1000kN capacity universal testing machine located in engineering research building at the University of Nottingham Malaysia. A gauge length of 200mm was marked at the mid-height of the sample to determine the strains in steel reinforcement. The tensile load was applied monotonically up to failure (Figure 3.6), and the test results were recorded by a data acquisition system connected to the testing machine. Typical failure of steel reinforcement is depicted in Figure 3.7.

The tensile test results of 12mm diameter steel reinforcement are summarised in Table 3.4 and illustrated in Figure 3.8. From the results, it is clear that the average yield strength of 12-mm longitudinal steel reinforcement was 550MPa. The tensile strength of transverse steel reinforcement was not measured due to the inavailability of a machine for testing small-diameter rebar.

Figure 3.6 Test setup for tensile testing of steel reinforcement

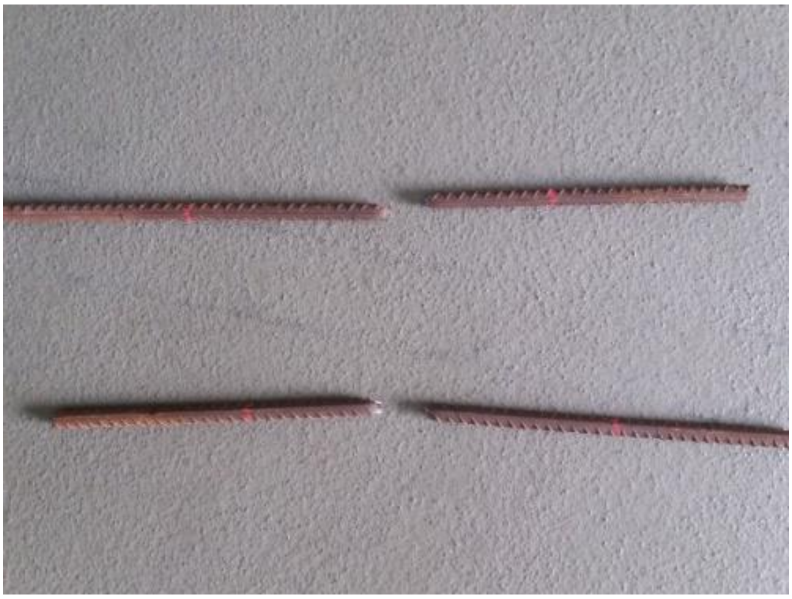

Figure 3.7 Typical failure of steel reinforcement

Table 3.4 Results of tensile testing of 12mm diameter steel bars

Sample no.	Nominal diameter (mm)	Yield load (N)	Yield stress (MPa)	Average yield stress (MPa)	Ultimate load (N)	Ultimate stress (MPa)	Average ultimate stress (MPa)
1	12	62133	549	550	73574	651	652
2	12	63999	545		73976	654	
3	12	62912	555		73468	650	

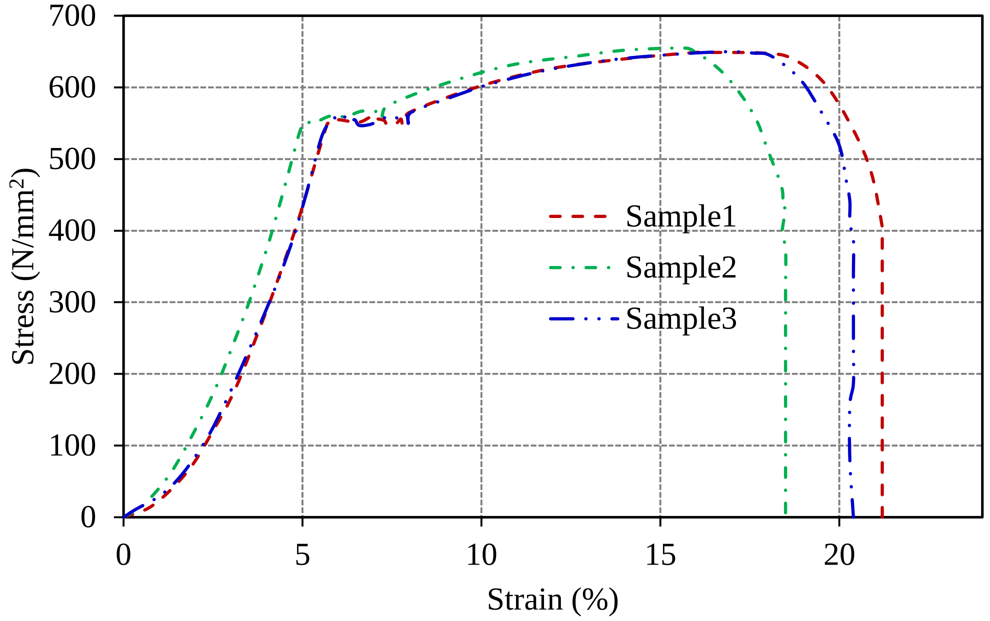

Figure 3.8 Stress-strain responses of 12mm diameter steel bars

3.5.3 FRP Composites Testing

The tensile test was conducted on bi-directional GFRP coupons to determine the in-plane tensile properties of the GFRP reinforcement. The test was conducted based on the recommendations of ASTM D3039 (2000) guidelines using a 50kN capacity LR50K-plus tensile testing machine located in the Mechanical Engineering Laboratory at the University of Nottingham Malaysia. A total of 9 rectangular GFRP coupons of 250mm in length and 25mm in width were prepared and tested (Figure 3.9). The test coupons were divided into three groups based on the number of GFRP layers (one, two and three layers), and each group consists of three samples, respectively. The GFRP coupons were tabbed using aluminium tabs measuring 50mm in length and 25mm in width, with a taper angle of 7^{o} and a thickness of 1.5mm, respectively. The surface of aluminium tabs was roughen using a sand paper, and a thinner was used to clean dust particles to ensure a strong bond between aluminium tabs and GFRP coupon. The tabs were bonded to the GFRP coupons using epoxy-resin, and were allowed to harden for seven days. Prior to application of tensile testing, the dimensions of each sample was measured and recorded. The specimen was then clamped in the grips of the testing machine, with a gauge length of 150mm between the two grips. The tensile load was applied by the load cell with a head-speed of 2mm/min until the failure of each specimen occurred. The details of GFRP coupons and the tensile test set-up are illustrated in Figure 3.10, respectively.

Figure 3.9 GFRP coupon samples

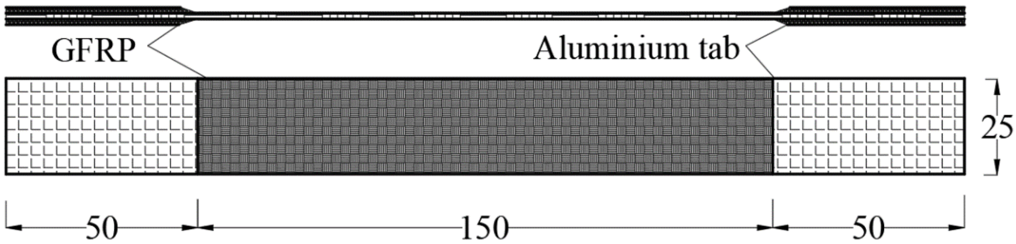

(a)

(b)

Figure 3.10 Tensile testing of GFRP coupons (a) Details of GFRP coupons (b) Tensile test setup

The results of tensile test of GFRP coupons are summarised in Table 3.5 and illustrated in Figure 3.11. It is clear from Table 3.5 that the three layers GFRP coupons achieved the highest ultimate load carrying capacity, followed by two layers, and eventually one layer GFRP coupons. The results clearly indicated that the tensile strength significantly increased with an increase in the number of GFRP layers. It is also evident from Figure 3.11 that the stress-strain response of 1 layer GFRP coupons demonstrated a softer nonlinear behaviour. This nonlinear trend might be attributed to the relatively low total fibre volume fractions in the GFRP composites and material imperfections such as voids and micro cracks. The failure pattern of GFRP coupons are illustrated in Figure 3.12.

Table 3.5 Results of tensile testing of GFRP coupons

Sample no.	Gauge dimension				Maximum Load, P (N)	Maximum Tensile Stress (MPa)	Strain at Maximum Load (%)	Modulus of Elasticity (MPa)
	Length (mm)	Width (mm)	Thickness (mm)	Cross Section Area (mm^2)				
One Layer GFRP Coupons (1L)								
1.	150	25	0.78	19.50	4638.30	237.86	4.34	10112.00
2.	150	25	0.74	18.50	4064.30	219.69	3.63	10477.00
3.	150	25	0.76	19.00	3563.00	189.79	3.68	12002.00
Average			0.76	19.00	4088.53	215.78	3.88	10863.67
Two Layers GFRP Coupons (2L)								
1.	150	25	1.35	32.50	7293.60	224.42	4.04	9683.40
2.	150	25	1.37	34.25	7398.70	216.02	4.09	10094.00
3.	150	25	1.35	33.75	6405.40	189.79	3.54	10471.00
Average			1.36	33.5	7032.57	210.08	3.89	10082.80
Three Layers GFRP Coupons (3L)								
1.	150	25	1.84	46.00	9842.50	213.97	5.04	9152.20
2.	150	25	1.84	46.00	11841.00	257.41	5.51	9495.20
3.	150	25	1.80	45.10	8310.70	184.27	4.26	9453.20
Average			1.83	45.7	9998.07	218.55	4.94	9366.87

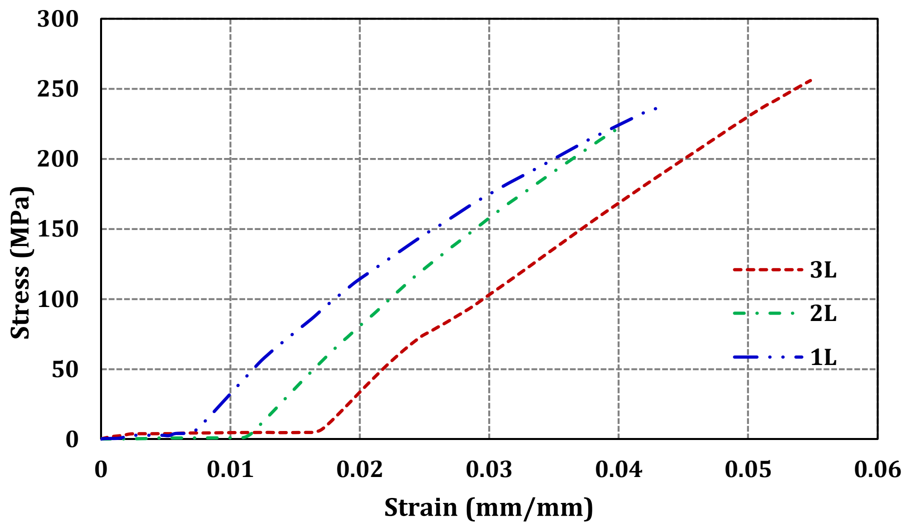

Figure 3.11 Stress-strain curves of GFRP coupons

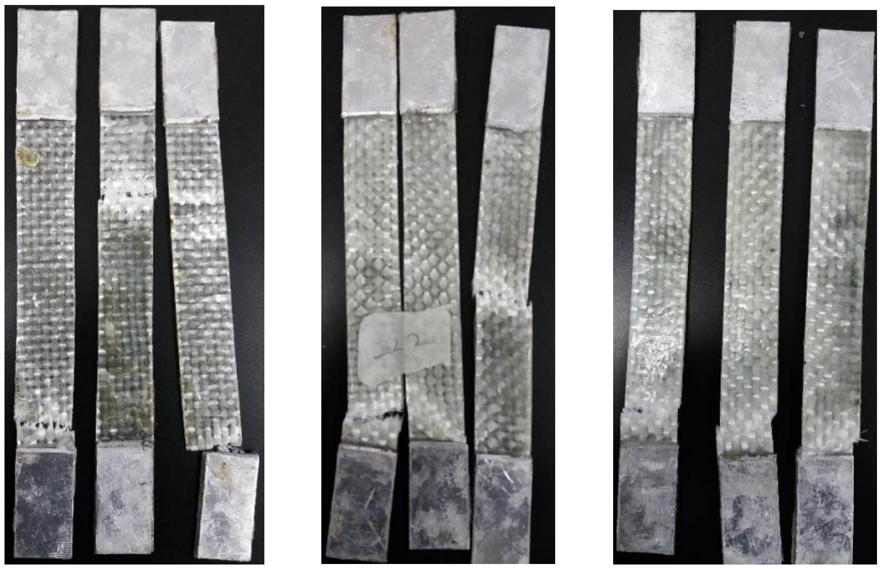

(a) (b) (c)

Figure 3.12 Typical failure of GFRP coupons (a) one layer (b) Two layers (c) Three layers

3.6 Instrumentation and Test Setup

The specimens were tested monotonically using a universal static compression-testing machine with 4000kN capacity in the heavy structures Laboratory located at the University of Malaya. The test setup and layout of specimen instrumentation are portrayed in Figure-3.13. The details of load and deformation were directly recorded using data acquisition system, which was connected to the testing machine. However, the strains in steel and GFRP were measured using data logger. The axially loaded columns were instrumented with a linear variable differential transformer (LVDT) to monitor the axial displacement of columns. The LVDT was connected vertically to the lower steel plate attached to the actuator (Figure 3.13 (a)). For the eccentrically loaded columns, the eccentricity was achieved using two steel rollers: one roller was attached to the lower end of steel plate attached to the actuator, and the second roller was welded to a strong steel base support (Figure 3.13 (b)). The steel base support was placed along the axis of the actuator to achieve the required eccentricity. The lateral displacement of the columns was measured with one LVDT mounted horizontally at mid-height of the columns. Similar to the concentrically loaded specimens, the axial displacement of the columns was measured using an LVDT mounted vertically at the lower steel plate attached to the actuator. The specimens were loaded to failure under displacement control system with a loading rate of 0.2 mm/min.

For specimens subjected to flexural loading, pure bending was achieved by four-point loading over a simply supported clear distance of 690mm and two shear spans of 230mm (Figure 3.13 (c)). During loading, the flexural load and mid-span deflection were recorded using the data acquisition system, which was connected to the testing machine. Additionally, a LVDT was fixed vertically at the mid-span to monitor the specimen’s mid-span deflection. The load was applied monotonically under displacement control system with a loading rate of 0.5 mm/min.

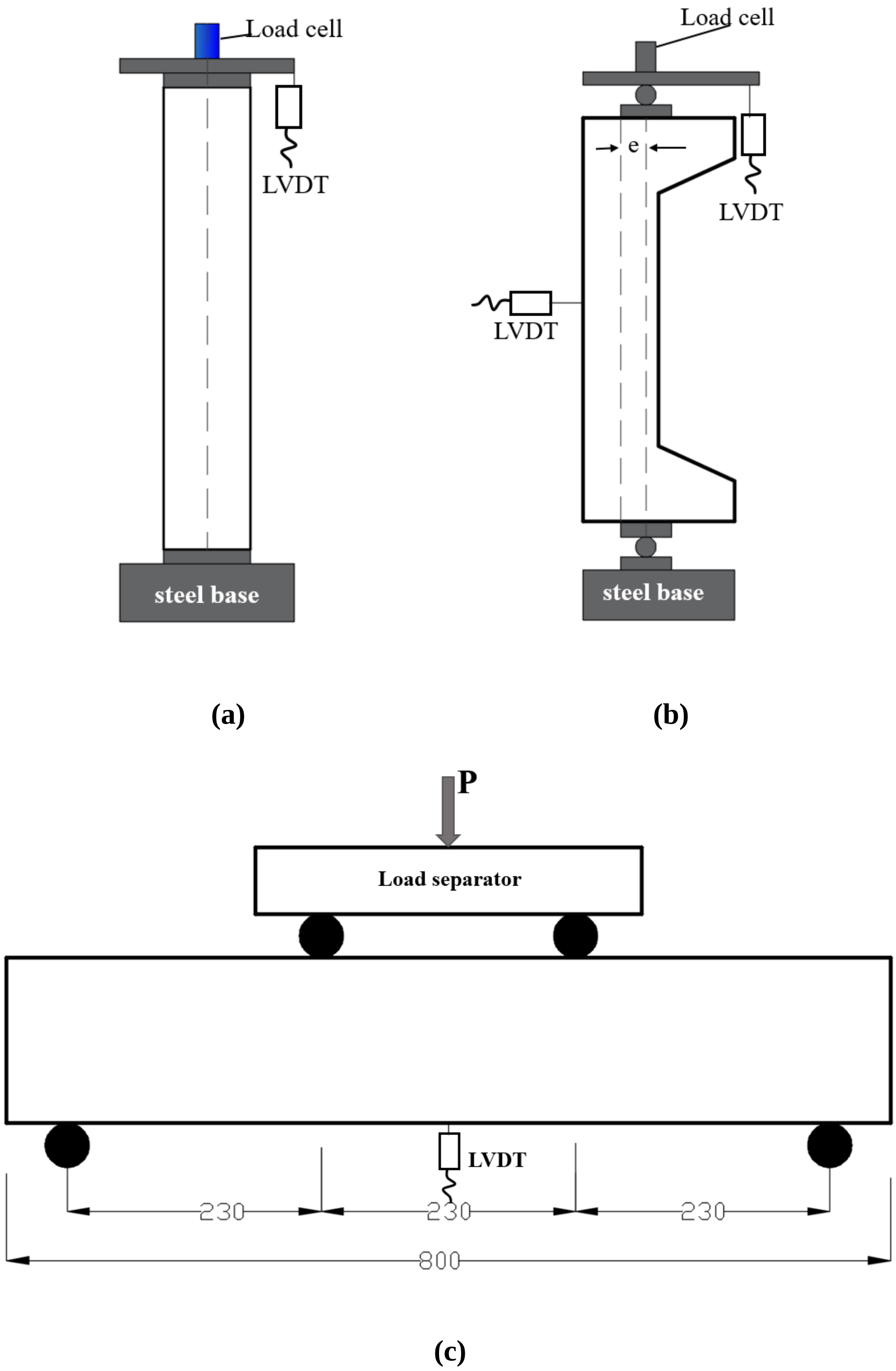

Figure 3.13 Test setup: (a) concentrically loaded specimens, (b) eccentrically loaded specimens and (c) specimens subjected to flexural loading

3.7 Summary

This chapter discussed the detailed description of specimens, preparation of specimens, instrumentation and test procedure of specimens. Moreover, preliminary testing of materials used in this research was described and the material properties summarised. The results obtained from the experimental programme are reported and discussed in the next chapter.

CHAPTER 4: EXPERIMENTAL RESULTS

4.1 Introduction

As described in chapter 3, a series of 16 rectangular reinforced concrete columns were prepared and divided into four distinct groups as per their FRP wrapping (unwrapped and fully wrapped) and loading conditions (concentric, eccentric and flexural loadings). Each group comprised four specimens in which one specimen was tested under axial loading, two columns were tested under different load eccentricities (25 and 50mm), and one specimen was tested under four-point bending test. All the RC specimens were tested under displacement control using a 4000kN capacity compression testing machine at University of Malaya. The experimental observations include load, displacement, and strains were recorded using data acquisition system and data logger. The main test variables considered in this study include the amount of GFRP wrap layers (i.e., one, two, and three) and the intensity of load eccentricities (i.e., 0, 25mm, and 50mm). The outcomes of the investigation and a comprehensive discussion of effects of test variables on failure patterns, percentage enhancement in load carrying capacity, ductility and load-displacement and load-strain behaviour of the rectangular RC specimens are presented in this chapter.

4.2 Failure Pattern of RC Columns

Figure 4.1 illustrates the modes of failure of axially loaded rectangular RC columns. The cracks of rectangular RC column 0UC were initiated at the upper end and followed by few minor cracks, which are slightly a distance away from the mid-span of column. As the applied load increased, a sudden crushing failure of concrete cover was observed in the upper region of the specimen. After crushing of concrete cover, an outward buckling of longitudinal steel reinforcement along with partial deformation of the hoop ties was also observed. As shown in Figure 4.1 the failure of axially loaded GFRP confined RC columns commenced with the development of FRP wrinkles at the sides of the specimens. At the later stages of axial loading, a snapping sound related to the initiation of concrete micro-cracking was observed, indicating the commencement of GFRP confinement action. At failure load, a sudden rupture of GFRP was observed near the upper and lower ends, which then propagated to the column ends, resulting in a drop in load. However, small rupture of GFRP was observed at the column corners near mid-height without concrete crushing. The GFRP confined columns under axial loading attained a concrete crushing failure followed by yielding of longitudinal steel and deformation of steel ties at the upper end of the columns.

(a) **(b)** **(c)** **(d)**

Figure 4.1 Failure of concentrically loaded specimens: (a) column 0UC, (b) column 1FWC (c) column 2FWC and (d) column 3FWC

The failure patterns of control and GFRP confined RC columns with 25mm and 50mm eccentricities are depicted in Figures 4.2 and 4.3, respectively. The vertical cracks of control column 0UC-25e with 25mm eccentricity at the initial stages of loading were observed at the upper part of the column's test region (i.e. close to the top corbel). At the maximum failure load, premature failure was observed due to spalling of concrete at the top of control column 0UC-25e. However, the mode of failure of control column 0UC-50e with 50mm eccentricity experienced a sudden crushing of the concrete cover, followed by yielding of longitudinal steel reinforcement. Moreover, the modes of failure of all GFRP confined columns were observed near the top end of column.

(a) **(b)** **(c)** **(d)**

Figure 4.2 Failure of specimens with 25mm eccentric load: (a) column 0UC-25e (b) column 1FWC-25e (c) column 2FWC-25e (d) column 3FWC-25e

Furthermore, the failure pattern of all fully wrapped columns subjected to 50mm eccentricity was similar to that of GFRP confined specimens with 25mm eccentricity. The failure of all GFRP confined columns with 50mm eccentricity were initiated due to the formation of FRP wrinkles at the compression face of the columns. When the applied load approached the maximum value, a snapping sounds was observed due to the confining action of GFRP reinforcement. Subsequently, the GFRP confined columns suffered premature failure by GFRP rupture followed by GFRP debonding, which initiated at the upper end of column, leading to a decline in load. All these GFRP confined columns specimens sustained a maximum load until rupture of the GFRP, followed by crushing of concrete at the lower end of corbel. However, a small FRP rupture was observed at the compression face near mid-height of GFRP confined columns.

(a) (b) (c) (d)

Figure 4.3 Failure of specimens with 50mm eccentric load: (a) column 0UC-50e (b) column 1FWC-50e (c) column 2FWC-50e (d) column 3FWC-50e

4.3 Behaviour of Columns

The experimental results of rectangular RC columns with bi-directional GFRP wrapping under axial and eccentric loadings are summarised in Table 4.1. The relationship between the applied load and the equivalent axial and lateral displacements for each group of tested columns was plotted to assess their behaviour and performance. Moreover, the ductility index of each column specimen was evaluated to describe the influence of GFRP wrapping on ductility of the specimens. Ductility is the capacity of structural members to suffer considerable deformation prior to failure (GangaRao et al., 2006). Ductility index 'λ' is commonly quantified as the ratio of maximum axial displacement

‘δ_u’ at ultimate load to the axial displacement ‘δ_y’ at yield load (Priestley et al., 1996).

$$\lambda = \frac{\delta_u}{\delta_y} \tag{4.1}$$

Two methods were employed to quantify the ductility index of the tested column specimens. In the first method, the ductility of the columns was quantified based on the expression given in equation (4.1) above. In the second method, the ductility index of the column specimens was quantified based on the ratio between the area under the axial load-displacement curve up to the ultimate axial displacement ‘A_1’ and the area under the curve up to the yield axial displacement ‘A_2’ (Hadi and Youssef, 2016; Mai et al., 2018).

$$\lambda = \frac{A_1}{A_2} \tag{4.2}$$

In both methods, the yield displacement is the axial displacement at the yield load, and the ultimate axial displacement was taken as the displacement at an axial load equivalent to 0.8 times the ultimate axial load in the descending branch of the axial load-displacement response (Priestley et al., 2007; Sheikh and Légeron, 2014).

Table 4.1 Experimental results of testing GFRP-wrapped rectangular RC specimens with concentric and eccentric loadings

Test specimen	Yield axial load P_y (kN)	Axial displacement at P_y (mm)	Ultimate axial load P_{ult} (kN)	Axial displacement at P_{ult} (mm)	Axial displacement at $0.8P_{ult}$ (mm)	Lateral displacement at P_{ult} (mm)	Increase in P_{ult} relative to the control column (%)	Ductility index λ	
								First Method	Second Method
0UC	388.17	2.86	403.07	3.40	8.10	-	-	2.83	4.46
1FWC	564.07	3.51	578.99	4.70	10.31	-	44	2.94	4.61
2FWC	799.17	4.00	878.35	6.30	11.95	-	118	2.99	5.60
3FWC	868.08	4.20	1155.00	7.96	13.44	-	187	3.20	7.27
0UC-25e	248.60	2.34	255.53	2.82	6.14	2.62	-	2.62	4.30
1FWC-25e	267.60	2.43	281.61	3.42	7.00	3.26	10	2.88	4.55
2FWC-25e	309.55	2.46	343.29	4.24	7.30	4.02	34	2.97	5.30
3FWC-25e	325.55	2.48	428.34	4.67	8.01	4.45	68	3.23	6.30
0UC-50e	163.28	1.69	181.69	2.18	2.78	1.98	-	1.64	2.64
1FWC-50e	169.42	1.74	203.43	2.94	4.00	2.74	12	2.30	3.79
2FWC-50e	186.54	1.96	219.25	3.23	5.31	3.07	21	2.71	5.17
3FWC-50e	255.28	3.29	276.19	4.23	10.35	4.07	52	3.14	5.92

4.3.1 Behaviour of Concentrically Loaded Columns

The axial load versus vertical displacement responses of axially loaded specimens are portrayed in Figure 4.4. It is evident that the linear ascending portion of the load-displacement response of both unconfined and GFRP confined columns had similar trend up to the yield axial load. Moreover, the axial load-displacement response of both GFRP confined and control columns demonstrated a post-peak descending branch, with a decline in axial load after achieving the peak point. It is clear that GFRP confinement leads to a substantial improvement in ultimate axial capacity and performance of rectangular RC specimens. Among all the axially loaded GFRP wrapped columns, column 3FWC with three layers of GFRP reinforcement achieved the highest maximum axial load followed by columns 2FWC and 1FWC, respectively. Moreover, maximum ultimate load enhancement of 187%, 118%, and 44% were attained by columns 3FWC (3 layers of GFRP), 2FWC (2 layers of GFRP), and 1FWC (1 layer of GFRP), respectively, over the control column 0UC. Regarding the GFRP confinement effect on the ductility of column specimens in this group, it is apparent that full GFRP wrapping of columns results in a significant increase in ductility. Column 3FWC with three layers of GFRP reinforcement achieved the highest ductility index of 7.27, followed by the columns 2FWC (2 layers of GFRP) and 1FWC (1 layer of GFRP) with ductility index values of 5.60 and 4.61, respectively. From the experimental results, it was found that the increasing the number of GFRP layers increased the ductility index of GFRP confined RC columns. The remarkable increase in ductility of the tested columns might be attributed to the confinement effect of GFRP wrapping which prevented spalling of concrete cover.

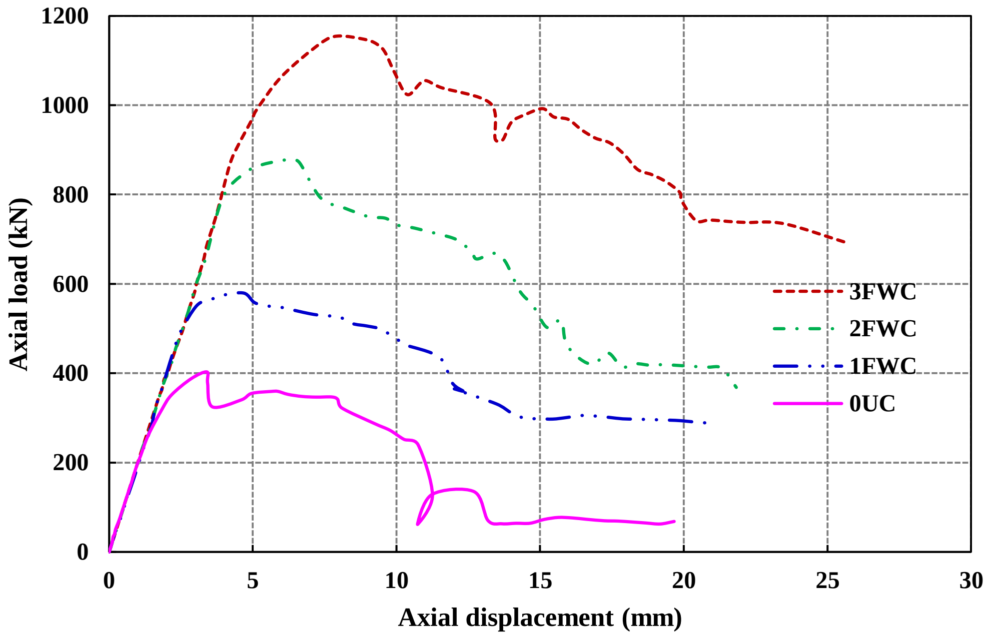

Figure 4.4 Axial load versus axial displacement responses of specimens with concentric loading

The relationship between the axial load and the corresponding longitudinal strain for GFRP confined columns subjected to axial loading are depicted in Figure 4.5. The longitudinal strains were obtained from the strain gauges attached to the GFRP reinforcement at mid-height of the column. It is worth noting that strain in steel reinforcement of GFRP confined columns were not reported due to malfunction of most of the strain gauges on steel bars. It is obvious from Figure

4.5 that the GFRP confinement remarkably enhanced the longitudinal strain of the tested columns at ultimate axial load. Among all the axially loaded GFRP-confined rectangular RC columns, column 3FWC with three layers of GFRP reinforcement exhibited the highest ultimate longitudinal strain of 0.151%, followed by columns 2FWC (2 layers of GFRP) and 1FWC (1 layer of GFRP) with ultimate longitudinal strains of 0.123% and 0.084%.

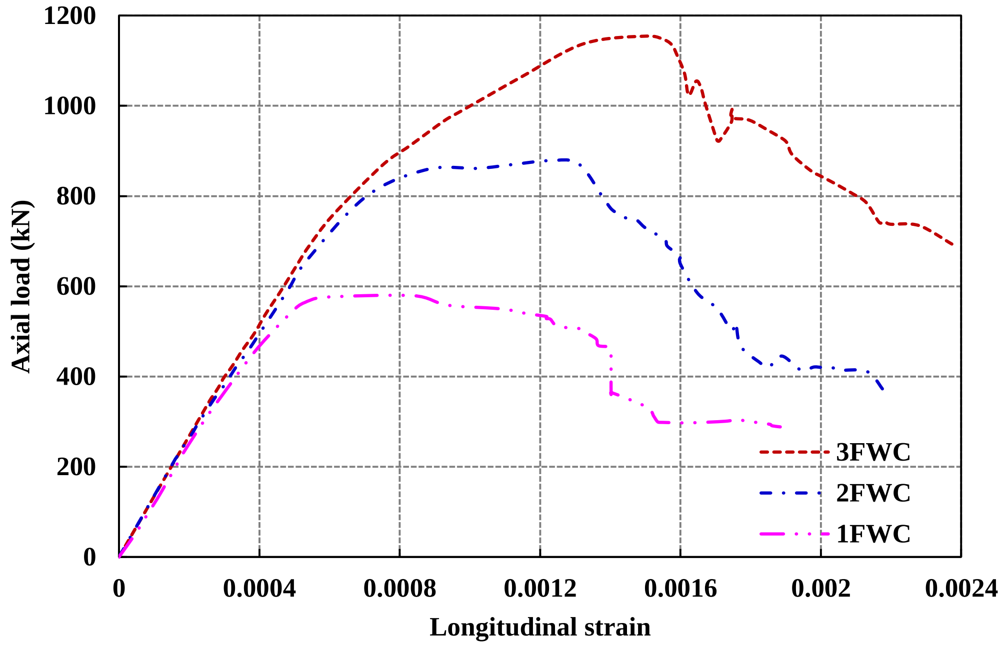

Figure 4.5 Axial load versus longitudinal strain relationships for columns subjected to concentric loading

4.3.2 Behaviour of Fully Wrapped Specimens with 25mm Eccentric Loading

Figure 4.6 portrays the axial load versus axial and lateral displacement responses of specimens with 25mm eccentric loading. The linear ascending portion of the load-displacement responses of the unconfined and GFRP confined columns shows similar stiffness behaviour up to the yielding of internal steel reinforcement. Similar to axially loaded columns, the axial load versus displacement responses of specimens in this group with 25mm eccentricity also indicates a descending trend in which the load decreased after achieving the peak point. Column 3FWC-25e with three layers of GFRP reinforcement sustained the highest peak load of 428.34kN, achieving a 68% increase in ultimate load over the control column 0UC-25e. However, ultimate load enhancement of 34% and 10% were achieved by columns 2FWC-25e and 1FWC-25e greater than the control column 0UC-25e. The significant increase in ultimate load carrying capacity of columns 3FWC-25e, 2FWC-25e and 1FWC-25e was mainly due to the confinement generated by GFRP to the compression region of the columns, which prevented severe crushing of concrete cover after yielding of longitudinal steel bars. It was found that the percentage of enhancement in GFRP confined columns was increased with increase in number of GFRP layers. The ductility index values of control and GFRP confined columns in this group are reported in Table 3. Column 3FWC-25e with three layers of GFRP reinforcement achieved a ductility index of 6.30, which is higher than the ductility index of two and one layers of GFRP confined columns 2FWC-25e (5.3), 1FWC-25e (4.55), and control column 0UC-25e (4.30). The higher ductility index of columns 3FWC-25e, 2FWC-25e and 1FWC-25e compared to control columns 0UC-25e was mainly due to the combined confinement action of the longitudinal and the transverse weaves of the bi-directional GFRP reinforcement, which resulted to an increase in axial deformation with a gradual decrease in ultimate axial load.

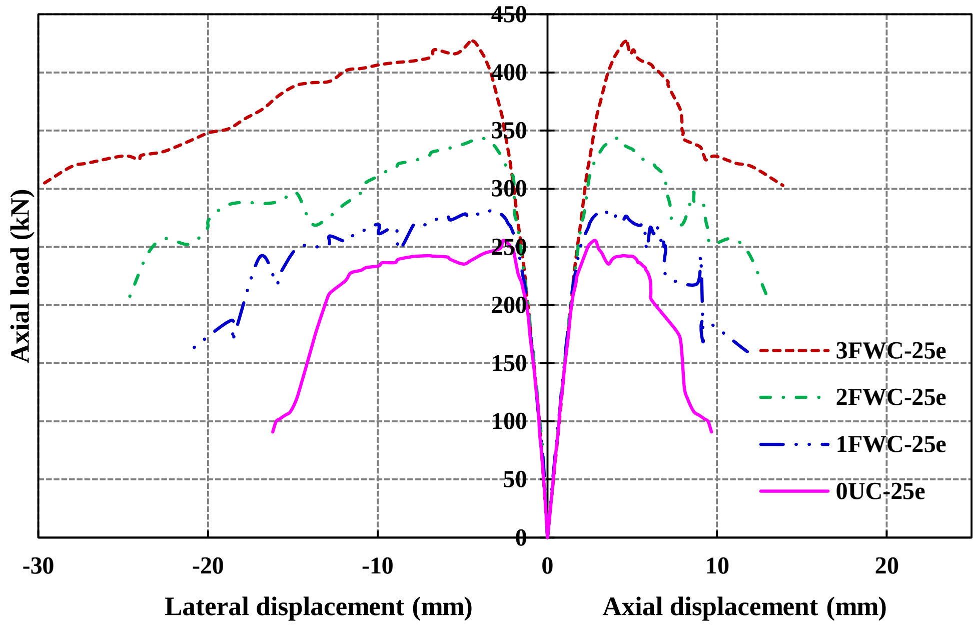

Figure 4.6 Axial load versus axial and lateral displacement responses of specimens with 25mm eccentric loading

Figure 4.7 portrays the axial load versus longitudinal and transverse strain behaviour for GFRP-confined rectangular RC columns subjected to 25mm eccentricity. It is clear that the GFRP confined columns exhibited a significant gain in both longitudinal and transverse strains with an increase in number of GFRP wraps. The highest gain in strain was observed in columns with three layers of GFRP wrapping, followed by columns with two and one layers of GFRP wrapping.

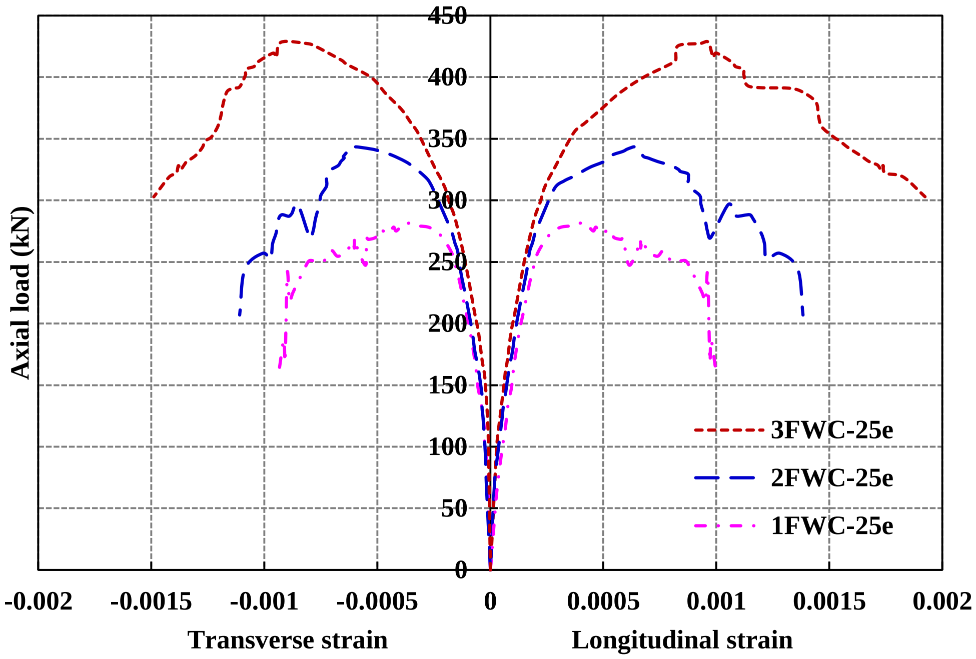

Figure 4.7 Axial load versus longitudinal and transverse strain responses of specimens under 25mm eccentric load

4.3.3 Behaviour of Fully Wrapped Columns Subjected to 50mm Load Eccentricity

The axial load versus axial and lateral displacement trends of specimens with 50mm eccentricity are shown in Figure 4.8 It is apparent that all the GFRP confined columns had bilinear behaviour. The post-peak axial load versus axial and lateral displacement responses of all the columns showed a descending response. The first part of the response curves of the fully confined columns indicates a similar linear ascending response up to the yielding of steel reinforcement. This linear ascending response characterises the typical behaviour of column specimens without GFRP wrapping. Beyond the yield point, the columns experienced a small reduction in stiffness with increased in axial load. The ultimate load of each column was achieved at the rupture of GFRP. Column 3FWC-50e with three layers of GFRP reinforcement sustained the highest maximum ultimate load of 276.19kN, achieving a 52% ultimate load enhancement over the control column (0UC-50e). However, columns 2FWC-50e (2 layers of GFRP) and 1FWC-50e (1 layer of GFRP) had maximum ultimate loads of 219.25kN and 203.43kN, with corresponding enhancement of 21% and 12% over the control column 0UC-50e. The significant enhancement in the GFRP confined columns was mainly attributed to the combined confinement effect generated by the longitudinal and transverse fibres of bi-directional GFRP reinforcement. In terms of ductility, the trend of ductility in GFRP confined columns with 50mm eccentricity was similar to that of GFRP confined columns with eccentricity of 25mm. The ductility index values of columns 3FWC-50e, 2FWC-50e, 1FWC-50e, and 0UC-50e were 5.92, 5.17, 3.79, and 2.64, respectively. The remarkable decrease in ductility of columns with 50mm eccentricity compared to columns with 25mm eccentricity was due to the decrease in the compression area of concrete confined by GFRP.

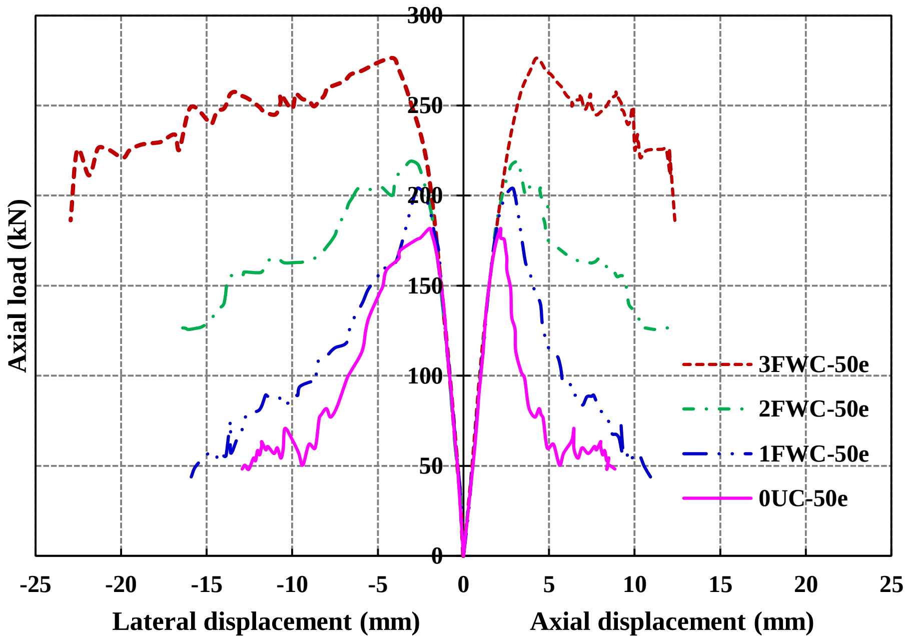

Figure 4.8 Axial load versus axial and lateral displacement trends of specimens with 50mm eccentric loading

Figure 4.9 depicts the axial load versus longitudinal and transverse strain relationships for GFRP-confined rectangular RC columns under to 50mm eccentricity. It is evident that the GFRP confined columns revealed a remarkable enhancement in longitudinal and transverse strains at peak load, which increases with an increase in number of layers of GFRP reinforcement. The highest attainment in strain was observed for column 3FWC-50e with three layers of GFRP reinforcement, followed by columns 2FWC-50e and 1FWC-50e, with two and one layers of GFRP reinforcement, respectively.

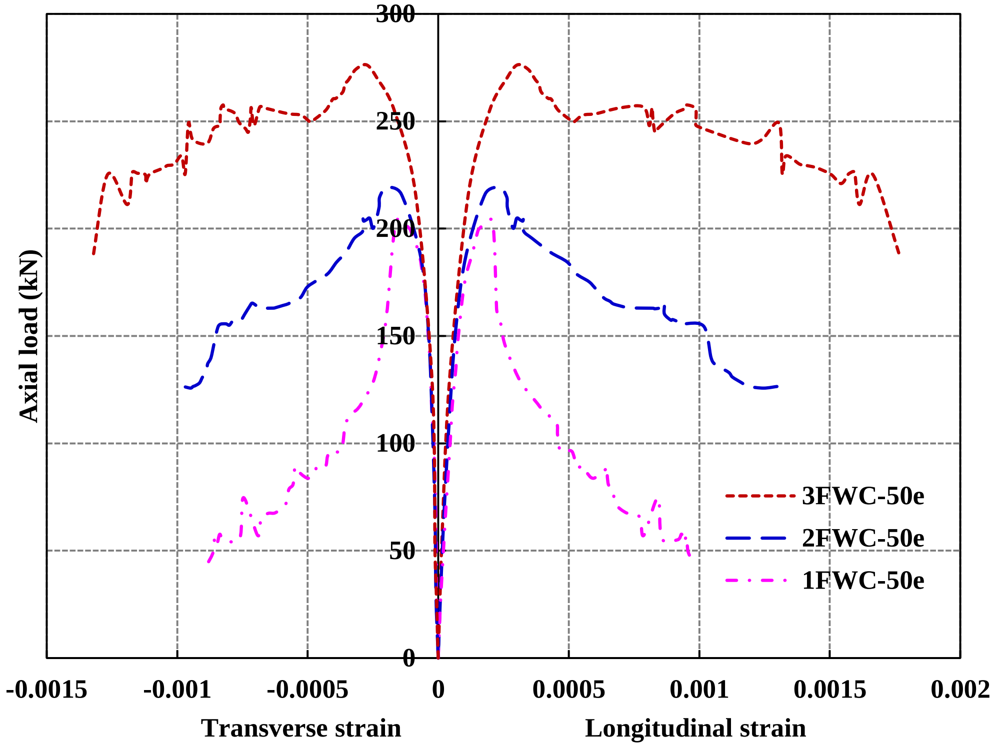

Figure 4.9 Axial load versus longitudinal and transverse strain responses of specimens under 50mm eccentric load

4.4 Effect of Eccentricity

Figure 4.10 depicts the axial load versus axial displacement curves for specimens under various eccentric loading conditions. The effect of the axial eccentric load on performance of the tested columns was determined by analysing the variation of their ultimate load capacity and ductility with eccentricity. Figure 4.11

portrays the variation of ductility with eccentric loading for rectangular RC specimens. It is apparent from Figures 4.10 and 4.11 that increasing the eccentricities of GFRP confined columns led to a decline in their ultimate load carrying capacity and ductility. This might be attributed to the reduction of the compression area of concrete confined by GFRP reinforcement. It is also evident from Figure 4.11 that when the number of GFRP layers is increased from 0-3 layers, the ductility of GFRP confined columns remarkably increases. But when eccentricity was introduced, the ductility of GFRP confined columns decreases with increased in eccentricity.

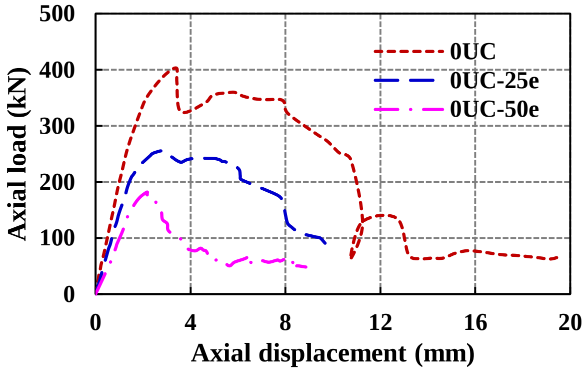

(a) Unwrapped columns

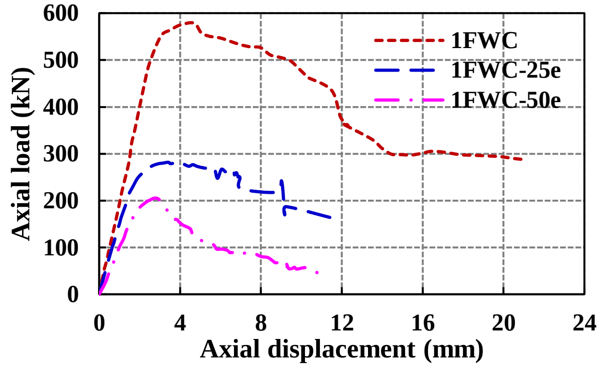

(b) One layer GFRP wrapped columns

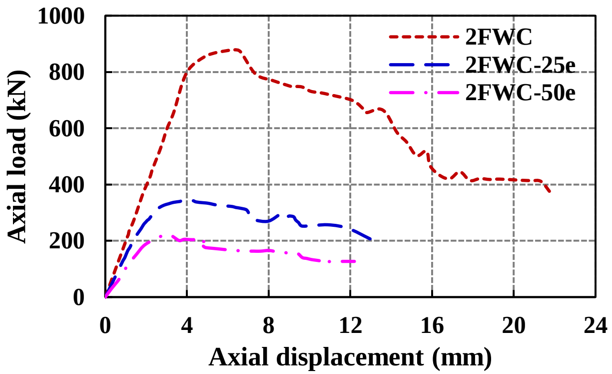

(c) Two layers GFRP wrapped columns

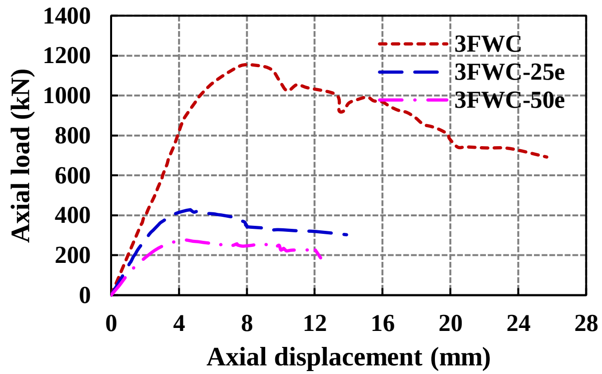

(d) Three layers GFRP wrapped columns

Figure 4.10 Axial load versus axial displacement curves for specimens subjected to various eccentric loadings

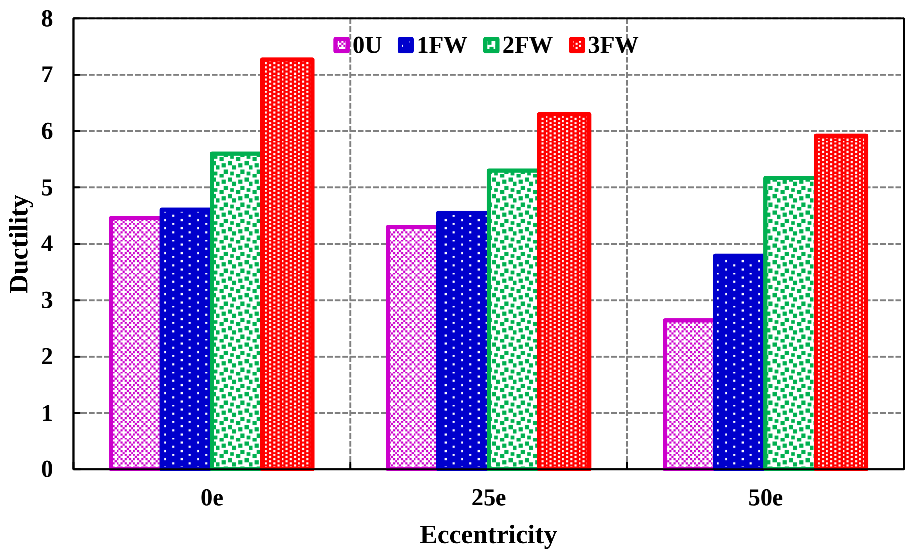

Figure 4.11 Variation of ductility with eccentricity

4.5 Behaviour of Beams

Typical flexural failure pattern of beam specimens is illustrated in Figure 4.12. The failure of beam 0UB commenced with the initiation of flexural cracks at the tension sides of the specimen due to the increase in flexural stresses. At the later stages of loading, the cracks were widened and further propagated towards the compression region of the beam. The control beam failed with the rupture of internal steel reinforcement followed by spalling of concrete cover in the tension region of the beam. Similar to the unconfined beam, the failure modes of fully wrapped beams commenced with initiation of vertical flexural cracks in the tension region at mid-span of the beams. These cracks in GFRP confined beams widened and propagated towards the compression region of the beams as the load approached maximum value. Beams 2FWB and 3FWB with two and three layers of GFRP failed in flexure with vertical rupture of GFRP at mid-span of the beams. Similarly, beam 1FWB with one layer of GFRP reinforcement failed due to GFRP rupture near the mid-span (Figure 4.12(b)). Moreover, all the GFRP wrapped beams exhibited crushing of concrete cover due to transverse cracking in the compression side. Yielding of internal steel reinforcement were obvious in all the GFRP wrapped beams.

(a) Beam 0UB

(b) Beam 1FWB

(c) Beam 2FWB

(d) Beam 3FWB

Figure 4.12 Typical Failure of specimens under flexural loading

Table 4.2 summarises the results of bending test of rectangular RC beams. The flexural load versus mid-span deflection responses of the specimens are plotted as shown in Figure 4.13. The ductility index of the specimens was quantified by applying the procedure described in Section 4.3 using the flexural load versus mid-span deflection curves of the specimens. The first part of the flexural load-mid-span deflection response of control beam 0UB demonstrated quasi-linear behaviour up to the yield load of 75.31kN, with a corresponding mid-span deflection of 2.32mm. Beyond the yield load, a slight ductile behaviour of the flexural load-deflection curve was obvious up to a maximum flexural load of 94.39kN and the corresponding mid-span deflection of 14.62mm. The flexural load-deflection response also showed descending trends in which the flexural load dropped immediately after reaching the peak load. The control beam 0UB had ductility index value of 7.39 and 15.63 based on the first and second methods of calculations (Table 4.2).

Furthermore, the flexural load-deflection responses of fully wrapped beams showed nearly similar stiffness trends before the yielding of internal steel reinforcement. Beams 1FWB, 2FWB, and 3FWB had a yielding load of 94.80kN, 110.43kN, and 117.63kN with corresponding mid-span deflections of 2.67mm, 2.77mm, and 2.79mm, respectively. From Figure 4.13, it is obvious that the post-peak flexural load-mid-span deflection responses of all the GFRP wrapped beams demonstrated an ascending behaviour up to the maximum flexural load. This could be attributed to the confinement effect of the longitudinal fibres of bi-directional GFRP reinforcement. Among all the GFRP wrapped beams, beam 3FWB with three layers of GFRP reinforcement sustained the highest maximum flexural load of 142.77kN and the corresponding enhancement of 51% over the control beam. However, beams 2FWB and 1FWB had attained a maximum failure load of 124.89kN and 116.69kN and the corresponding enhancement of 32% and 24% higher than control beam 0UB, respectively. From Table. 4.2., it is evident that wrapping beam specimens with up to three layers of GFRP composites led to a significant improvement in their ductility. This could be attributed to the good elongation characteristic of GFRP fibres at rupture. Consequently, this result contradicts the generally accepted idea that RC beams strengthened with FRP composites are affected by a decrease in ductility, which could lead to a brittle and sudden collapse.

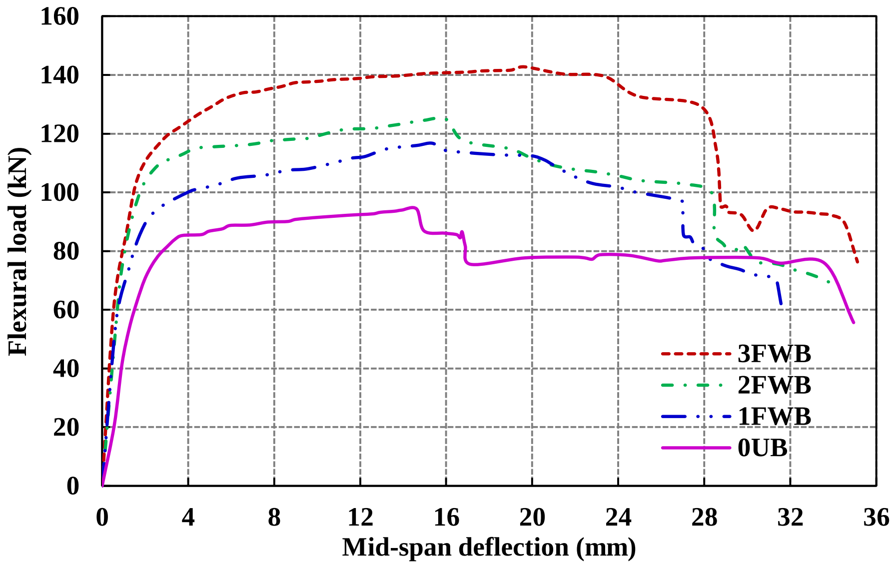

Figure 4.13 Flexural load versus mid-span deflection responses of specimens subjected to flexural loading

Table 4.2 Experimental results of flexural testing of rectangular RC specimens

Test Specimen	**Yield flexural load P_y (kN)**	**Mid-Span deflection at P_y (mm)**	**Ultimate flexural load P_{ult} (kN)**	**Mid-Span deflection at P_{ult} (mm)**	**Mid-span displacement at $0.8P_{ult}$ (mm)**	**Increase in P_{ult} relative to control specimen (%)**	**Ductility index λ**	
							First method	**Second method**
0UB	75.31	2.32	94.39	14.62	17.14	-	7.39	15.63
1FWB	94.80	2.67	116.69	15.35	27.01	24	10.12	16.75
2FWB	110.43	2.77	124.89	16.00	28.35	32	10.23	17.79
3FWB	117.63	2.79	142.77	19.63	28.57	51	10.24	18.99

4.6 Axial Load-Bending Moment Interaction Diagrams of the Columns

Figure 4.14 presents experimental axial load versus bending moment interaction diagrams (P-M) of rectangular RC specimens tested in this study. The P-M interaction diagrams are plotted as a chain of straight lines linking four characteristic points (Rocca et al., 2009; Wight and MacGregor, 2011). The first point is the pure axial compression case for axially loaded specimens. The second and third points are the axial load and bending moment of specimens with 25mm and 50mm eccentric loadings. The fourth point represents the pure bending case for specimens subjected to a flexural load. Equations 4.3 and 4.4 below were used to evaluate the bending moments M_u for columns under eccentric loading and M_{uf} for specimens under flexural loading, respectively.

$$M_u = P_{ult}(e + \delta) \tag{4.3}$$

$$M_{uf} = \frac{1}{2} P_{ult} L \tag{4.4}$$

where M_u = ultimate bending moment of columns under eccentric load and M_{uf} = ultimate bending moment of beams under flexural load, P_{ult} = ultimate load, e

= eccentricity of axial loading, δ = lateral mid-span displacement at ultimate load, L = Length of span between support and loading point (shear span length), which was taken as 230mm in the present study.

The ultimate experimental load and the calculated bending moments of specimens tested in this study are portrayed in Table 4.3. It is clear that the ultimate axial load and ultimate bending moment of GFRP wrapped specimens significantly increases with increased in number of layers of GFRP reinforcement. The bending moment of columns 3FWC-25e, 2FWC-25e, and 1FWC-25e were 79%, 41% and 13% higher than the bending moment of control column 0UC-25e, respectively. Similarly, the column 3FWC-50e with 50mm eccentricity achieved an ultimate bending moment enhancement of 58% over the control column 0UC-50e. The enhancement of ultimate bending moment of 23% and 14% were achieved by columns 2FWC-50e and 1FWC-50e compared to the control column 0UC-50e. The superior performance in ultimate load and bending moment capacity of GFRP confined columns was mainly due to the increase in ultimate axial load and lateral displacement at peak load. The significant increase in ultimate axial load and lateral displacement at peak load of GFRP wrapped RC columns was as a result of the lateral confining pressure generated by the GFRP wraps, which resisted the lateral dilation of concrete. For GFRP wrapped specimens subjected to pure flexural loading, the bending moment increases with increased in number of GFRP layers. The beam 3FWB with three layers of GFRP reinforcement achieved the highest ultimate bending moment enhancement of 51%, followed by beams 2FWB (2 layers of GFRP) and 1FWB (1 layer of GFRP) with an ultimate bending moment enhancement of 32% and 24%, over the control beam. The significant gain in ultimate bending moment of the GFRP strengthened beams was as a result of the confinement action of bi-directional GFRP reinforcement. Because the confinement action generated by the longitudinal and the transverse fibres of bi-directional GFRP improved the flexural capacity and compressive capacity of the compression zone of the strengthened beams.

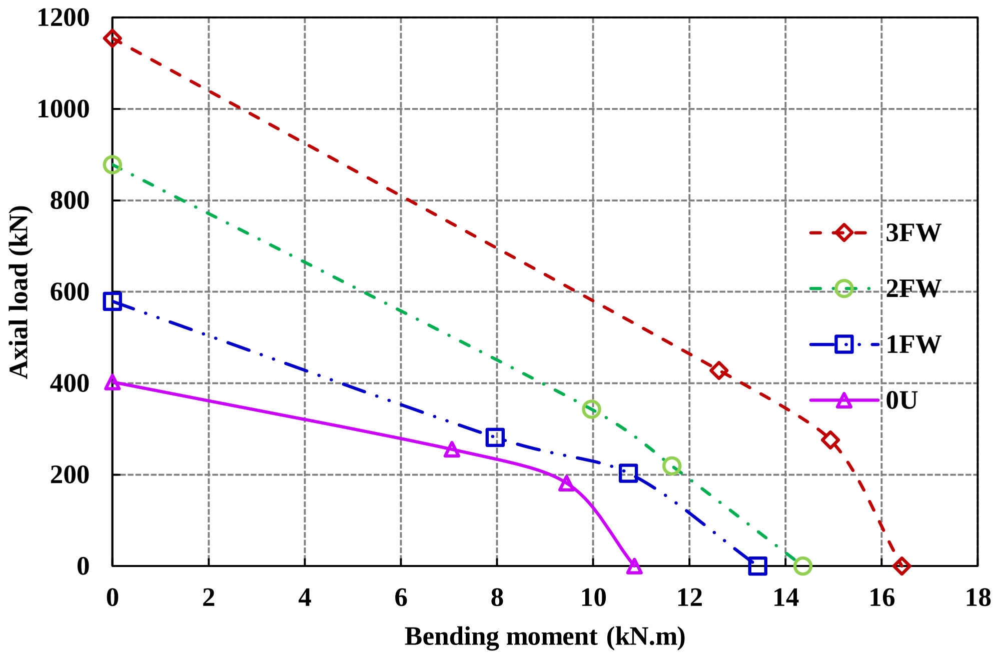

Figure 4.14 Axial load versus bending moment interaction diagrams

Table 4.3 Experimental ultimate load and the calculated bending moment of the tested specimens

Test specimen	**Eccentricity of loading '*e*' (mm)**	**Ultimate axial load P_{ult} (kN)**	**Lateral displacement at Ultimate load 'δ' (mm)**	**Ultimate bending moment 'M_u' (kN.m)**
0UC	-	403.07	-	-
0UC-25e	25	255.53	2.62	7.06
0UC-50e	50	181.69	1.98	9.44
0UB	-	94.39	-	10.85
1FWC	-	578.99	-	-
1FWC-25e	25	281.61	3.26	7.96
1FWC-50e	50	203.43	2.74	10.73
1FWB	-	116.69	-	13.42
2FWC	-	878.35	-	-
2FWC-25e	25	343.29	4.02	9.96
2FWC-50e	50	219.25	3.07	11.64
2FWB	-	124.89	-	14.36
3FWC	-	1155.00	-	-
3FWC-25e	25	428.34	4.45	12.61
3FWC-50e	50	276.19	4.07	14.93
3FWB	-	142.77		16.42

4.7 Summary

Experimental results of 16 rectangular reinforced concrete columns confined with bi-directional GFRP reinforcement under three loading conditions (concentric, eccentric and flexural loadings) were discussed in this chapter. The influence of test variables considered in this study on the behaviour and performance of rectangular RC specimens was discussed. The results of specimens tested as beams under flexural loadings was also discussed. In addition, the axial load versus bending moment interaction behaviour of the rectangular RC columns tested in this study was also discussed. The axial load versus bending moment interaction diagrams revealed significant improvement in the overall performance of specimens with GFRP wrapping.

The next chapter presents the detailed formulation of finite element analysis (FEA) of GFRP wrapped rectangular RC columns under concentric and eccentric loadings.

CHAPTER 5: FINITE ELEMENT ANALYSIS OF GFRP WRAPPED RECTANGULAR RC BEAMS AND COLUMNS UNDER COMBINED AXIAL AND BENDING LOADINGS

5.1 Introduction

This study develops a nonlinear finite element model for FRP confined rectangular RC columns under concentric, eccentric and flexural loading conditions. A series of 100 × 150 × 800mm rectangular RC beams and columns were confined with one, two and three layers of GFRP sheets. The control and GFRP confined RC specimens have a uniform concrete compressive strength of f'_{co}= 42MPa. The details of the beams and columns are described in chapter 3. All the control and GFRP confined rectangular RC specimens were simulated in ANSYS workbench (Products 18.1) at the University of Nottingham Malaysia. ANSYS is a very famous FE program in engineering simulation that could execute simple static analysis and sophisticated non-linear dynamic analysis. However, like all other finite element packages, ANSYS program also has its own nomenclature and analysis procedures that need to be included before executing any analysis.

The nonlinear finite element analysis performed in this study was aimed at contributing to the understanding of the behaviour of rectangular RC beams and columns wrapped with FRP under three loading conditions (i.e. concentric, eccentric, and bending loadings). The primary effort focused on the influence of number of GFRP layers and load eccentricity on the load carrying capacity and ductility of rectangular RC specimens wrapped with GFRP reinforcement. The detailed formulation of the finite element analysis is described below.

5.2 Element Types

ANSYS program has a large library of element types for use in performing finite element analysis (FEA). Each element type is recognized by its names (maximum of eight characters), for instance, SHELL181, which consist of a group label SHELL, and a particular identification number 181. The description of each element in the element library is organized in order of this identification number. The element is carefully chosen from the library for use in the FEA by inputting its name in the element command box. The following sub-sections highlight the detailed element types employed in developing the finite element model.

5.2.1 Reinforced Concrete

A reinforced concrete solid element SOLID65 was used to model concrete. This element is capable of cracking in tension, crushing in compression and can resist plastic deformations. SOLID65 element is outlined by 8-nodes with three degrees of freedom at each node: translations within the nodal x, y, and z directions. This element is used in the modelling of 3-Dimensional solids with or without internal steel reinforcement. The geometry, node positions and the coordinate systems for a SOLID65 element are depicted in Figure 5.1.

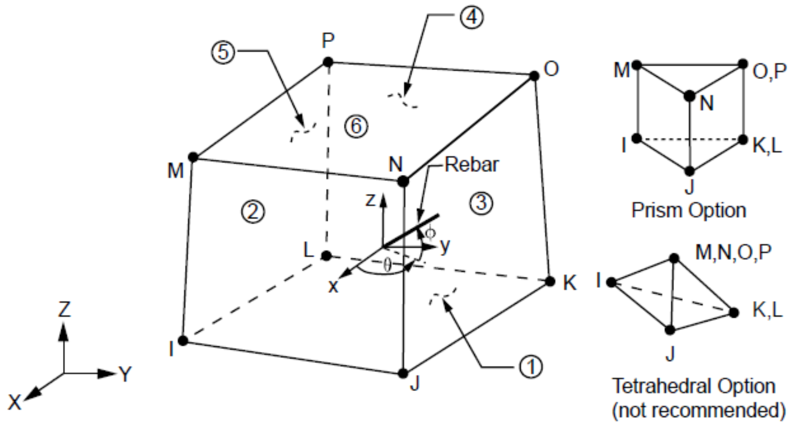

Figure 5.1 SOLID65 element geometry and coordinate system (ANSYS Release 18.1, 2017a)

5.2.2 Steel Reinforcement

Steel reinforcement was modelled with a 3-Dimensional spar LINK180 element, which is a uniaxial tension-compression element with three translational degrees of freedom at each node: translations within the nodal x, y, and z directions. LINK180 is used in the modelling of trusses, sagging cables, links, springs e.t.c. The geometry, node positions and coordinate systems for LINK180 element are illustrated in Figure 5.2.

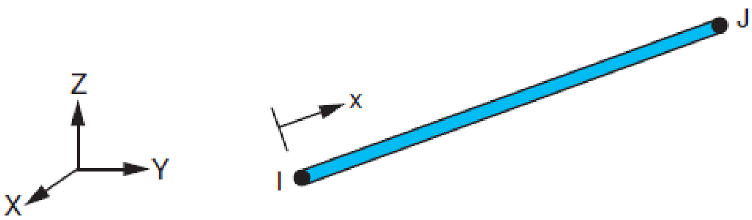

Figure 5.2 LINK180 geometry and coordinate system (ANSYS Release 18.1, 2017a)

5.2.3 Fibre Reinforced Polymer Composites

A four-node structural shell element SHELL181 was used to model GFRP composites. Each node is characterised by six degrees of freedom: translations within the nodal x, y, and z directions, and rotations about the x, y, and z-axes. This element is suitable for linear, large rotation, as well as large strain non-linear analysis. Figure 5.3 depicts the geometry, node locations and the element coordinate systems for SHELL181 element.

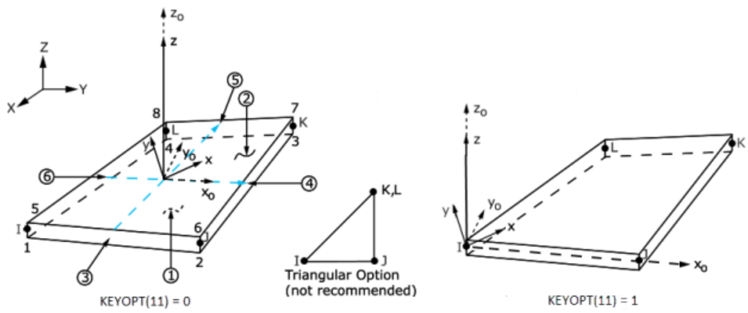

Figure 5.3 Geometry, node locations and element coordinate systems for SHELL181 element (ANSYS Release 18.1, 2017a)

5.3 Material Properties

The material properties of concrete, steel reinforcement and GFRP composites are required in ANSYS to define each of the selected element types. The following sub-sections highlight the detailed descriptions of the material properties of concrete, steel reinforcement and GFRP composites.

5.3.1 Concrete

The concrete, in modern fracture mechanics, is considered as a quasi-brittle material and its behaviour under loading is entirely different in compression and tension (Anderson, 2005). Illustrated in Figure 5.4 is the uniaxial stress-strain response of concrete. The stress-strain response of concrete in compression is linearly elastic up to about 30% of the maximum compressive strength. Beyond this point, the stress steadily increases up to the maximum compressive strength f_{co}. After achieving the maximum compressive strength, any further application of load result to an increase in strain at constant stress and finally concrete crushing failure occurs at an ultimate strain ε_{cu}. Moreover, the stress-strain response of concrete in tension is approximately linearly elastic up to the maximum tensile strength. Once the maximum tensile strength is reached, subsequent damage is concentrated in a local fracture zone (Anderson, 2005).

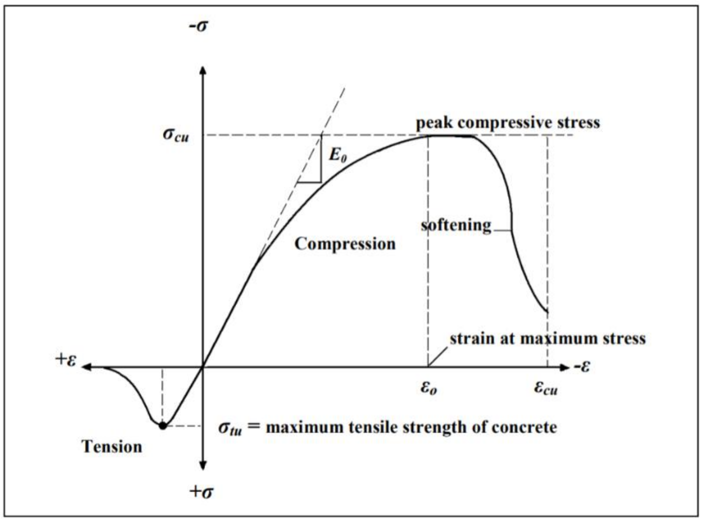

Figure 5.4 Uniaxial stress-strain response of concrete (Kachlakev et al., 2001)

The material properties required for a SOLID65 element in ANSYS include elastic modulus (E_{co}), ultimate uniaxial compressive strength (f_{co}), ultimate uniaxial tensile strength (modulus of rupture f_t), Poisson's ratio (v), shear transfer coefficient (β_t) and the uniaxial stress-strain relationship for concrete in compression. The elastic modulus and tensile strength (modulus of rupture) of concrete are calculated using the equations below (McCormac and Brown, 2013).

$$E_{co} = 4700\sqrt{f_c'} \tag{5.1}$$

$$f_t = 0.7\sqrt{f_c'} \tag{5.2}$$

The concrete material model in ANSYS is based on William-Warnke's five parameter constitutive model for triaxial behaviour of concrete. In the present study, the failure behaviour of concrete was simulated using this criteria (ANSYS Release 18.1, 2017b). The shear transfer coefficient is 0.5 for a smooth crack (complete loss of shear transfer) and 0.9 for a rough crack (no loss of shear transfer). The Poisson's ratio of concrete was assumed to be 0.2 for all the GFRP confined specimens.

To accurately predict the structural behaviour of unconfined concrete in compression, ANSYS requires the complete uniaxial stress-strain relationship of concrete. For unconfined concrete in compression, the stress-strain curve is divided into ascending and descending branches. Several numerical equations have been developed for the complete stress-strain curve (Hognestad et al., 1955; Desayi and Krishnan, 1964; Popovics, 1973; Wang et al., 1978). In the present study, the multilinear isotropic stress-strain curve for concrete was constructed using the following numerical expressions proposed by Popovics (1973) due to its ability in simulating strain softening behaviour:

$$f_c = \frac{f_c' \cdot x \cdot p}{p-1+x^p} \tag{5.3}$$

$$x = \frac{\varepsilon_c}{\varepsilon_c'} \tag{5.4}$$

$$p = \frac{E_{co}}{E_{co}-E_{sec}} \tag{5.5}$$

$$E_{sec} = \frac{f_c'}{\varepsilon_c'} \tag{5.6}$$

Being f_c the stress at a given axial strain ε_c, f_c' the unconfined concrete strength corresponding to the strain ε_c', E_{co} and E_{sec} the tangent and secant modulus of concrete. E_{co} was calculated using equation 5.1. The constructed uniaxial stress-strain curve for concrete in compression is shown in Figure 5.5.

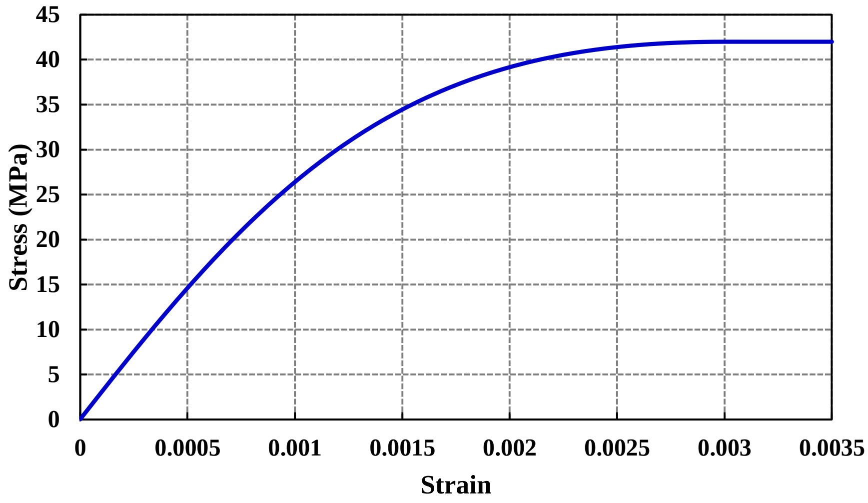

Figure 5.5 Stress-Strain curve of concrete 42MPa

5.3.2 Steel Reinforcement

In finite element modelling, the steel reinforcement is assumed to be elastic-perfectly plastic material and exhibits a similar stress-strain behaviour in compression and tension as shown in Figure 5.6 (Kwak and Filippou 1990; Chansawat et al. 2009). The steel reinforcement in RC columns used in this study consists of 12mm diameter bar as longitudinal reinforcement and 6mm diameter bar as transverse reinforcement with nominal properties $E_{se} = 2 \times 10^5$MPa, E_{sp} = 0.01 E_{se}, f_y = 550MPa, $f_y' = 290$MPa and v=0.3. Being E_{se} and E_{sp} the elastic and plastic modulus, f_y the yield strength of longitudinal steel, f_y' the yield strength of transverse steel (assumed) and v the Poison's ratio.

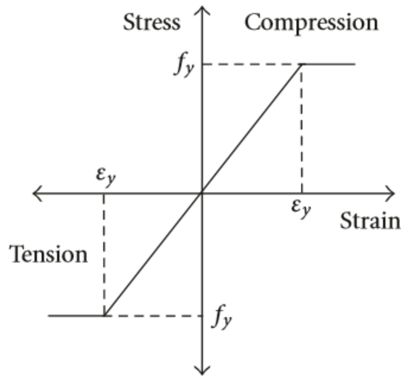

Figure 5.6 Uniaxial Stress-strain response for steel reinforcement (Chansawat et al., 2009)

5.3.3 FRP Composites

The FRP composites were simulated as orthotropic and transversely isotropic material. In other words, the mechanical properties are similar in any direction perpendicular to the direction of fibres. GFRP composites used in this study has a nominal thickness of 0.76mm/ply. The essential input data to describe the material model for FRP composites include: thickness of FRP layers, the orientation of fibre for each layer, elastic modulus of FRP in three directions (E_x, E_y and E_z), shear modulus of FRP for three planes (G_{xy}, G_{yz} and G_{xz}) and major Poisson's ratio for the three planes (v_{xy}, v_{yz} and v_{xz}). The orthotropic material properties of FRP composites used in the present study are portrayed in Table 5.1 below.

Table 5.1 Orthotropic material properties of the GFRP composites (Feng et al., 2002)

Elastic Modulus (MPa)	Poisson's Ratio	Ultimate Strength (MPa)	Shear Modulus (MPa)
$E_x = 65000$	$v_{xy} = 0.31$		$G_{xy} = 1761$
$E_y = 4000$	$v_{yz} = 0.39$	900	$G_{yz} = 1660$
$E_z = 4000$	$v_{xz} = 0.02$		$G_{xz} = 1761$

5.3.4 End Corbels

The corbels were provided at the ends of column to apply the eccentric loading conditions. The primary function of the end corbel is to transfer load to the column in the test region. In this study, the end corbel was modelled as a single mass element: MASS21. However, the stiffness behaviour of the end corbels was characterised as rigid to prevent deformation and damage in the corbels during the solution process. In this model, a modulus of 200,000MPa was used for the end corbels.

5.4 Modelling and Meshing of Rectangular RC columns

The geometry was modelled using ANSYS workbench design modeller. Due to the longitudinal symmetry, only one-half of the full-size rectangular column was modelled in this study. On the other hand, only half of the beam specimen was modelled considering the symmetric dimension and loading pattern of the beam. A rectangular solid with end corbels was first modelled with specified dimensions and corner radii. A hollow rectangular surface body with a specified thickness and corner radius was also modelled. A corner radius of 20mm was maintained for all the specimens. The internal steel reinforcement was also modelled as line bodies within the rectangular solid. In this model, the rectangular solid represents the concrete and the hollow rectangular surface body acts as the bonded FRP composites. Mapped meshing was used to mesh the generated model because it helps in controlling the number of elements/nodes. An element size of 20mm is used to mesh the model. The adjacent mesh nodes of concrete and end corbels were connected using the node merge tool. The perfect bond between the interfaces of concrete and steel reinforcement was achieved using CEINTF command. This command is used to tie together two regions with different mesh patterns by creating constraint equations that bond the designated nodes of one region to the designated elements of the other region. In the present FE analysis, the boundary between concrete and FRP composites was simulated as a perfect bond because perfect bond could make the stiffness of FRP confined concrete columns stronger (Hu et al., 2011). The bonded command was used to tie the boundaries between concrete and FRP. Figure 5.7 shows the finite element model of GFRP wrapped rectangular RC beam and column.

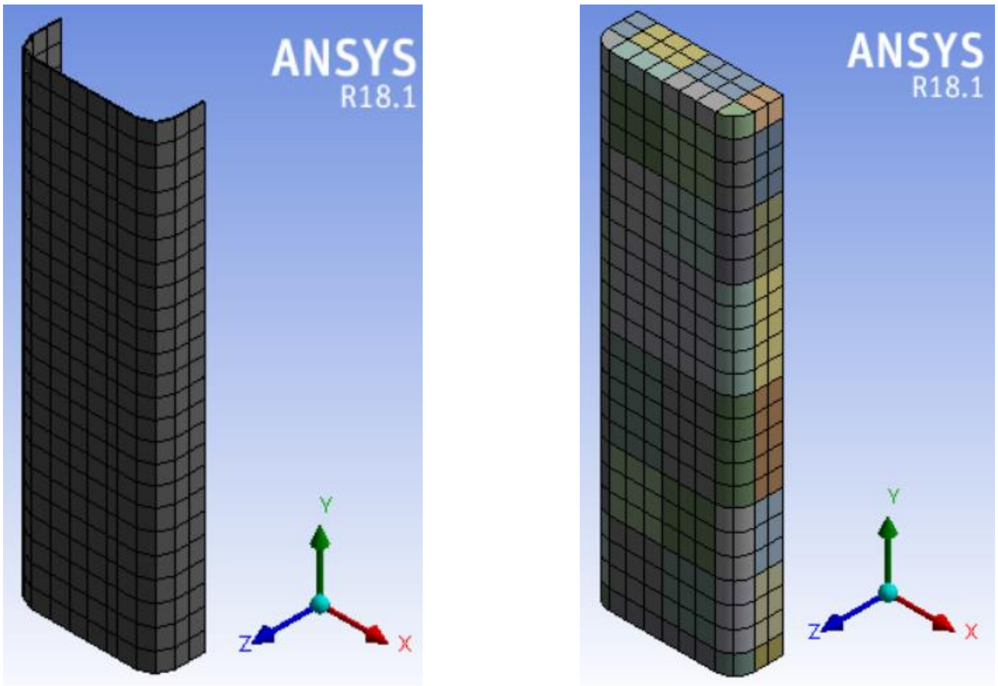

(a) GFRP **(b)** Reinforced concrete

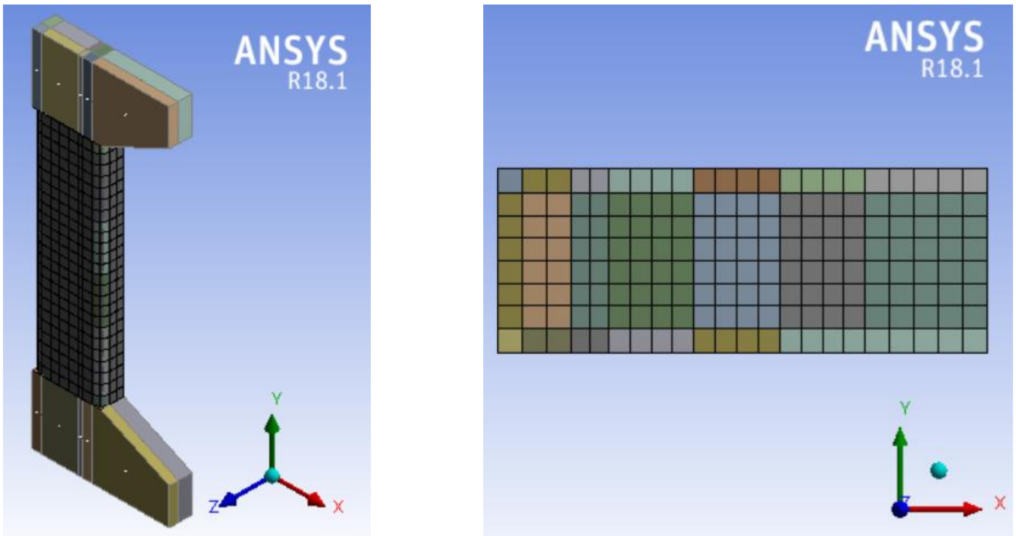

(c) Geometry of column **(d)** Geometry of beam

Figure 5.7 Finite element model of GFRP wrapped rectangular RC beam and column

5.5 Boundary Conditions and Load Application

In this model, the y-axis (Figure 5.7) of the coordinate system corresponds to the axis of the rectangular RC column, whereas the x-axis of the coordinate system corresponds to the axis of the beams. The following boundary conditions were applied:

- The bottom surface of the column was sliced according to the location of the fixed support. All the coupled nodes on the bottom sliced line are restrained from all degrees of freedom in three directions.
- The top of the column was sliced according to the location of the applied load. The load was applied normal to the axis of the column.
- The finite element beams were loaded and supported at the same locations as the experimental beams.

5.6 Simulation

The ANSYS program employs the Newton-Raphson method to solve problems that involve non-linear structural behaviour. In this approach, the load is segmented into a series of load increments. The load increments can be applied over several load steps. The analysis follows an iterative procedure until the problem converges. In the present non-linear FE analysis, the automatic load stepping feature was activated, as it enabled the solver to predict and control the number of load steps. However, the automatic time stepping was defined in terms of sub-steps to enable loads to be applied gradually. The number of sub-steps used varied from 20 to 100 with the minimum sub-step set to 1/100th of the applied load. The large deflection feature in the solver control was also activated.

5.7 Summary

The detailed formulation of the finite element analysis implemented in this study was discussed in this chapter. The finite element analysis was carried out using ANSYS finite element software. The element types assigned to describe the behaviour of concrete, steel reinforcement and FRP composites were introduced first. Then the essential input data to define the material model for concrete, steel reinforcement and FRP composites were described. Moreover, the mapped meshing was considered the suitable mesh for the FE analysis.

The results of FE analysis of GFRP-wrapped rectangular RC specimens under concentric, eccentric and flexural loadings are discussed in the next chapter. However, comparison of FE analysis results with experimental results was also discussed.

CHAPTER 6: DISCUSSION OF FEA RESULTS

6.1 Introduction

As described in chapter 5, a series of sixteen rectangular reinforced concrete specimens wrapped with GFRP under concentric, eccentric and flexural loads were analysed in ANSYS 18.1 (ANSYS Release 18.1, 2017c). The variables considered in the finite element (FE) model include the number of GFRP layers and load eccentricity. The results obtained from the finite element modelling of rectangular RC specimens confined with GFRP under the three loading conditions are presented and discussed in this chapter. A comparison of experimental and finite element analysis (FEA) results is also discussed.

6.2 Behaviour of GFRP Confined Columns

The contours of axial deformation of the simulated GFRP confined columns with three layers of GFRP are portrayed in Figure 6.1. It is clear that the deformation contours for columns subjected to axial loading are maximum at the upper part of the column. The negative values in the legend box (Figure 6.1 (b) and (c)) are the axial deformations of eccentrically loaded columns. It is clear that the columns with 25mm and 50mm eccentricities exhibited maximum deformation contours in the compression zones. Summarized in Table 6.1 are the results of FEA of rectangular RC columns with GFRP wrapping under axial and eccentric loadings.

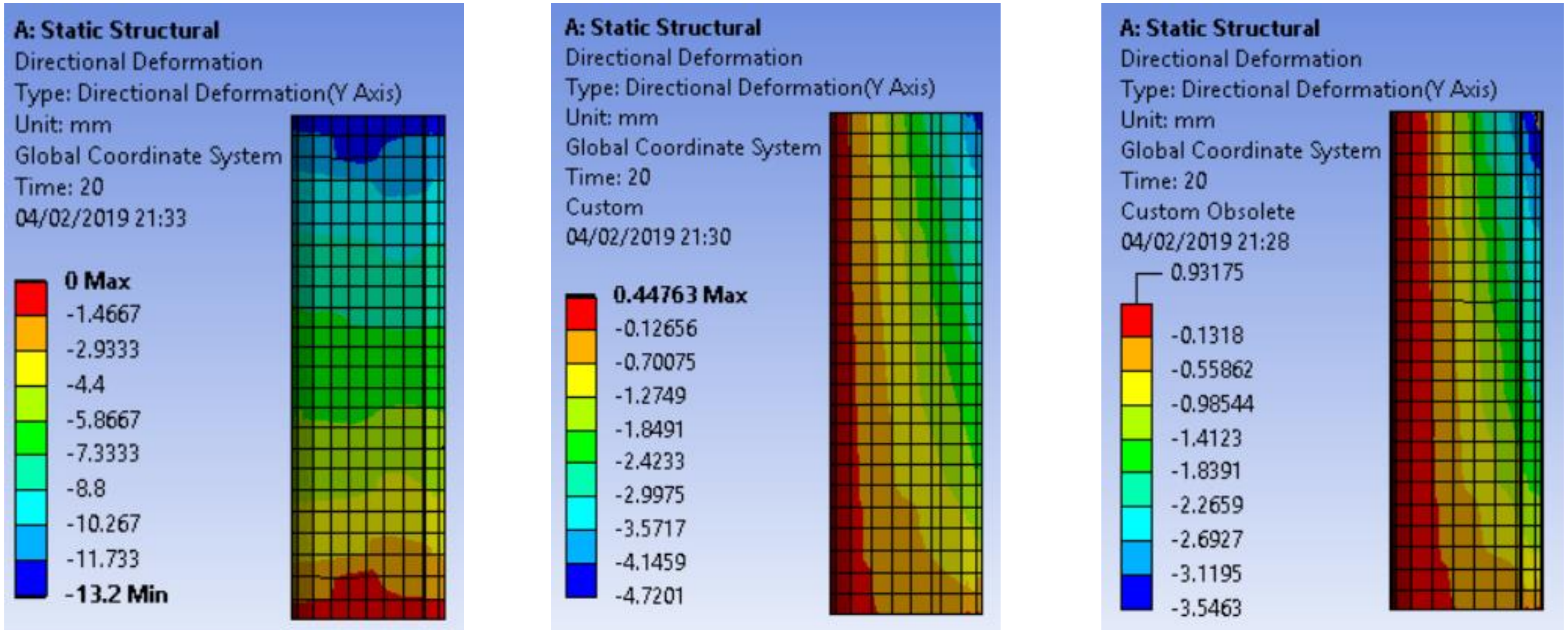

(a) **(b)** **(c)**

Figure 6.1 Axial deformation contour for (a) Concentrically loaded column, (b) Column with 25mm eccentricity, (c) Column with 50mm eccentricity

Table 6.1 Summary of FE analysis results

Specimen	Yield axial load (kN)	Axial displacement at yield load (mm)	Ultimate axial load (kN)	Axial displacement at ultimate load (mm)	Increase in ultimate load relative to control specimen (%)	Lateral displacement at ultimate load (mm)
0UC	357.16	1.20	381.89	7.23	-	-
1FWC	367.51	1.20	564.16	12.72	48	-
2FWC	391.23	1.24	881.65	12.81	131	-
3FWC	428.23	1.32	1363.80	13.20	257	-
0UC-25e	180.20	1.19	245.48	3.69	-	7.56
1FWC-25e	209.97	1.51	280.78	5.54	14	11.05
2FWC-25e	225.52	1.54	346.62	6.38	41	12.01
3FWC-25e	253.11	1.66	444.89	6.70	81	12.21
0UC-50e	113.60	1.13	175.52	3.21	-	6.75
1FWC-50e	125.62	1.26	193.74	4.56	10	9.74
2FWC-50e	139.38	1.37	222.42	4.91	27	10.06
3FWC-50e	162.75	1.59	274.99	6.00	57	11.99

6.2.1 Axial Load-Displacement Behaviour

Figure 6.2 illustrates the axial load versus axial displacement responses of axially loaded columns. It is obvious that the axial load-displacement curves of columns indicated a bi-linear response. The first part of the linear ascending portion of the load-displacement response of all the control and GFRP confined columns in this group proceeds in a similar trend up to yielding of longitudinal steel reinforcement. After yielding of steel reinforcement, a ductile behaviour of load-displacement response of control column OUC was obvious up to the maximum ultimate axial load of 381.89kN with a corresponding axial displacement of 7.23mm. Beyond the ultimate load, the axial load-displacement response of the control column indicated a slight decrease in axial load with an increase in axial displacement. However, the axial load-displacement response of all the GFRP confined columns demonstrated a post-peak ascending response, with a significant increase in axial load until the maximum peak load is achieved. It is evident from the figure that GFRP confinement leads to a significant enhancement in ultimate axial load and performance of rectangular RC columns. The highest enhancement in the ultimate axial load was achieved by column 3FWC with 257% increase in ultimate load relative to the control column 0UC. Columns 2FWC and 1FWC achieved an ultimate load enhancement of 131% and 48% higher than the control column 0UC, respectively.

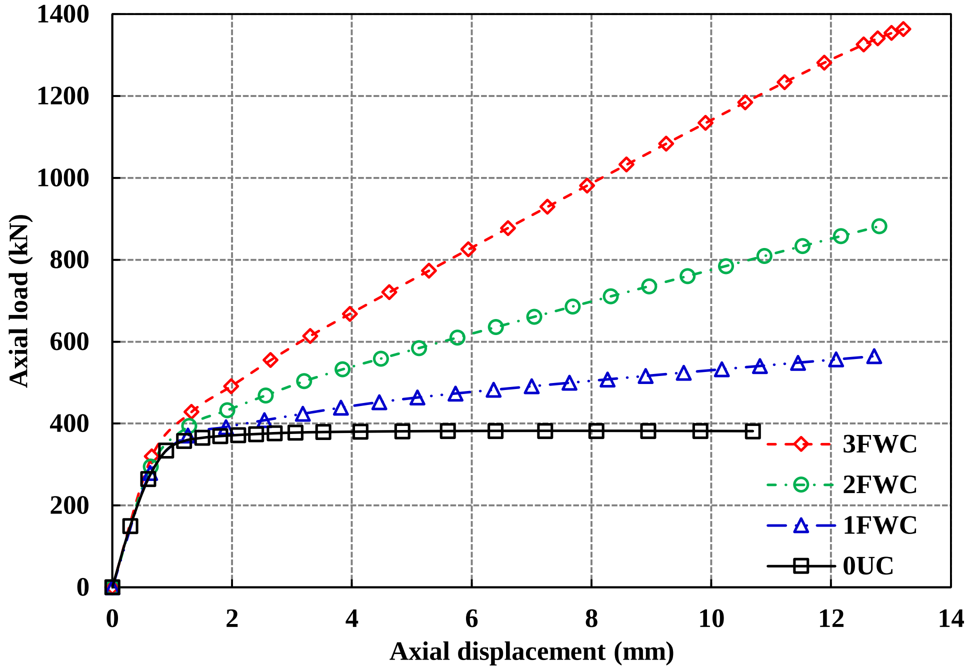

Figure 6.2 Axial load versus axial displacement responses of concentrically loaded columns

The axial load versus axial and lateral displacement curves of columns under 25mm eccentricity are portrayed in Figure 6.3. Similar to the axially loaded columns, the load-displacement responses of columns in this group indicated a bi-linear trend. Column 3FWC-25e with three layers of GFRP achieved the highest ultimate load enhancement of 81% over the control column 0UC-25e. The columns 2FWC-25e (2 layers of GFRP) and 1FWC-25e (1 layer of GFRP) achieved a 41% and 14% gains in ultimate load over the control column 0UC-25e.

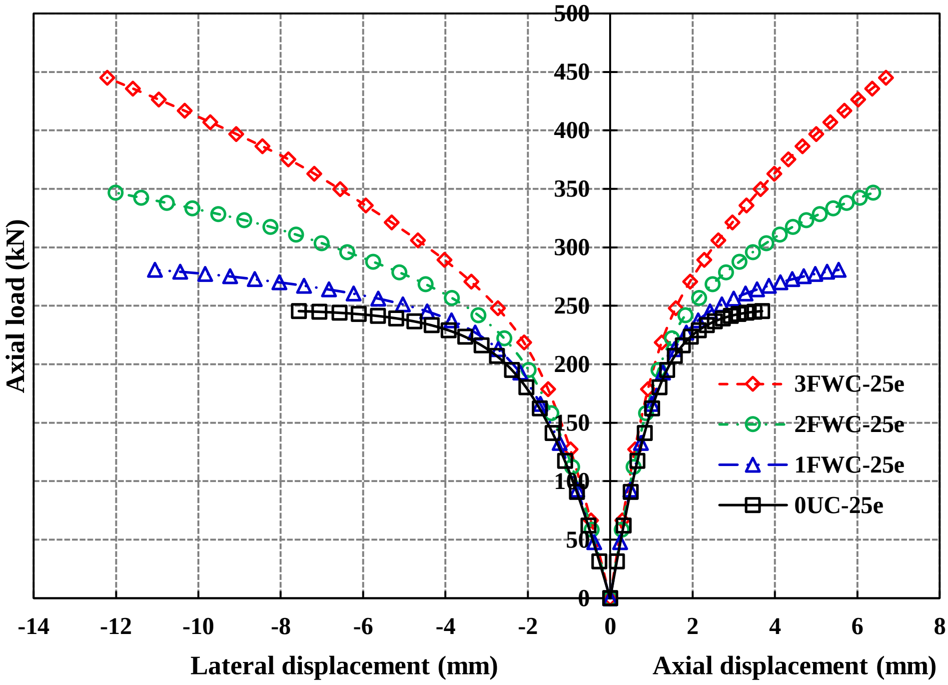

Figure 6.3 Axial load versus axial and lateral displacement curves of columns under 25mm load eccentricity

Figure 6.4 portrays the axial load versus axial and lateral displacement responses of columns simulated under 50mm eccentricity. It is evident that the load-displacement response demonstrated a significant gain in performance and ultimate load carrying capacity of the rectangular RC columns with GFRP confinement. A maximum load capacity gain of 57%, 27% and 10% were attained by columns confined with three, two and one layers of GFRP over the control column.

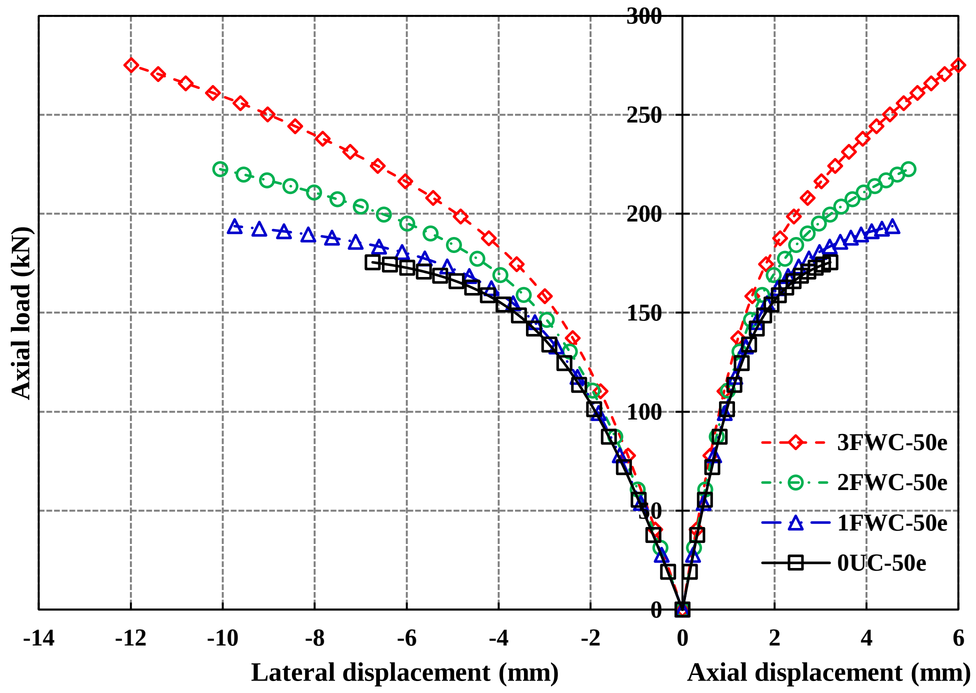

Figure 6.4 Axial load versus axial and lateral displacement responses of specimens under 50mm eccentric load

6.3 Influence of Eccentricity

Figure 6.5 depicts the axial load versus axial displacement responses for columns simulated under different loading conditions. It is clear that the GFRP confined rectangular RC columns demonstrated a decrease in ultimate load capacity and performance by increasing the eccentricity.

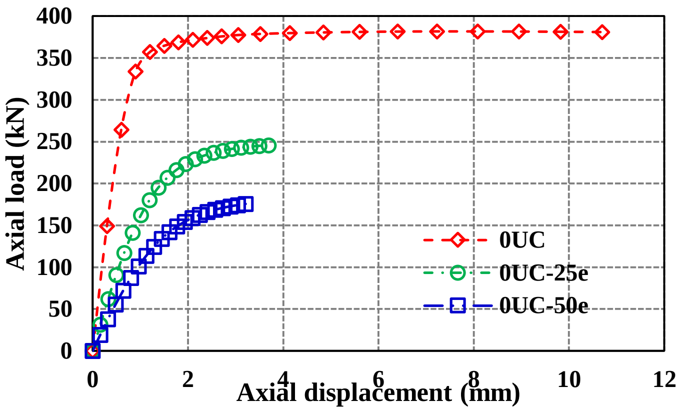

(a) Unwrapped

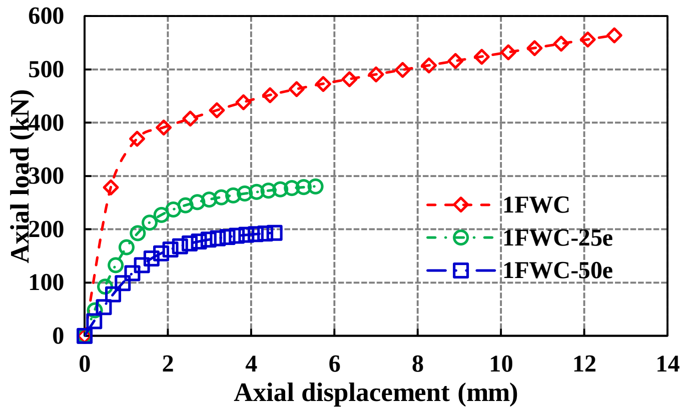

(b) Wrapped with one layer

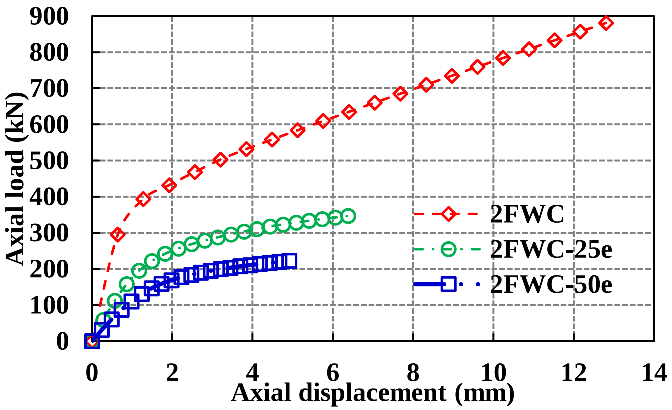

(c) Wrapped with two layers

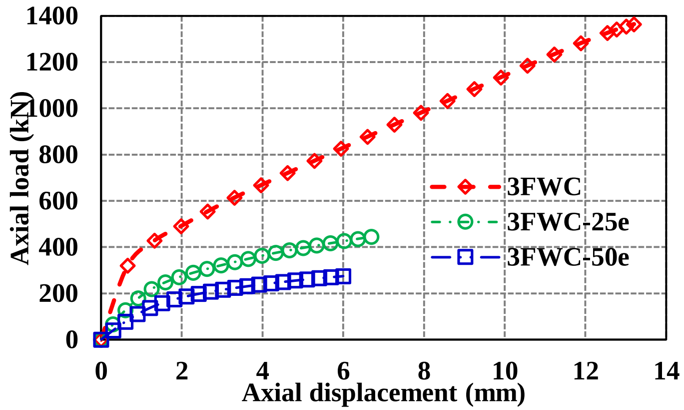

(d) Wrapped with three layers

Figure 6.5 Axial load versus axial displacement responses for columns simulated under different loading conditions

6.4 Ductility

The ductility index was used in this FE analysis to evaluate the effect of the number of GFRP layers on the performance of rectangular RC columns confined with GFRP reinforcement. The ductility index 'λ' of the simulated columns was quantified using the first method described in chapter 4. The results of the ductility index of the simulated columns are presented in Table 6.2. It is apparent that the GFRP confined columns exhibited a significant gain in ductility index over the control columns. The gain in ductility of the concentrically loaded GFRP confined columns was more significant in columns confined with three layers of GFRP reinforcement. For columns governed by eccentric loading, the ductility significantly increases with increased in GFRP layers and remarkably decreases when the eccentricity is increased.

Table 6.2 Ductility index of the simulated columns

Specimen	**Axial displacement at yield load δ_y (mm)**	**Axial displacement at ultimate load δ_u (mm)**	**Ductility index λ**
0UC	1.20	7.23	6.03
1FWC	1.20	12.72	10.60
2FWC	1.24	12.81	10.33
3FWC	1.32	13.20	10.00
0UC-25e	1.19	3.69	3.10
1FWC-25e	1.51	5.54	3.67
2FWC-25e	1.54	6.38	4.14
3FWC-25e	1.66	6.70	4.04
0UC-50e	1.13	3.21	2.84
1FWC-50e	1.26	4.56	3.62
2FWC-50e	1.37	4.91	3.58
3FWC-50e	1.59	6.00	3.77

6.5 Variation of Axial Stress over the Rectangular Column Section

Figure 6.6 illustrates the variations of axial stress contours over the section for rectangular RC columns with FRP confinement under axial and eccentric loadings. The axial stresses in the concrete section are indicated as the negative values in the legend box. The variations of axial stress over the transverse section of rectangular columns are plotted at different points in the section (Figure 6.7). It is evident from Figure 6.7 (a) that the axial stress distribution for axially loaded columns varies significantly over the column section, with maximum values at the corners and minimum along the edges. This confirmed that the FRP confinement is effective at the corners and less effective at the edges. This stress variation aligns with the observations reported by other researchers (Mirmiran et al., 2000; Feng et al., 2002; Youssef et al., 2007; Hajsadeghi et al., 2011; Yu et al., 2010b). From Figure 6.7 (b) and (c), it is evident that the distribution of stress for eccentrically loaded columns varies significantly over the column’s section, with maximum values in the compression zone and minimum in the tension zone. For specimens under 25mm load eccentricity, the distribution of stress across the concrete section drops gradually from maximum around the corners of the compression side to minimum edges of the tension side of the columns. Moreover, the stress distribution across the concrete section of columns with 50mm eccentricity gradually drops from maximum value around the corners of the compression side to zero at corners and edges of the tension side. This further confirms that the presence of load eccentricity in FRP confined RC columns generally affect the strength and load carrying capacity of the columns due to the decreased in compression area of concrete confined by GFRP.

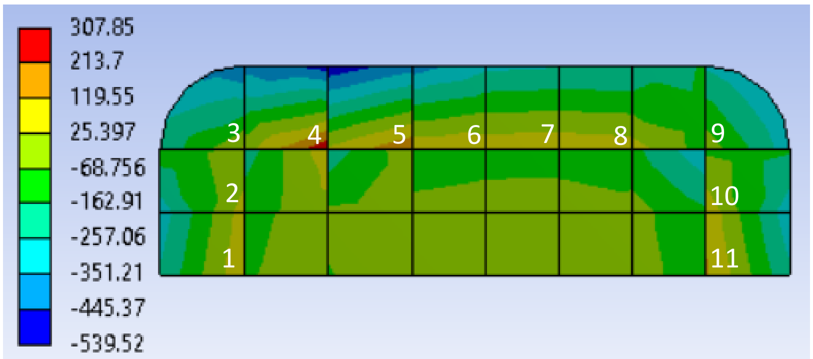

(a) Concentrically loaded column

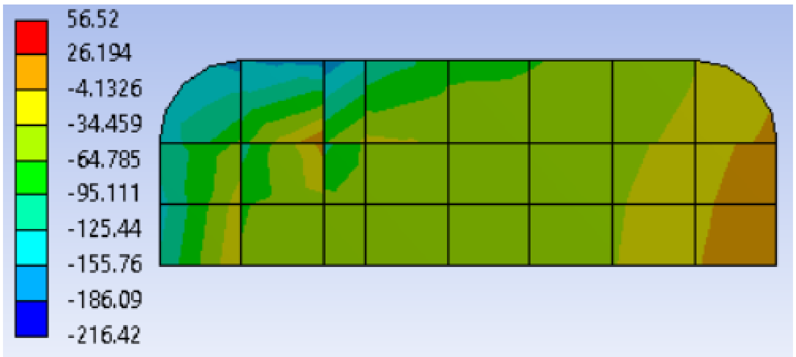

(b) Columns under 25mm eccentric load

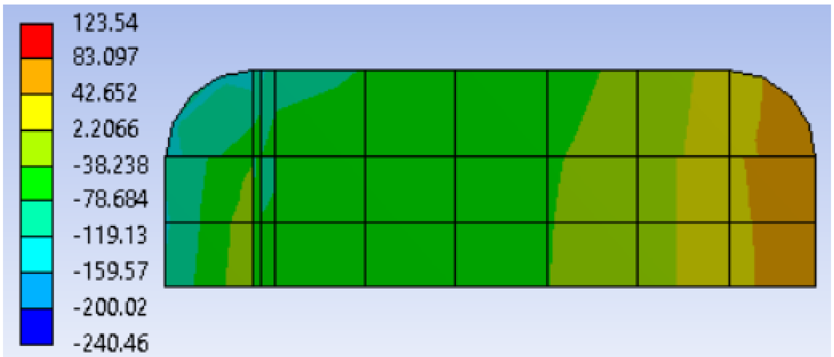

(c) Columns under 50mm eccentric load

Figure 6.6 Distribution of axial stress contours over the section

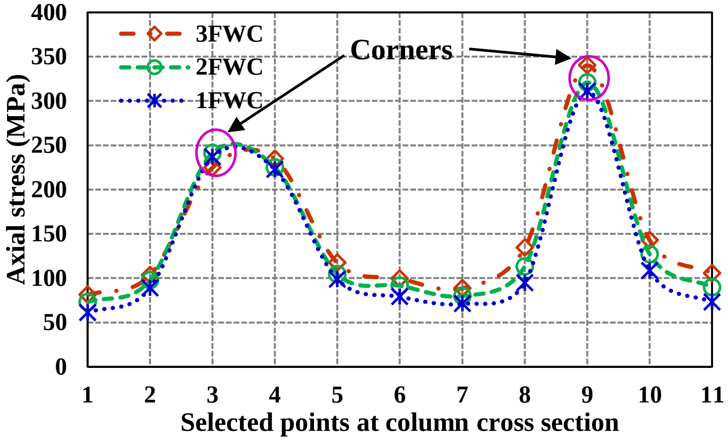

(a) Columns under concentric load

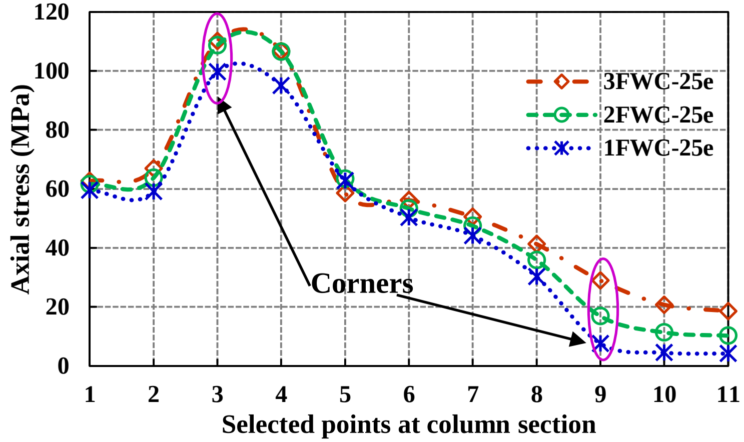

(b) Columns with 25mm eccentricity

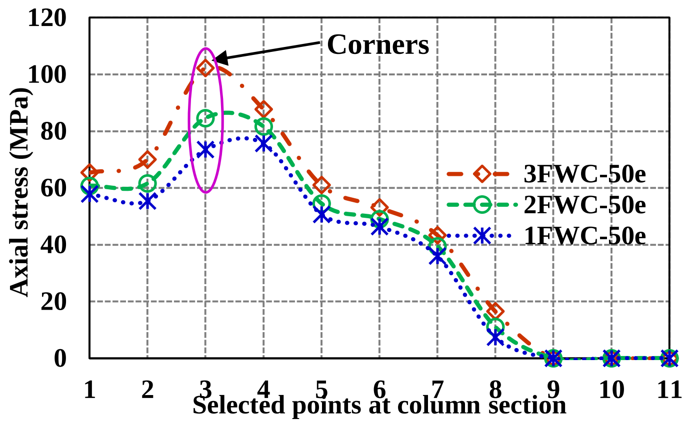

(c) Columns with 50mm eccentricity

Figure 6.7 Variations of axial stress over the rectangular column section

6.6 Behaviour of Simulated beams under Flexural Load

The results of the finite element analysis of rectangular RC beams with GFRP wrapping under bending load are summarised in Table 6.3 below. The ductility index of the simulated beams was calculated based on the first method described in section 4.3 chapter 4 using the flexural load versus mid-span deflection curves of the beams. Figure 6.8 portrays the flexural load versus mid-span plots of rectangular RC beams wrapped with GFRP under flexural loading. From the figure, it is clearly seen that the flexural load-deflection plot of the control beam 0UB exhibited a tri-linear behaviour, which is a typical load-deflection relationship of unwrapped RC beam. At the early stages of loading, the first part of the load-deflection plot indicates the beam behaviour prior to concrete cracking and this characterises the stiffer part of the curve. As the applied load increases, the load-deflection curve exhibited a post-cracking response with a loss in stiffness and slope. This part of the curve extends up to the yield load of 73.84kN with a corresponding mid-span deflection of 1.98mm. Beyond the yield load, the load-deflection curve forms a yielding plateau up to the ultimate applied flexural load of 101kN with a corresponding mid-span deflection of 17.17mm.

Table 6.3 Results of FE analysis of GFRP wrapped rectangular RC beams under flexural loadings

Specimen	Yield flexural load P_y (kN)	Mid-Span deflection at P_y (mm)	Ultimate flexural load P_{ult} (kN)	Mid-Span deflection at P_{ult} (mm)	Increase in P_{ult} relative to control specimen (%)	Ductility index λ
0UB	73.84	1.98	101	17.17	-	8.67
1FWB	97.48	1.71	189	19.42	87.13	11.36
2FWB	118.02	2.02	230	24.07	127.72	11.92
3FWB	141.78	2.42	278	30.42	175.25	12.57

It is also evident from Figure 6.8 that the load-deflection responses of all the GFRP wrapped beams demonstrated stiffer and more ductile behaviour relative to the control beam 0UB. This might be attributed to the confinement effect of GFRP reinforcement on concrete in compression after yielding of tensile longitudinal steel reinforcements. However, the confinement effect generated by the GFRP reinforcement increases with increased in the layers of GFRP wraps. Specimen 3FWB with three layers of GFRP sustained the highest ultimate flexural load of 278kN with 175.25% ultimate flexural load enhancement compared with the control beam 0UB. Specimen 2FWB achieved an ultimate flexural load of 230kN lower than beam 3FWB and 127.72% higher ultimate flexural load than the control beam 0UB. The ultimate flexural load of specimen 1FWB was 189kN, respectively lower than that of specimen 2FWB and 87.13% ultimate flexural load enhancement relative to the control beam 0UB.

In terms of ductility, the GFRP wrapping resulted in a significant enhancement in ductility of the rectangular RC beams, which increases with increased in number of GFRP layers. The ductility of specimen 1FWB and specimen 2FWB were almost similar but higher than the ductility of specimen 0UB by approximately 31.03% and 37.49%, respectively. The specimen 3FWB with three layers of GFRP reinforcement achieved the highest ductility of 12.57, which is higher than the ductility of beam 0UB by approximately 44.98%. However, this results further refutes the generally accepted idea that RC beams with FRP wrapping are affected by a drop in ductility, which could lead to a brittle and sudden failure.

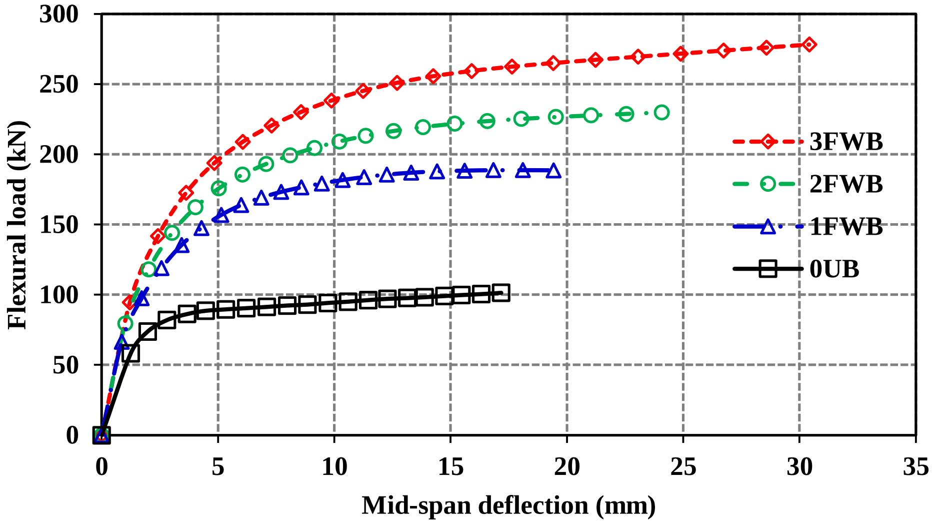

Figure 6.8 Flexural load versus mid-span deflection curves of simulated beams under flexural loadings

6.7 Validation of FEA Results

The comparison between the experimental and FEA ultimate axial loads of rectangular RC columns are presented in Table 6.4. It is evident that only one FEA ultimate axial load for GFRP confined column 3FWC is approximately 18.08% higher than the experimental value, but all other columns demonstrated less than 10% difference in the ultimate axial load between the experimental and FEA results. This might be attributed to the fact that the models of concrete, steel reinforcement and GFRP composites are too stiff compared to the experimental specimens. On the other hand, the difference may probably be due to the difference between the boundary conditions of the experimental columns and the finite element models.

Figure 6.9 portrays the comparison between FEA results and experimental results for control columns under axial and eccentric loadings, in terms of the axial load-axial displacement response. It is obvious that the experimental axial load-displacement curve for all the columns is divided into two branches: the linear ascending and post-peak descending parts. Conversely, the FEA axial load-displacement curves for all simulated control columns indicated linear ascending branch and post-peak ascending response except control columns 0UC which exhibited a slight decrease in axial load after reaching the peak axial load. From Figure 6.9, it is clear that the FE model provides a reasonably close prediction of ultimate axial load-displacement response for all the columns except control column 0UC, which indicated slight discrepancies in stiffness between experimental and FEA axial load-displacement curves. However, these discrepancies may be related to the inaccurate alignment of the test specimen during loading, possible spalling of concrete cover and loss of composite action between concrete and steel reinforcement due to bond slippage (Jiang and Teng, 2012).

The comparisons between FEA and experimental axial load-displacement responses for columns with one layer of GFRP confinement under axial and eccentric loadings are depicted in Figure 6.10. It is evident that the numerical FE model provides reasonably close predictions of axial load-displacement response for all the GFRP confined columns except column 1FWC with one layer of GFRP reinforcement. Considerable discrepancies in stiffness exist between experimental and FEA axial load-displacement curves for column 1FWC. This might be attributed to the geometric and material imperfections as well as inaccurate alignment of the column specimens during testing. The geometric imperfection may probably be due to the variation in the dimensions of the columns, or lack of straightness or verticality of the column specimens. However, the material imperfection always arises from the deviation in the assumed material properties of concrete and steel reinforcements.

Table 6.4 Comparison between the experimental and FEA ultimate axial loads of rectangular RC columns

Specimen	**Ultimate axial load (kN)**		**Axial displacement at ultimate load (mm)**		**Difference in ultimate load (%)**	**Difference in axial displacement at ultimate load (%)**
	Experimental	**FEM**	**Experimental**	**FEM**		
0UC	403.07	381.89	8.10	7.23	-5.25	10.74
1FWC	578.99	564.16	10.31	12.72	-2.56	23.38
2FWC	878.35	881.65	11.95	12.81	0.38	7.20
3FWC	1155.00	1363.80	13.44	13.20	18.08	-1.79
0UC-25e	255.53	245.48	6.14	3.69	-3.93	-39.90
1FWC-25e	281.61	280.78	7.00	5.54	-0.29	-20.86
2FWC-25e	343.29	346.62	7.30	6.38	0.97	-12.60
3FWC-25e	428.34	444.89	8.01	6.70	3.86	-16.35
0UC-50e	181.69	175.52	2.78	3.21	-3.40	15.47
1FWC-50e	203.43	193.74	4.00	4.56	-4.76	14.00
2FWC-50e	219.25	222.42	5.31	4.91	1.45	-7.53
3FWC-50e	276.19	274.99	10.35	6.00	-0.43	-42.03

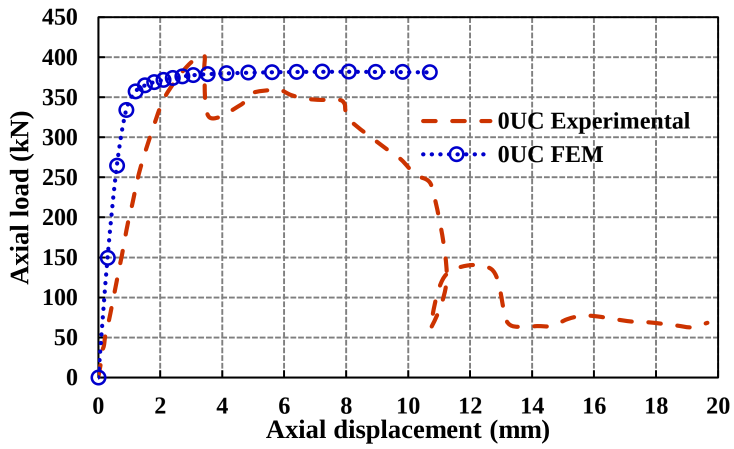

(a) Concentrically loaded column

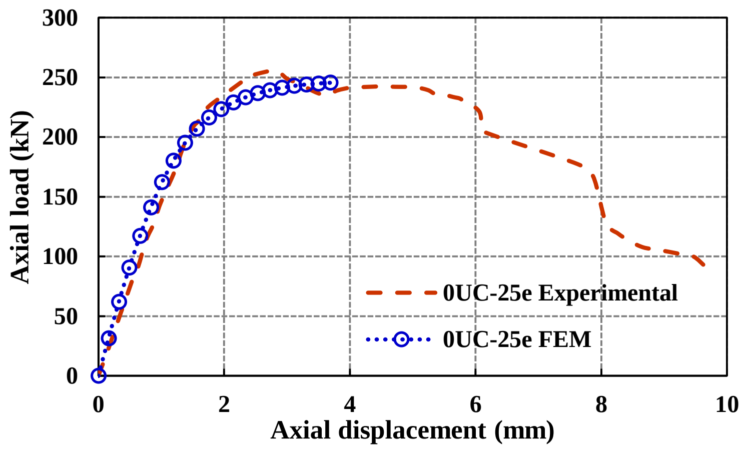

(b) Column subjected to 25mm load eccentricity

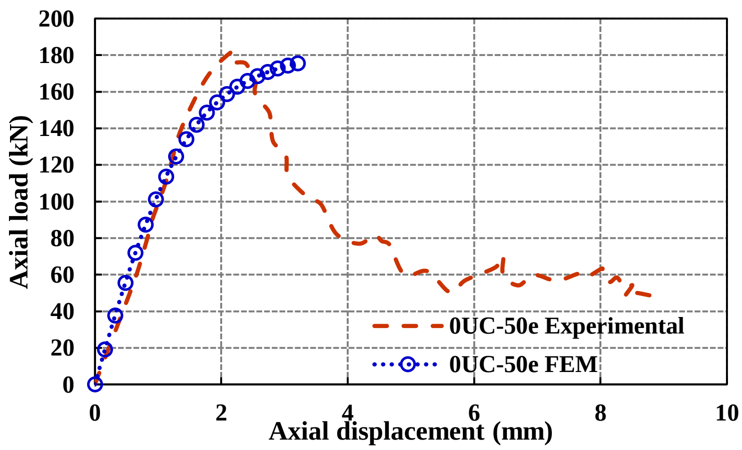

(c) Column subjected to 50mm load eccentricity

Figure 6.9 Comparison of axial load-displacement responses between experimental and FEA results for unwrapped columns

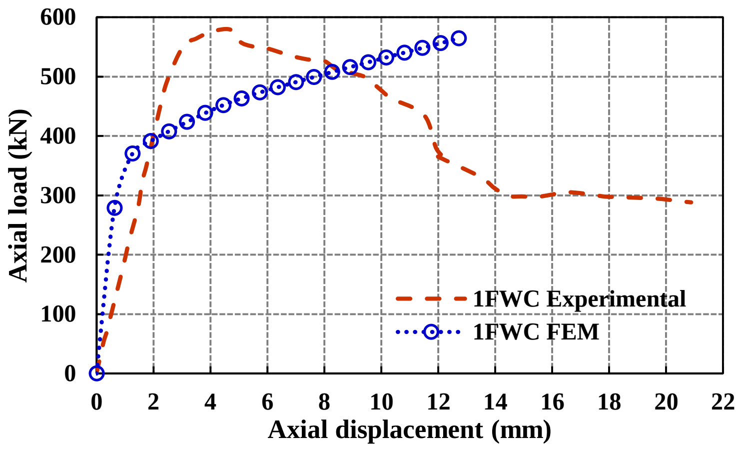

(a) Concentrically loaded column

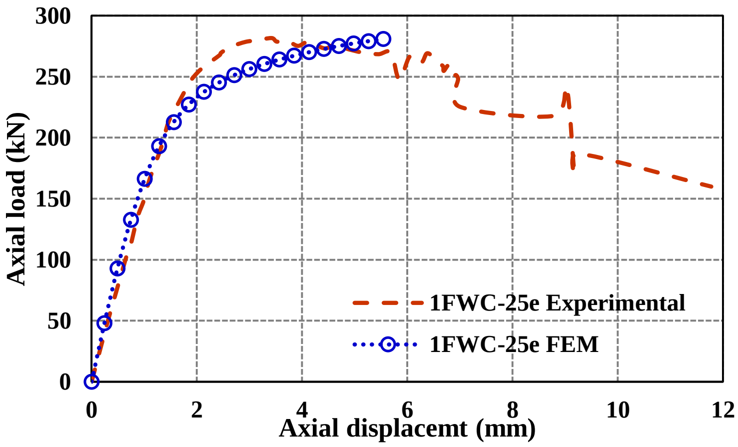

(b) Column subjected to 25mm load eccentricity

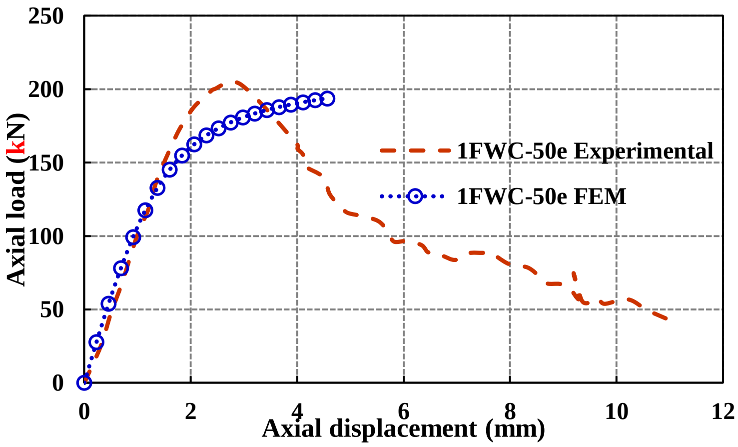

(c) Column subjected to 50mm load eccentricity

Figure 6.10 Comparison of axial load-displacement responses between experimental and FEA results for GFRP wrapped columns

For specimens subjected to flexural loading, the results of comparison between the experimental and FEA ultimate flexural load and mid-span deflection at ultimate flexural load are presented in Table 6.5. Figure 6.11 depicts the comparisons between flexural load-deflection plots of the experimental beams and load-deflection plots of beams from the FEA. For the control beam 0UB (Figure 6.11 (a)), the FEA load-deflection plot agrees quite well with the load-deflection plot of the actual beam. In the linear range, the load-deflection plots of both FE and experimental beams attained almost similar stiffness behaviour up to the yielding of longitudinal steel. Beyond the yielding point, it is evident that the load-deflection curve of the FE beam is slightly stiffer than that of the actual beam. The ultimate flexural load of the FE beam 0UB is 101kN, which is higher than 94.39kN of the experimental beam by approximately 7%.

Figure 6.11 (b-d) portrays the comparisons of load-deflection plots of FE and experimental beams wrapped with GFRP reinforcement. It is evident from the figure that the linear range of the load-deflection plots of the FE beams and the actual beams exhibited almost similar stiffness behaviour up to the first cracking region of the curves. Furthermore, the load-deflection curves of the FE beams are much stiffer than that of the experimental beams in the nonlinear range of the curves. It is important to note that for all the GFRP wrapped beams, the FE ultimate flexural load is considerably higher than the experimental value. In general, the finite element analysis results underestimate the load carrying capacity and stiffness of the experimental beams by approximately 7% - 94%.

This underestimation might be interpreted as being attributed to the presence of micro cracks in concrete resulting from drying shrinkage and handling of beams. In the finite element analysis, micro cracks are not accounted for because it could reduce the stiffness of the tested beams to some extent. the underestimation might also be attributed to the assumptions made in some of the material properties of concrete, steel and GFRP. Moreover, the assumption of perfect bond between the interfaces of concrete and steel, as well as the interfaces of concrete and GFRP in the FE analysis could increase the stiffness of the beams. But in real scenario, this assumption cannot hold true because bond slip could occur, and composite action between concrete and steel, and, concrete and GFRP could be lost.

Table 6.5 Comparison between the experimental results and FEA results for GFRP wrapped beams under flexural loadings

Specimen	**Ultimate flexural load (kN)**		**Mid-span deflection at ultimate load (mm)**		**Difference in ultimate flexural load (%)**	**Difference in mid-span deflection at ultimate load (%)**
	Experimental	**FEM**	**Experimental**	**FEM**		
0UB	94.39	101	17.14	17.17	7.00	0.18
1FWB	116.69	189	27.01	19.42	61.97	-28.10
2FWB	124.89	230	28.35	24.07	84.16	-15.10
3FWB	142.77	278	28.57	30.42	94.72	6.48

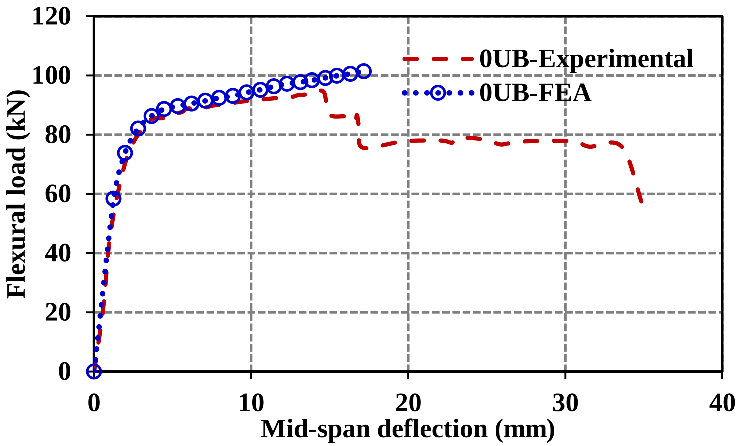

(a) Control beams

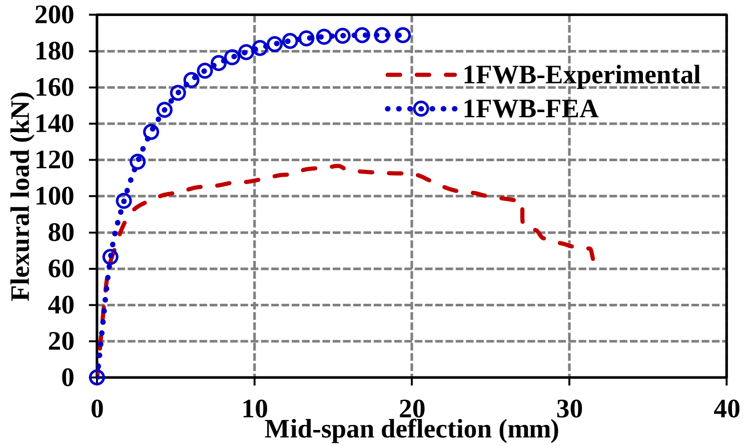

(b) Beams wrapped with one layer of GFRP

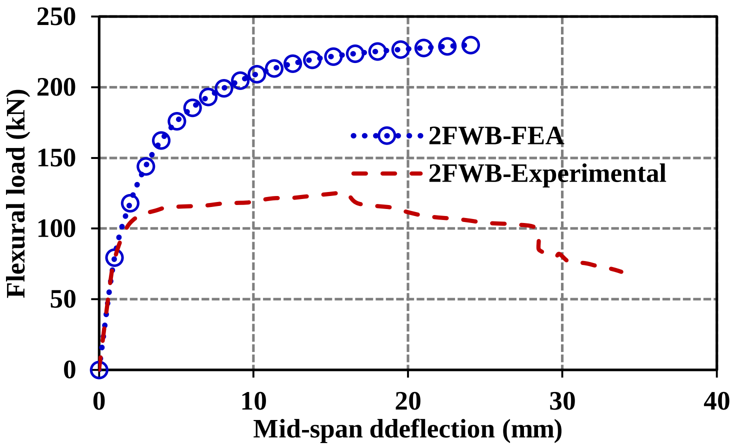

(c) Beams wrapped with two layers of GFRP

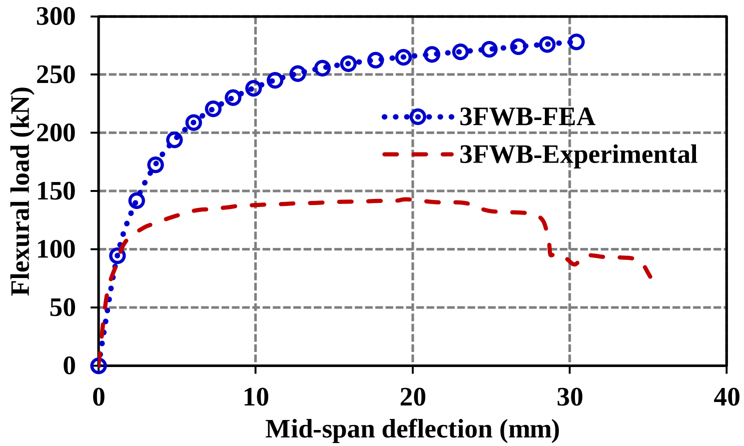

(d) Beams wrapped with three layers of GFRP

Figure 6.11 Comparison of flexural load versus mid-span responses between experimental and FEA results for GFRP wrapped beams

6.8 Comparisons of axial load-bending moment interaction diagrams

The results of comparisons between the experimental and FEA ultimate bending moment of rectangular GFRP wrapped column and beam specimens are presented in Table 6.6. Meanwhile, the corresponding plots of ultimate load versus ultimate bending moment interaction diagrams of the column specimens are portrayed in Figure 6.12. It is evident from those figures that under eccentric loading, the finite element analysis gave ultimate bending moment values that ware higher than the experimental results (i.e. overestimation). For one and two layers GFRP wrapped columns under concentric loading, the finite element analysis gave axial load values that ware very close to the experimental results. However, the FE axial load values of control column under concentric loading underestimate axial load of experimental column. On the other hand, the ultimate axial load of FE column with three layers of GFRP overestimate that of the experimental column. For specimens under pure flexural loading, it can be seen clearly from Figure 6.12 that the finite element analysis gave bending moment values that ware much higher than those of the experimental results. In general, the theoretical axial load-bending moment interaction diagram (P-M) of GFRP wrapped specimens demonstrated that the FEA P-M are not in good agreement with those of the experiment results. But for specimens without GFRP wrapping, the FEA P-M exhibited almost close agreement with the experimental P-M.

Table 6.6 Results of comparisons between the experimental and FEA ultimate bending moment of rectangular GFRP wrapped RC column and beam specimens

Test specimen	**Eccentricity of loading '*e*' (mm)**	**Ultimate bending moment 'M_u' (kN.m)**		**Difference in ultimate bending moment (%)**
		Experimental	**FEA**	
0UC	-	-	-	-
0UC-25e	25	7.06	7.99	13.17
0UC-50e	50	9.44	9.96	5.51
0UB	-	10.85	11.62	7.10
1FWC	-	-	-	
1FWC-25e	25	7.96	10.12	27.14
1FWC-50e	50	10.73	11.57	7.83
1FWB	-	13.42	21.74	62.00
2FWC	-	-	-	
2FWC-25e	25	9.96	12.83	28.82
2FWC-50e	50	11.64	13.36	14.78
2FWB	-	14.36	26.45	84.19
3FWC	-	-	-	
3FWC-25e	25	12.61	16.55	31.25
3FWC-50e	50	14.93	17.05	14.20
3FWB	-	16.42	31.97	94.70

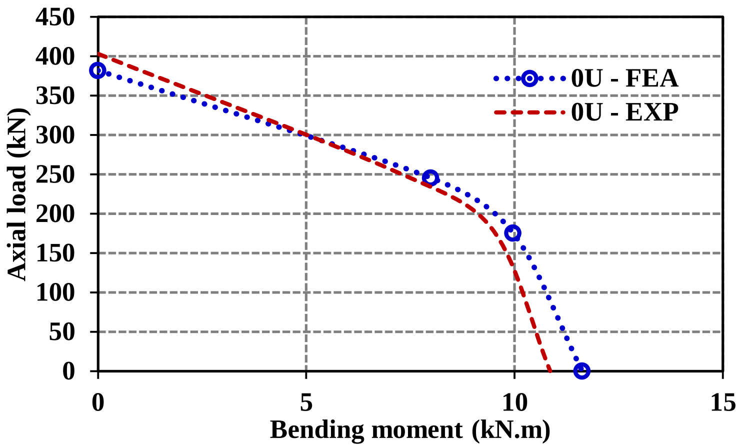

(a) Control specimens

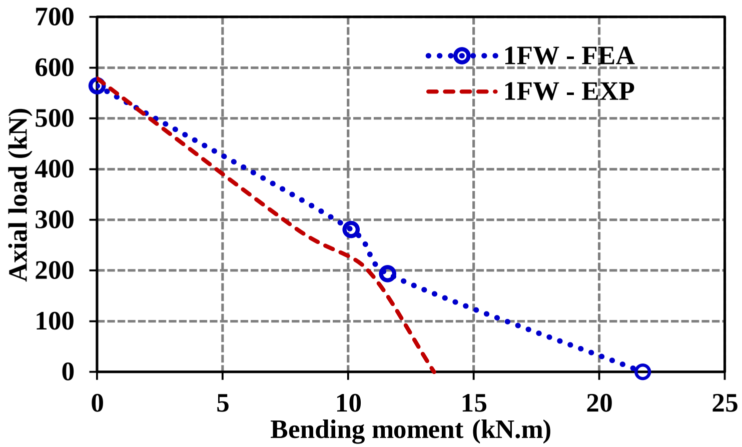

(b) One layers GFRP wrapped specimens

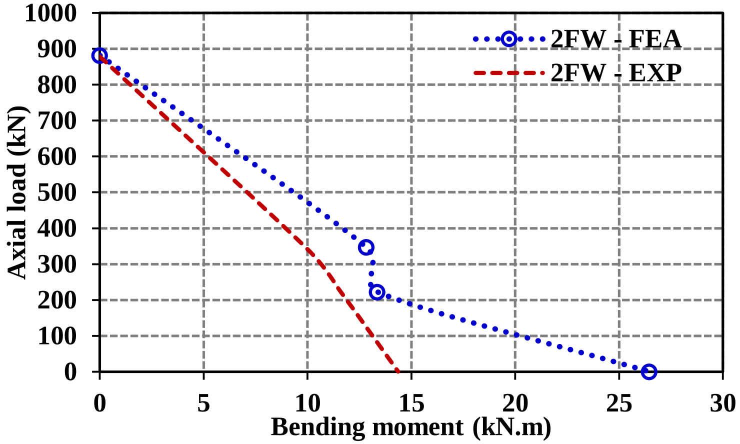

(c) Two layers GFRP wrapped specimens

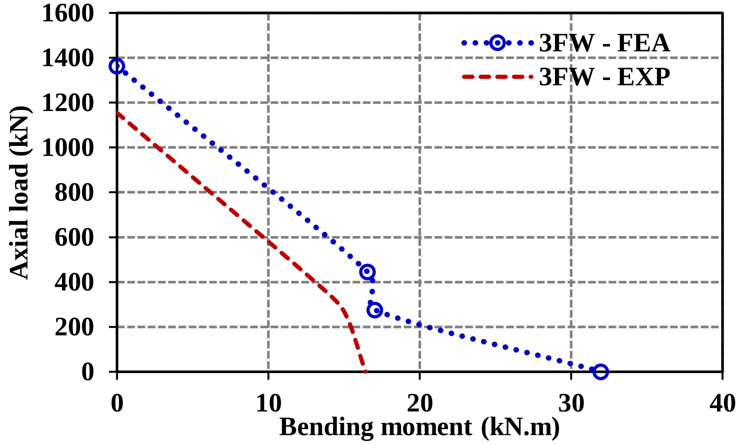

(d) Three layers GFRP wrapped specimens

Figure 6.12 Comparison of axial load-bending moment interaction diagrams between experimental and FEA results

6.9 Summary

The results of finite element analysis of rectangular RC specimens with GFRP confinement under concentric eccentric and flexural loading conditions were discussed in this chapter. The influence of GFRP layers and three load eccentricities on the performance of the simulated rectangular RC columns were also discussed. The results obtained from the FE model were validated with the experimental results. For column specimens under concentric and eccentric loadings, a reasonably close agreement was obtained, except in columns subjected to concentric loadings. For specimens subjected to bending loadings, it was found that the finite element analysis results underestimate the load carrying capacity of the experimental beams.

In the next chapter, conclusions that can be drawn from the outcomes of this study along with the recommendations suggested as a way forward for future research on RC columns wrapped with FRP under eccentric load are summarised.

CHAPTER 7: CONCLUSIONS AND RECOMMENDATION FOR FUTURE RESEARCH

7.1 Summary

The primary objective of the current study was to examine the behaviour of rectangular RC columns confined with bi-direction GFRP under various loading conditions. The main test variables considered in this study include the amount of GFRP wrap layers (i.e., one, two, and three) and three load eccentricities (i.e., 0, 25mm, and 50mm). To achieve the objectives of this investigation, 16 rectangular RC specimens confined with bi-directional GFRP were prepared and tested under different loading conditions. Four specimens were tested under axial loading, eight were tested under eccentric loading, and four were tested under flexural loading.

Furthermore, the numerical investigation presented in this study was performed via finite element analysis utilising ANSYS finite element software. sixteen rectangular RC columns with GFRP wrapping were simulated under three loading conditions (i.e. concentric, eccentric and flexural loadings). The results obtained from the finite element analysis were compared with the experimental results.

7.2 Conclusions

From the outcomes of this investigation, the following conclusions are summarised:

1. Based on the experimental results, wrapping the rectangular RC columns using GFRP composites was effective for improving the ultimate capacity and performance of the columns under axial compression loadings as well as flexural loading. The enhancement in ultimate capacity and performance of the specimens increases significantly with increasing number of GFRP layers. Concentrically loaded columns achieved maximum ultimate capacity enhancement of 187%, but columns with 25mm and 50mm eccentricities achieved maximum ultimate capacity enhancement of 68%, and 52%, respectively. However, specimens subjected to pure bending achieved a maximum flexural capacity enhancement of 51%. In terms of ductility, the GFRP confined rectangular RC columns subjected to axial loading exhibited significant gains in ductility. This was mainly attributed to the higher confinement pressure generated by the longitudinal and transverse fibres of bi-directional GFRP wrap layers, which effectively increased axial deformation of the columns. However, the GFRP confinement resulted in a significant enhancement in ductility of specimens subjected to flexural loading, with higher ductility enhancement in specimens confined with three layers of GFRP reinforcement. The increase in ductility of the beam specimens contradicts the generally accepted idea that RC beams with FRP confinement are affected by a decrease in ductility, which could lead to a brittle and sudden collapse.

2. From the experimental results, the eccentricity of loading resulted in a general decline in ultimate axial strength of GFRP wrapped columns by about 76%, with a ductility decrease of about 19%. Conversely, the loss in ultimate capacity and ductility of the specimens increased when the eccentricity was increased.

3. Based on the FE analysis results, the axial stress distribution in concrete for concentrically loaded columns varies significantly over the column section, with maximum values at the corners and minimum along the edges. However, the axial stress distribution in concrete for eccentrically loaded columns is maximum in the compression zone and drop gradually to a minimum in the tension zone. The finite element analysis provided reasonably close predictions in estimating the ultimate capacity of the GFRP confined rectangular RC columns except in columns under concentric loading. For specimens subjected to flexural loading, the FE load-deflection plot of the control beam agrees quite well with the load-deflection plot of the actual beam in both linear and nonlinear range. Moreover, the load-deflection curves of the FE GFRP wrapped beams are much stiffer than that of the experimental beams in both linear and nonlinear range of the curves.
4. The theoretical axial load-bending moment interaction diagram (P-M) of GFRP wrapped specimens demonstrated that the finite element analysis P-M are not in good agreement with those of the experiment results. But for specimens without GFRP wrapping, the finite element analysis P-M and the experimental P-M exhibited almost close agreement.

7.3 Recommendations for Future Research

From the outcomes of this investigation, the following recommendations are suggested as a way forward for future research:

1. The axial stress distribution over the section of FRP confined concrete column described in the present study utilising finite element method is difficult to verify experimentally, due to constraints in Laboratory measurement procedures. It is recommended that additional investigation on some new methods of monitoring the axial stress distribution over the section of concrete columns with FRP wrapping is valuable.
2. From the literature review presented in Chapter 2, it is clear that research contributions towards FRP-confined rectangular or square RC sections under eccentric loadings are lacking. Further investigation on the behaviour of FRP wrapped rectangular or square RC columns with variation in their corner radius under eccentric loading is still worthwhile.
3. The test columns in the present work are fully wrapped with FRP under eccentric load. Further research on the influence of partial FRP wrapping on the behaviour of rectangular or square RC columns under eccentric loading is recommended.
4. The influence of cross-section size on the behaviour of FRP-confined rectangular/square RC columns under eccentric loading can be investigated utilising experimental and finite element methods.

REFERENCES

Al-Salloum, Y.A. (2007), "Influence of edge sharpness on the strength of square concrete columns confined with FRP composite laminates", *Composites Part B: Engineering*, Vol. 38 No. 5–6, pp. 640–650.

Alecci, V., Briccoli Bati, S. and Ranocchiai, G. (2014), "Concrete columns confined with CFRP wraps", *Materials and Structures/Materiaux et Constructions*, Vol. 47 No. 3, pp. 397–410.

Almusallam, T.H. (2007), "Behavior of normal and high-strength concrete cylinders confined with E-glass/epoxy composite laminates", *Composites Part B: Engineering*, Vol. 38 No. 5–6, pp. 629–639.

Altunışı, A.C., Kalkan, E. and Ba, H.B. (2018), "Structural response relationship between scaled and prototype concrete load bearing systems using similarity requirements", *Computers and Concrete*, Vol. 21 No. 4, pp. 385–397.

Anderson, T.L. (2005), *Fracture Mechanics: Fundamentals and Applications*, edited by CRC Press*Taylor and Francis Group*, 3rd edition.

ANSYS Release 18.1. (2017a), "ANSYS Mechanical APDL Element Reference", ANSYS Inc, Canonsburg, PA 15317 USA.

ANSYS Release 18.1. (2017b), "ANSYS Mechanical APDL Theory Reference", ANSYS Inc, Canonsburg, PA 15317 USA.

ANSYS Release 18.1. (2017c), "Workbench User's Guide", ANSYS Inc, Canonsburg, PA 15317 USA.

ASTM A370-8a. (2008), "Standard Test Methods and Definitions for Mechanical Testing of Steel Products", ASTM International, West Conshohocken, PA, USA.

ASTM D3039. (2000), "Standard Test Method for Tensile Properties of Polymer Matrix Composite Materials 1", ASTM International, West Conshohocken, PA, USA.

Benzaid, R. and Mesbah, H.-A. (2014), "The confinement of concrete in compression using CFRP composites–effective design equations", *Journal of Civil Engineering and Management*, Vol. 20 No. 5, pp. 632–648.

Berthet, J.F., Ferrier, E. and Hamelin, P. (2005), "Compressive behavior of concrete externally confined by composite jackets. Part A: experimental study", *Construction and Building Materials*, Vol. 19 No. 3, pp. 223–232.

Bousias, S., Spathis, A.-L. and Fardis, M.N. (2007), "Seismic Retrofitting of Columns with Lap Spliced Smooth Bars Through FRP or Concrete Jackets", *Journal of Earthquake Engineering*, Vol. 11 No. 5, pp. 653–674.

Bousias, S.N., Spathis, A.-L. and Fardis, M.N. (2006), "Concrete or FRP Jacketing of Columns with Lap Splices for Seismic Rehabilitation", *Journal of Advanced Concrete Technology*, Vol. 4 No. 3, pp. 431–444.

BS 1881 part 125. (1986), "Method of mixing and sampling fresh concrete in the laboratory", 389 Chiswick high road London.

BS 8500-1. (2006), "Concrete-complementary british standard to BS EN 206-1-part 1 : method of specifying and guidnace for the specifier", *British*

Standard, BSI, London, U.K.

BS EN 12390-3. (2009), "Testing hardened concrete. Compressive strength of test specimens", BSI, London, U.K.

Campione, G. (2012), "Load carrying capacity of RC compressed columns strengthened with steel angles and strips", *Engineering Structures*, Ltd, Vol. 40, pp. 457–465.

Chaallal, O., Hassan, M. and Shahawy, M. (2003), "Performance of axially loaded short rectangular columns strengthened with fiber-reinforced polymer wrapping", *Journal of Composites for Construction*, Vol. 7 No. 3, pp. 200–208.

Chaallal, O., Shahawy, M., and Al-Saad, A., (2000), "Behaviour of Axially Loaded Short Rectangular Columns Strengthened With CFRP Composite Wrapping", *Technical Report, FDOT, Structures Research Center*.

Chaallal, O. and Shahawy, M. (2000), "Performance of Fiber-Reinforced Polymer-Wrapped Reinforced Concrete Column under Combined Axial-Flexural Loading", *ACI Structural Journal*, Vol. 97 No. 4, pp. 659–668.

Chakrabarti, A. (2011), "Confinement behaviour of eccentrically loaded RCC columns using FRP sheets", *Advances in FRP Composites in Civil Engineering - Proceedings of the 5th International Conference on FRP Composites in Civil Engineering, CICE 2010*, pp. 607–609.

Chakrabarti, A., Chandra, A. and Bharagava, P. (2008), "Finite Element Analysis of Concrete Columns Confined with FRP Sheets", *Journal of Reinforced Plastics and Composites*, Vol. 27 No. 12, pp. 1349–1373.

Chansawat, K., Potisuk, T., Miller, Thomas H.Yim, S.C. and Kachlakev, D.I. (2009), "FE models of GFRP and CFRP strengthening of reinforced concrete beams", *Advances in Civil Engineering*, Vol. 2009, p. 13.

Chellapandian, M., Prakash, S.S. and Rajagopal, A. (2018), "Analytical and finite element studies on hybrid FRP strengthened RC column elements under axial and eccentric compression", *Composite Structures*, Vol. 184, pp. 234–248.

Choi, E., Chung, Y.S., Park, K. and Jeon, J.S. (2013), "Effect of steel wrapping jackets on the bond strength of concrete and the lateral performance of circular RC columns", *Engineering Structures*, Vol. 48, pp. 43–54.

Cui, C. and Sheikh, S.A. (2010), "Experimental Study of Normal- and High-Strength Concrete Confined with Fiber-Reinforced Polymers", *Journal of Composites for Construction*, Vol. 14 No. 5, pp. 553–561.

Cusson, D. and Paultre, P. (1995), "Stress-Strain Model for Confined High-Strength Concrete", *Journal of Structural Engineering*, Vol. 121 No. 3, pp. 468–477.

Daugevičius, M., Valivonis, J., Beinaravičius, A., Skuturna, T. and Budvytis, M. (2013), "Experimental Investigation of the Load Carrying Capacity of Eccentrically Loaded Reinforced Concrete Elements Strengthened with CFRP", *Procedia Engineering*, Vol. 57, pp. 232–237.

Desayi, P. and Krishnan, S. (1964), "Equation for the Stress-strain Curve of Concrete", *Journal of the American Concrete Institute*, Vol. 61 No. 3, pp. 345–350.

El-Hacha, R., Green, M.F. and Wight, G.R. (2010), "Effect of Severe Environmental Exposures on CFRP Wrapped Concrete Columns", *Journal of Composites for Construction*, Vol. 14 No. 1, pp. 83–93.

Fam, A.Z., Flisak, B. and Rizkalla, S. (2003), "Experimental and Analytical Modeling of Concrete-Filled Fiber-Reinforced Polymer Tubes Subjected to Combined Bending and Axial Loads", *ACI Structural Journal*, Vol. 100 No. 4, pp. 499–509.

Feng, P., Lu, X.Z. and Ye, L.P. (2002), "Experimental research and finite element analysis of square concrete columns confined by FRP sheets under uniaxial compression", *17th Australasian Conference on the Mechanics of Structures and Materials*, Gold Coast, Australia, pp. 60–65.

GangaRao, H., Taly, N. and Vijay, P. (2006), *Reinforced Concrete Design with FRP Composites*, CRC Press, Boca Raton.

Garzón-Roca, J., Adam, J.M. and Calderón, P.A. (2011), "Behaviour of RC columns strengthened by steel caging under combined bending and axial loads", *Construction and Building Materials*, Vol. 25 No. 5, pp. 2402–2412.

Ghali, K., Rizkalla, S., Kassem, M., Fawzy, T. and Mahmoud, M. (2003), "FRP-Confined Circular Columns under small Eccentric Loading", *Proceedings of the Fifth Alexandria International Conference on Structural and Geotechnical Engineering, Alexandria, Egypt, December*, pp. 20–22.

Hadi, M.N.S. (2007a), "Behaviour of FRP strengthened concrete columns under eccentric compression loading", *Journal of Composite Structures*, Vol. 77 No. 1, pp. 92–96.

Hadi, M.N.S. (2007b), "The behaviour of FRP wrapped HSC columns under different eccentric loads", *Journal of Composite Structures*, Vol. 78 No. 4, pp. 560–566.

Hadi, M.N.S. (2009), "Behaviour of eccentric loading of FRP confined fibre steel reinforced concrete columns", *Construction and Building Materials*, Vol. 23 No. 2, pp. 1102–1108.

Hadi, M.N.S., Algburi, A.H.M., Sheikh, M.N. and Carrigan, A.T. (2018), "Axial and flexural behaviour of circular reinforced concrete columns strengthened with reactive powder concrete jacket and fibre reinforced polymer wrapping", *Construction and Building Materials*, Vol. 172, pp. 717–727.

Hadi, M.N.S. and Li, J. (2004), "External reinforcement of high strength concrete columns", *Journal of Composite Structures*, Vol. 65 No. 3–4, pp. 279–287.

Hadi, M.N.S. and Widiarsa, I.B.R. (2012), "Axial and Flexural Performance of Square RC Columns Wrapped with CFRP under Eccentric Loading", *Journal of Composites for Construction*, Vol. 16 No. 6, pp. 640–649.

Hadi, M.N.S. and Youssef, J. (2016), "Experimental Investigation of GFRP-Reinforced and GFRP-Encased Square Concrete Specimens under Axial and Eccentric Load, and Four-Point Bending Test", *Journal of Composites for Construction*, Vol. 20 No. 5, p. 04016020.

Hajsadeghi, M., Alaee, F.J. and Shahmohammadi, A. (2011), "Investigation on Behaviour of Square/Rectangular Reinforced Concrete Columns Retrofitted with FRP Jacket", *Journal of Civil Engineering and*

Management, Vol. 17 No. 3, pp. 400–408.

Hassan, W.M., Hodhod, O.A., Hilal, M.S. and Bahnasaway, H.H. (2017), "Behavior of eccentrically loaded high strength concrete columns jacketed with FRP laminates", *Construction and Building Materials*, Vol. 138, pp. 508–527.

Hognestad, E., Hanson, N.. and McHenry, D. (1955), "Concrete Stress Distribution in Ultimate Strength Design", *ACI Journal Proceedings*, Vol. 52 No. 12, pp. 455–480.

Hollaway, L.C. (2010), "A review of the present and future utilisation of FRP composites in the civil infrastructure with reference to their important in-service properties", *Construction and Building Materials*, Vol. 24 No. 12, pp. 2419–2445.

Hosseinpour, F. and Abbasnia, R. (2014), "Experimental investigation of the stress-strain behavior of FRP confined concrete prisms", *Advances in Concrete Construction*, Vol. 2 No. 3, pp. 177–192.

Houssam A. Toutanji. (1999), "Toutanji - stress-strain characteristics of concrete columns externaly confined with FRP", *ACI Materials Journal*, Vol. 96 No. 3, pp. 397–404.

Hu, B., Wang, J. and Li, G. (2011), "Numerical simulation and strength models of FRP-wrapped reinforced concrete columns under eccentric loading", *Construction and Building Materials*, Vol. 25 No. 5, pp. 2751–2763.

Ilki, A. and Kumbasar, N. (2003), "Compressive Behaviour of Carbon Fibre Composite Jacketed Concrete with Circular and Non-Circular Cross-

Sections”, *Journal of Earthquake Engineering*, Vol. 7 No. 3, pp. 381–406.

Ilki, A., Peker, O., Karamuk, E., Demir, C. and Kumbasar, N. (2008), “FRP Retrofit of Low and Medium Strength Circular and Rectangular Reinforced Concrete Columns”, *Journal of Materials in Civil Engineering*, Vol. 20 No. 2, pp. 169–188.

Jiang, C. and Wu, Y.-F. (2020), “Axial Strength of Eccentrically Loaded FRP-Confined Short Concrete Columns”, *Polymers*, Vol. 12 No. 6, pp. 1–14.

Jiang, T. and Teng, J.G. (2012), “Theoretical model for slender FRP-confined circular RC columns”, *Construction and Building Materials*, Vol. 32, pp. 66–76.

Jin, L., Li, P., Wang, Z. and Du, X. (2021), “Effect of Size on Eccentric Compression Behavior of CFRP-Confined RC Columns : Experimental and Numerical Investigation”, *Journal of Composites for Construction*, Vol. 25 No. 4, p. 04021032.

Julio, E.N.B.S. and Branco, F. (2008), “Reinforced Concrete Jacketing-Interface Influence on Cyclic Loading Response”, *ACI Structural Journal*, Vol. 105 No. 4, pp. 471–477.

Kachlakev, D., Miller, T., Yim, S., Chansawat, K. and Potisuk, T. (2001), *Finite Element Modelling of Reinforced Concrete Structures Strengthening with FRP Laminates*, *Final Report, SPR*, Vol. 316, Washington, DC.

Kaish, A.B.M.A., Alam, M.R., Jamil, M. and Wahed, M.A. (2013), “Ferrocement jacketing for restrengthening of square reinforced concrete column under concentric compressive load”, *Procedia Engineering*, Vol.

54, pp. 720–728.

Kaish, A.B.M.A., Alam, M.R., Jamil, M., Zain, M.F.M. and Wahed, M.A. (2012), “Improved ferrocement jacketing for restrengthening of square RC short column”, *Construction and Building Materials*, Vol. 36, pp. 228–237.

Karabinis, A.I., Rousakis, T.C. and Manolitsi, G.E. (2008), “3D Finite-Element Analysis of Substandard RC Columns Strengthened by Fiber-Reinforced Polymer Sheets”, *Journal of Composites for Construction*, Vol. 12 No. 5, pp. 531–540.

Kumutha, R., Vaidyanathan, R. and Palanichamy, M.S. (2007), “Behaviour of reinforced concrete rectangular columns strengthened using GFRP”, *Cement and Concrete Composites*, Vol. 29 No. 8, pp. 609–615.

Kwak, H. and Filippou, F. (1990), *Finite Element Analysis of Reinforced Concrete Structures under Monotonic Loads*, *Structural Engineering, Mechanics and Materials,* Vol. UCB/SEMM-9, California USA.

Lai, M.H. and Ho, J.C.M. (2015), “Axial strengthening of thin-walled concrete-filled-steel-tube columns by circular steel jackets”, *Thin-Walled Structures*, Vol. 97, pp. 11–21.

Lam, L. and Teng, J.G. (2003), “Design-Oriented Stress-Strain Model for FRP-Confined Concrete in Rectangular Columns”, *Journal of Reinforced Plastics and Composites*, Vol. 22 No. 13, pp. 1149–1186.

Lam, L. and Teng, J.G. (2004), “Ultimate Condition of Fiber Reinforced Polymer-Confined Concrete”, *Journal of Composites for Construction*, Vol. 8 No. 6, pp. 539–548.

Li, J. and Hadi, M.N.S. (2003), "Behaviour of externally confined high-strength concrete columns under eccentric loading", *Journal of Composite Structures*, Vol. 62 No. 2, pp. 145–153.

Limbrunner, G.F. (2013), *Reinforced Concrete Design*, 8th ed., Pearson Education, Inc, Upper Saddle River, NJ, USA.

Lin, G. and Teng, J.G. (2017), "Three-Dimensional Finite-Element Analysis of FRP-Confined Circular Concrete Columns under Eccentric Loading", *Journal of Composites for Construction*, Vol. 21 No. 4, p. 04017003.

Lin, G., Zeng, J.J., Teng, J.G. and Li, L.J. (2020), "Behavior of large-scale FRP-confined rectangular RC columns under eccentric compression", *Engineering Structures*, Vol. 216 No. May, pp. 1–17.

De Lorenzis, L. and Tepfers, R. (2003), "Comparative Study of Models on Confinement of Concrete Cylinders with Fiber-Reinforced Polymer Composites", *Journal of Composites for Construction*, Vol. 7 No. 3, pp. 219–237.

M.N.S Hadi; I.B.R Widiarsa. (2012), "Axial and Flexural Performance of Square RC Columns Wrapped with CFRP under Eccentric Loading", *Journal of Composites for Construction*, Vol. 16 No. December, pp. 640–649.

Maaddawy, T. El. (2009), "Strengthening of Eccentrically Loaded Reinforced Concrete Columns with Fiber-Reinforced Polymer Wrapping System: Experimental Investigation and Analytical Modeling", *Journal of Composites for Construction*, Vol. 13 No. 1, pp. 13–24.

Mai, A.D., Sheikh, M.N. and Hadi, M.N.S. (2018), "Investigation on the behaviour of partial wrapping in comparison with full wrapping of square RC columns under different loading conditions", *Construction and Building Materials*, Vol. 168, pp. 153–168.

Malvar, L.J., Morrill, K.B. and Crawford, J.E. (2004), "Numerical Modeling of Concrete Confined by Fiber-Reinforced Composites", *Journal of Composites for Construction*, Vol. 8 No. 4, pp. 315–322.

Mander, J.B., Priestley, M.J.N. and R.Park. (1988), "Theoretical Stress Strain Model for Confined Concrete", *Journal of Structural Engineering*, Vol. 114 No. 8, pp. 1804–1825.

Masia, M.J., Gale, T.N. and Shrive, N.G. (2004), "Size effects in axially loaded square-section concrete prisms strengthened using carbon fibre reinforced polymer wrapping", *Canadian Journal of Civil Engineering*, Vol. 31 No. 1, pp. 1–13.

Matthys, S. (2000), *Structural Behaviour and Design of Concrete Members Strengthened with Externally Bonded FRP Reinforcement*, Ghent University.

Matthys, S., Toutanji, H., Audenaert, K. and Taerwe, L. (2005), "Axial load behavior of large-scale columns confined with fiber-reinforced polymer composites", *ACI Structural Journal*, Vol. 102 No. 2, pp. 258–267.

Matthys, S., Toutanji, H. and Taerwe, L. (2006), "Stress – Strain Behavior of Large-Scale Circular Columns Confined with FRP Composites", *Structural Engineering*, Vol. 132 No. 1, pp. 123–133.

McCormac, C.J. and Brown, H.B. (2013), *Design of Reinforced Concrete*, *ACI*

318-11 Code Edition, Ninth., John Wiley & Sons, United State of America,

Mirmiran, A., Shahawy, M., Samaan, M., Echary, H. El, Mastrapa, J.C. and Pico, O. (1998), "Effect of Column Parameters on FRP-Confined Concrete", *Journal of Composites for Construction*, Vol. 2 No. 4, pp. 175–185.

Mirmiran, A., Zagers, K. and Yuan, W. (2000), "Nonlinear finite element modeling of concrete confined by fiber composites", *Finite Elements in Analysis and Design*, Vol. 35, pp. 79–96.

Moshiri, N., Hosseini, A. and Mostofinejad, D. (2015), "Strengthening of RC columns by longitudinal CFRP sheets: Effect of strengthening technique", *Construction and Building Materials*, Vol. 79, pp. 318–325.

Mostofinejad, D. and Saadatmand, H. (2010), "A Procedure for Predicting the Behavior of FRP Confined Concrete Using the FE Method", *Scientia Iranica Transaction A-Civil Engineering*, Vol. 17 No. 6, pp. 471–481.

Nilson, A.H., Darwin, D. and Dolan, C.W. (2010), *Design of Concrete Structures*, 14th ed., McGraw-Hill Higher Education, New York, USA.

Ozbakkaloglu, T. and Oehlers, D.J. (2008), "Concrete-Filled Square and Rectangular FRP Tubes under Axial Compression", *Journal of Composites for Construction*, Vol. 12 No. 4, pp. 469–477.

Parghi, A. and Alam, M.S. (2016), "Seismic behavior of deficient reinforced concrete bridge piers confined with FRP – A fractional factorial analysis", *Engineering Structures*, Vol. 126, pp. 531–546.

Parghi, A. and Alam, M.S. (2017), "Seismic collapse assessment of non-seismically designed circular RC bridge piers retrofitted with FRP composites", *Composite Structures*, Vol. 160, pp. 901–916.

Parghi, A. and Alam, M.S. (2018), "A review on the application of sprayed-FRP composites for strengthening of concrete and masonry structures in the construction sector", *Composite Structures*, Vol. 187, pp. 518–534.

Park, R. and Paulay, T. (1975), *Reinforced Concrete Structures*, Vol. 154, John Wiley and Sons, New York, USA.

Parvin, A. and Wei, W. (2001), "Bahaviour of FRP Jacketed Concrete Conrete Columns under Eccentric Loading", *Journal of Composites for Construction*, Vol. 5 No. 3, pp. 146–152.

Pessiki, S., Harries, K.A., Kestner, J.T., Sause, R. and Ricles, J.M. (2001), "Axial Behavior of Reinforced Concrete Columns Confined with FRP Jackets", *Journal of Composites for Construction*, Vol. 5 No. 4, pp. 237–245.

Popovics, S. (1973), "A numerical approach to the complete stress-strain curve of concrete", *Cement and Concrete Research*, Vol. 3 No. 5, pp. 583–599.

Priestley, M.J.N., Calvi, G.M. and Kowalsky, M.J. (2007), *Displacement-Based Seismic Design of Structures*, IUSS Press : Distributed by Fondazione EUCENTRE, Pavia, Italy.

Priestley, M.J.N., Seible, F., Calvi, G.M. and Calvi, G.M. (1996), *Seismic Design and Retrofit of Bridges*, John Wiley & Sons.

Rasheed, H.A. (2014), *Strengthening Design of Reinforced Concrete with FRP*, Taylor and Fancis Group, New York, USA.

Rocca, S., Galati, N. and Nanni, A. (2009), "Interaction diagram methodology for design of FRP-confined reinforced concrete columns", *Construction and Building Materials*, Vol. 23 No. 4, pp. 1508–1520.

Rousakis, T.C., Rakitzis, T.D. and Karabinis, A.I. (2012), "Design-Oriented Strength Model for FRP-Confined Concrete Members", *Journal of Composites for Construction*, Vol. 16 No. December, pp. 724–736.

Saafi, M., Toutanji, H. and Zongjin, L. (1999), "Behavior of Concrete Columns Confined with Fiber Reinforced Polymer Tubes", *ACI Materials Journal*, Vol. 96 No. 4, pp. 500–509.

Sadeghian, P., Rahai, A.R. and Ehsani, M.R. (2010), "Experimental Study of Rectangular RC Columns Strengthened with CFRP Composites under Eccentric Loading", *Journal of Composites for Construction*, Vol. 14 No. 4, pp. 443–450.

SeismoStruct. (2015), "A computer program for static and dynamic nonlinear analysis of framed structures", Seismosft Ltd, Italy.

Sezen, H. and Miller, E.A. (2011), "Experimental Evaluation of Axial Behavior of Strengthened Circular Reinforced-Concrete Columns", *Journal of Bridge Engineering*, Vol. 16 No. 2, pp. 238–247.

Shehata, I.A.E.M., Carneiro, L.A. V. and Shehata, L.C.D. (2002), "Strength of short concrete columns confined with CFRP sheets", *Materials and Structures*, Vol. 35 No. 1, pp. 50–58.

Sheikh, M.N. and Légeron, F. (2014), "Performance based seismic assessment of bridges designed according to Canadian Highway Bridge Design Code", *Canadian Journal of Civil Engineering*, Vol. 41 No. 9, pp. 777–787.

Sheikh, S.A., Jaffry, S.A.. and Cui, C. (2007), "Investigation of glass-fibre-reinforced-polymer shells as formwork and reinforcement for concrete columns", *Canadian Journal of Civil Engineering*, Vol. 34 No. 3, pp. 389–402.

Siddiqui, N., Abbas, H., Almusallam, T., Binyahya, A. and Al-salloum, Y. (2020), "Compression behavior of FRP-strengthened RC square columns of varying slenderness ratios under eccentric loading", *Journal of Building Engineering*, Vol. 32 No. April, p. 101512.

Siddiqui, N.A., Alsayed, S.H., Al-Salloum, Y.A., Iqbal, R.A. and Abbas, H. (2014), "Experimental investigation of slender circular RC columns strengthened with FRP composites", *Construction and Building Materials*, Vol. 69, pp. 323–334.

Silva, M.A.G. and Rodrigues, C.C. (2006), "Size and Relative Stiffness Effects on Compressive Failure of Concrete Columns Wrapped with Glass FRP", *Journal of Materials in Civil Engineering*, Vol. 18 No. 3, pp. 334–342.

Tao, Z., Teng, J.G. and Ran, L. (2004), "Experimental Behaviour of FRP-Confined Slender RC Columns under Eccentric Loading", *2nd Int. Conf. on Advanced Polymer Composites for Structural Applications in Construction*, Woodhead Publishing Limited, Cambridge, UK, pp. 203–212.

Teng, J.G., Chen, J.F., Smith, S.T. and Lam, L. (2002), *FRP Strengthened RC Structures*, Wiley-Blackwell, Chichester.

Toutanji, H. (1999), "Stress-Strain Characteristics of Concrete Columns Externally Confined with Advanced Fiber Composite Sheets", *ACI*

Materials Journal, Vol. 96 No. 3, pp. 397–404.

Toutanji, H. and Balaguru, P. (1998), “Durability Characteristics of Concrete Columns Wrapped with FRP Tow Sheets”, *Journal of Materials in Civil Engineering*, Vol. 10 No. 1, pp. 52–57.

Toutanji, H., Han, M., Gilbert, J. and Matthys, S. (2010), “Behavior of Large-Scale Rectangular Columns Confined with FRP Composites”, *Journal of Composites for Construction*, Vol. 14 No. 1, pp. 62–71.

Triantafyllou, G.G., Rousakis, T.C. and Karabinis, A.I. (2015), “Axially loaded reinforced concrete columns with a square section partially confined by light GFRP straps”, *Journal of Composites for Construction*, Vol. 19 No. 1, p. 4014035.

Vandoros, K.G. and Dritsos, S.E. (2006), “Interface treatment in shotcrete jacketing of reinforced concrete columns to improve seismic performance”, *Structural Engineering and Mechanics*, Vol. 23 No. 1, pp. 43–61.

Vandoros, K.G. and Dritsos, S.E. (2008), “Concrete jacket construction detail effectiveness when strengthening RC columns”, *Construction and Building Materials*, Vol. 22 No. 3, pp. 264–276.

Vincent, T. and Ozbakkaloglu, T. (2015), “Compressive Behavior of Prestressed High-Strength Concrete-Filled Aramid FRP Tube Columns : Experimental Observations”, *Journal of Composites for Construction*, Vol. 19 No. 6, p. 04014029.

Wang, L.M. and Wu, Y.F. (2008), “Effect of corner radius on the performance of CFRP-confined square concrete columns: Test”, *Engineering Structures*, Vol. 30 No. 2, pp. 493–505.

Wang, P.., Shah, S.. and Naaman, A.. (1978), "Stress-Strain Curves of Normal and Lightweight Concrete in Compression", *ACI Journal Proceedings*, Vol. 75 No. 11, pp. 603–611.

Wang, W., Sheikh, M.N., Hadi, M.N.S., Gao, D. and Chen, G. (2017), "Behaviour of concrete-encased concrete-filled FRP tube (CCFT) columns under axial compression", *Engineering Structures*, Vol. 147, pp. 256–268.

Widiarsa, I.B.R. and Hadi, M.N.S. (2013), "Performance of CFRP Wrapped Square Reinforced Concrete Columns Subjected to Eccentric Loading", *Procedia Engineering*, Vol. 54, pp. 365–376.

Wight, J.K. and MacGregor, J.G. (2011), *Reinforced Concrete : Mechanics and Design*, 6th ed., Prentice Hall Inc, Upper Saddle River, NJ, USA.

William, K. and Warnke, E. (1974), "Constitutive model for the triaxial behavior of concrete", *Proceedings of International Association for Bridge and Structural Engineering 19*, ISMES, Bergamo, Italy, pp. 1–30.

Wu, H.-C. and Eamon, C.D. (2017), *Strengthening of Concrete Structures Using Fiber Reinforced Polymers (FRP): Design, Construction and Practical Applications*, Woodhead Publishing Limited, Royston Road, Duxford, United Kingdom.

Wu, H.-L., Wang, Y.-F., Yu, L. and Li, X.-R. (2009), "Experimental and Computational Studies on High-Strength Concrete Circular Columns Confined by Aramid Fiber-Reinforced Polymer Sheets", *Journal of Composites for Construction*, Vol. 13 No. 2, pp. 125–134.

Wu, Y.-F. and Jiang, C. (2013), “Effect of load eccentricity on the stress–strain relationship of FRP-confined concrete columns”, *Composite Structures*, Vol. 98, pp. 228–241.

Xiao, Y. and Wu, H. (2003a), “Retrofit of Reinforced Concrete Columns Using Stiffened Steel Jackets”, *Journal of Structural Engineering*, Vol. 129 No. 6, pp. 725–732.

Xiao, Y. and Wu, H. (2003b), “Compressive Behavior of Concrete Confined by Various Types of FRP Composite Jackets”, *Journal of Reinforced Plastics and Composites,* Vol. 22 No. 13, pp. 1187–1201.

Xing, L., Lin, G. and Chen, J.F. (2020), “Behavior of FRP-Confined Circular RC Columns under Eccentric Compression”, *Journal of Composite for Construction*, Vol. 24 No. 4, pp. 1–11.

Youssef, M.N., Feng, M.Q. and Mosallam, A.S. (2007), “Stress-strain model for concrete confined by FRP composites”, *Composites Part B: Engineering*, Vol. 38 No. 5–6, pp. 614–628.

Yu, T., Teng, J.G., Wong, Y.L. and Dong, S.L. (2010a), “Finite element modeling of confined concrete-I: Drucker–Prager type plasticity model”, *Engineering Structures*, Vol. 32 No. 3, pp. 665–679.

Yu, T., Teng, J.G., Wong, Y.L. and Dong, S.L. (2010b), “Finite element modeling of confined concrete-II: Plastic-damage model”, *Engineering Structures*, Vol. 32 No. 3, pp. 680–691.

Zeng, J., Guo, Y., Li, L. and Chen, W. (2018), “Behavior and three-dimensional finite element modeling of circular concrete columns partially wrapped with FRP strips”, *Polymers*, Vol. 10 No. 3, p. 253.

APPENDIX A: CONCRETE MIX DESIGN FORM

Table 1 Concrete mix design form

Job title ....

Stage	Item		Reference or calculation	Values
1	1.1	Characteristic strength	Specified	20 N/mm² at 28 days; Proportion defective / %
	1.2	Standard deviation	Fig 3	/ N/mm² or no data / N/mm²
	1.3	Margin	C1 or Specified	(k = /) / × / = / N/mm²; 10 N/mm²
	1.4	Target mean strength	C2	20 + 10 = 30 N/mm²
	1.5	Cement strength class	Specified	42.5/52.5
	1.6	Aggregate type: coarse Aggregate type: fine		Crushed/uncrushed Crushed/uncrushed
	1.7	Free-water/cement ratio	Table 2, Fig 4	0.64 } Use the lower value $\boxed{0.64}$
	1.8	*Maximum free-water/cement ratio*	*Specified*	/
2	2.1	Slump or Vebe time	Specified	Slump 30 - 60 mm or Vebe time / s
	2.2	Maximum aggregate size	Specified	20 mm
	2.3	Free-water content	Table 3	$\boxed{210}$ kg/m³
3	3.1	Cement content	C3	210 ÷ 0.64 = 330 kg/m³
	3.2	*Maximum cement content*	*Specified*	/ kg/m³
	3.3	*Minimum cement content*	*Specified*	/ kg/m³
				use 3.1 if ≤ 3.2 use 3.3 if > 3.1 $\boxed{330}$ kg/m³
	3.4	Modified free-water/cement ratio		$\boxed{/}$
4	4.1	Relative density of aggregate (SSD)		2.6 known/assumed
	4.2	Concrete density	Fig 5	2380 kg/m³
	4.3	Total aggregate content	C4	2380 − 330 − 210 = 1840 kg/m³
5	5.1	Grading of fine aggregate	Percentage passing 600 µm sieve	70 %
	5.2	Proportion of fine aggregate	Fig 6	Say 30 %
	5.3	Fine aggregate content	C5	1840 × 0.3 = $\boxed{550}$ kg/m³
	5.4	Coarse aggregate content	C5	1840 − 550 = $\boxed{1290}$ kg/m³

Quantities	Cement (kg)	Water (kg or litres)	Fine aggregate (kg)	Coarse aggregate (kg) 10 mm	20 mm	40 mm
per m³ (to nearest 5 kg)	330	210	550		1290	
per trial mix of 0.0163 m³	5.38	3.42	8.97		21.03	

Items in italics are optional limiting values that may be specified (see Section 7).
Concrete strength is expressed in the units N/mm². 1 N/mm² = 1 MN/m² = 1 MPa. (N = newton; Pa = pascal.)
The internationally known term 'relative density' used here is synonymous with 'specific gravity' and is the ratio of the mass of a given volume of substance to the mass of an equal volume of water.
SSD = based on the saturated surface-dry condition.

APPENDIX B: DESIGN AND SCALING OF RC COLUMN SPECIMEN

B.1 Scaling of Rectangular Columns

The relationship between the prototype and the scaled model of the column specimen can be described based on the Buckingham Π theorem. The frequency changes *(f_n)* in the columns with the cross-sectional dimensions and height *a, b,* h, respectively, are formulated by the Buckingham Π theorem. In the calculation of the frequency, the following equations are used.

$$f_n = \frac{\omega_n}{2\pi} \tag{APP.1}$$

$$\omega_n = \sqrt{\frac{k}{m}} \tag{APP.2}$$

$$k = \frac{Eab^3}{h^3} \tag{APP.3}$$

$$m = \frac{abh\gamma}{g} \tag{APP.4}$$

Where, m = mass, k = rigidity, E = modulus of elasticity and γ = unit weight volume of concrete.

The detailed calculations of frequency values for the prototype and the 1/3 scaled model of the rectangular column specimens are presented below:

Prototype data of rectangular RC column

Column dimensions; 0.3 × 0.45 × 2.4m

γ = 23.80kN/m^3

E_p = 25401750kN/m^2

g = 9.81m/s^2

System rigidity $k = \frac{3E_pI}{h^3}$

$I = \frac{ab^3}{12} = \frac{0.3\times0.45^3}{12} = 0.002278m^4$

$k = \frac{3\times25401750\times0.002278}{2.4^3} = 12558.238kN/m$

$m = \frac{0.3\times0.45\times23.80\times2.4}{9.81} = 0.786kNs^2/m$

$\omega_n = \sqrt{\frac{k}{m}} = \sqrt{\frac{12558.238}{0.786}} = 126.4017rads/s$

$f_{n(p)} = \frac{\omega_n}{2\pi} = \frac{126.4017}{2\pi} = 20Hz$

1/3 geometry and mass scaling model data for the rectangular RC column

Column dimensions 0.1 × 0.15 × 0.8m

γ = 23.80kN/m^3

E_p = 25401750kN/m^2

g = 9.81m/s^2

System rigidity $k = \frac{3E_pI}{h^3}$

$I = \frac{ab^3}{12} = \frac{0.1\times0.15^3}{12} = 0.000028125m^4$

$$k = \frac{3 \times 25401750 \times 0.000028125}{0.8^3} = 4186.079 kN/m$$

$$m = \frac{0.1 \times 0.15 \times 23.80 \times 0.8}{9.81} = 0.029113 kNs^2/m$$

$$\omega_n = \sqrt{\frac{k}{m}} = \sqrt{\frac{4186.079}{0.029113}} = 379.1929 rads/s$$

$$f_{n(m)} = \frac{\omega_n}{2\pi} = \frac{379.1929}{2\pi} = 60Hz$$

The ratio of the frequency values between the prototype and the scaled model is given by;

$$\frac{f_{n(m)}}{f_{n(p)}} = \frac{60}{20} = 3.0000$$

B.2 Design of RC Columns

The Specimens in the test region are designed based on Eurocode 2 (EC2) design guideline. For the given geometry and reinforcement, the axial load capacity and Moment capacity of the section are calculated below:

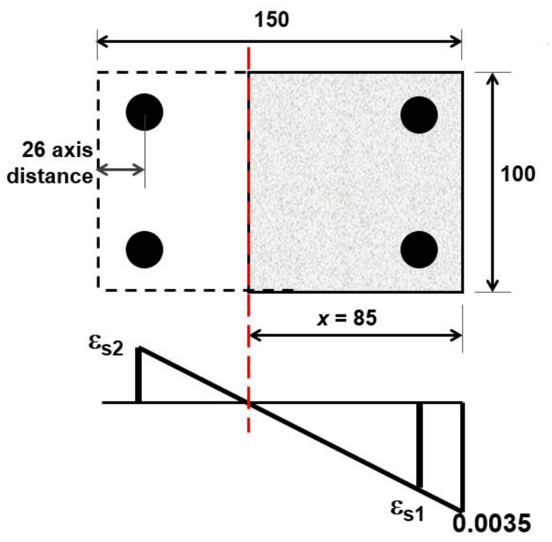

4 no. Y12 bars

A_{sc} = 452 mm^2

= 226 per face

Assume a depth of neutral axis $x = 85mm$

$f_{ck} = 29.21N/mm^2$

$f_{yk} = 550N/mm^2$

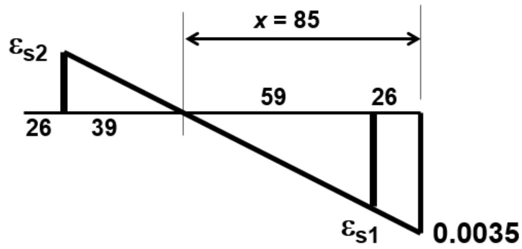

Determination of steel strains ε_{s1} and ε_{s2}:

$$\varepsilon_{s1} = 0.0035 \times \left(\frac{59}{85}\right) = 0.002429 \quad \text{Steel yielded} \quad \varepsilon_{s1} > 0.002$$

$$\varepsilon_{s2} = 0.0035 \times \left(\frac{39}{85}\right) = 0.00161$$

Steel stresses f_{s1} and f_{s2} are calculated as:

$$f_{s1} = 0.87f_{yk} = 0.87 \times 550 = 478.50\ N/mm^2$$

$$f_{s2} = 0.00161 \times 200{,}000 = 322N/mm^2$$

Final forces in the bars F_{s1} and F_{s2} are:

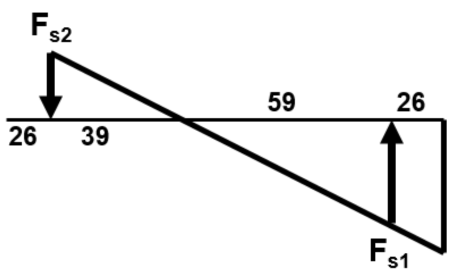

$$F_{s1} = +478.50 \times 226 \times 10^{-3} = +108.14KN$$

$$F_{s2} = 322 \times 226 \times 10^{-3} = 72.77KN$$

Determination of force due to the concrete in compression:

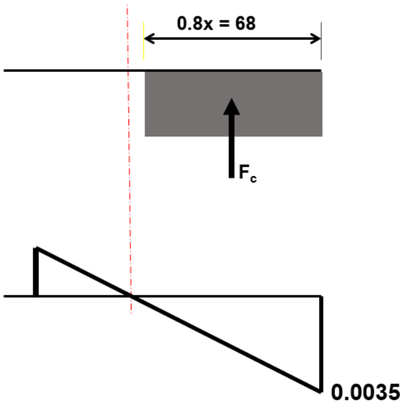

$$f_c = 0.567\, f_{ck} = 0.567 \times 29.21$$

$$= 16.56\, N/mm^2$$

$$F_c = 0.567\, f_{ck}\, b0.8x = 16.56 \times 100 \times 68 \times 10^{-3} = 112.61\, kN$$

Final axial capacity in column:

$$N_{Rd} = 108.14 + 112.61 - 72.77 = 147.98\, kN$$

$$M_{Rd} = (112.61\, x\, 0.041) + [(108.14 + 72.77)\, x\, 0.049]$$

$$= 4.78 + 8.86 = 13.64\, kNm$$

Therefore, the axial and moment capacity of the column are:

$$N_{Rd} = 147.98\, kN$$

$$M_{Rd} = 13.64\, kNm$$

Links:

Minimum links $= \frac{1}{4} \times$ size of compression bar but not less than 6mm

Therefore links $= \frac{1}{4} \times 12 = 3mm$ Provide 6mm links

Spacing between links:

Maximum spacing should not exceed the lesser of 20 × size of the smallest compression bar or the least lateral dimension of the column. This should be reduced by 0.60.

Therefore, spacing $= 20 \times 12 \times 0.6 = 144mm$

The maximum spacing for the column is 144mm, but considering the size of the column a spacing of 120 is also adequate.

Provide 6mm links at 120 c/c.

APPENDIX C: ANSYS COMMANDS FOR MODELLING OF REINFORCED CONCRETE

C.1 Concrete commands

The following ANSYS commands were utilised in the present study to define the material model for concrete.

```
ET,MATI,SOLID65
R,MATID,0,0,0,0,0,0
RMORE,0,0,0,0,0

MP,EX,MATID, 3.040439/0.0001
MP,NUXY,MATID,0.2

TB,CONCR,MATID,1,9
TBTEMP,22
TBDATA,1,0.5,0.9,4.5,42

TB,MISO,MATID,1,35,0
TBTEMP,22
TBPT,DEFI,0.0001,3.040439
TBPT,DEFI,0.0002,6.046658
TBPT,DEFI,0.0003,8.991751
TBPT,DEFI,0.0004,11.85285
TBPT,DEFI,0.0005,14.6106
TBPT,DEFI,0.0006,17.249
TBPT,DEFI,0.0007,19.75535
TBPT,DEFI,0.0008,22.1201
TBPT,DEFI,0.0009,24.33667
TBPT,DEFI,0.001,26.40119
TBPT,DEFI,0.0011,28.31221
TBPT,DEFI,0.0012,30.07042
TBPT,DEFI,0.0013,31.67829
TBPT,DEFI,0.0014,33.13978
TBPT,DEFI,0.0015,34.46005
TBPT,DEFI,0.0016,35.64516
TBPT,DEFI,0.0017,36.70181
TBPT,DEFI,0.0018,37.63718
TBPT,DEFI,0.0019,38.45865
```

```
TBPT,DEFI,0.002,39.17374
TBPT,DEFI,0.0021,39.78991
TBPT,DEFI,0.0022,40.31448
TBPT,DEFI,0.0023,40.75456
TBPT,DEFI,0.0024,41.11698
TBPT,DEFI,0.0025,41.40824
TBPT,DEFI,0.0026,41.63451
TBPT,DEFI,0.0027,41.80159
TBPT,DEFI,0.0028,41.91488
TBPT,DEFI,0.0029,41.97946
TBPT,DEFI,0.0030,42.00000
TBPT,DEFI,0.0031,42.00000
TBPT,DEFI,0.0032,42.00000
TBPT,DEFI,0.0033,42.00000
TBPT,DEFI,0.0034,42.00000
TBPT,DEFI,0.0035,42.00000
```

C.2 Steel Bars Commands

The material model for steel bars was defined using the following ANSYS commands:

C.2.1 Longitudinal Reinforcement

```
ET,matid,LINK180

MPDATA,EX,matid,,2e5
MPDATA,PRXY,matid,,0.3
TB,BISO,matid,1,2,
TBDATA,,560,2000,,,,
R,matid,113.1,,0
```

C.2.2 Transverse Reinforcement

```
ET,matid,LINK180

MPDATA,EX,matid,,2e5
MPDATA,PRXY,matid,,0.3
TB,BISO,matid,1,2,
TBDATA,,290,2000,,,,
R,matid,28.27,,0
```

C.3 Pre Processor Commands

The boundary between concrete and steel reinforcements was simulated using the following ANSYS commands:

```
/PREP7
ESEL,S,ENAME,,65
ESEL,A,ENAME,,180
ALLSEL,BELOW,ELEM
CEINTF,ALL,0.001,
ALLSEL,ALL
/SOLU
OUTRES,ALL,ALL
```

APPENDIX D: NEWTON-RAPHSON METHOD

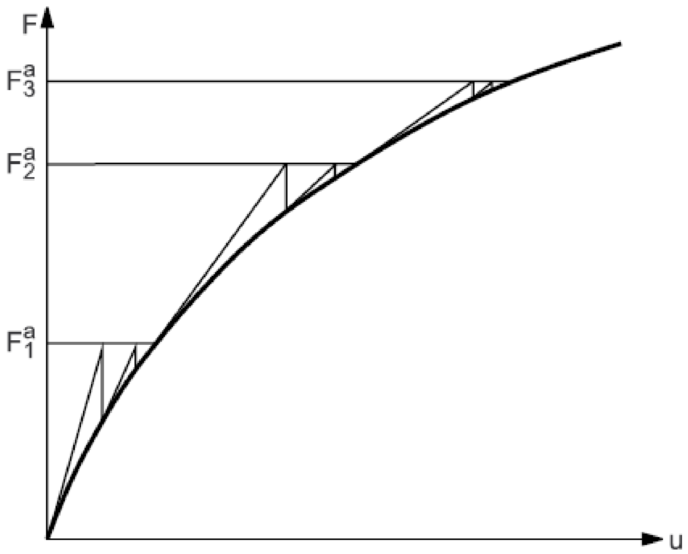

Figure APP-D.1 Incremental Newton-Raphson procedure (ANSYS Release 18.1, 2017b)

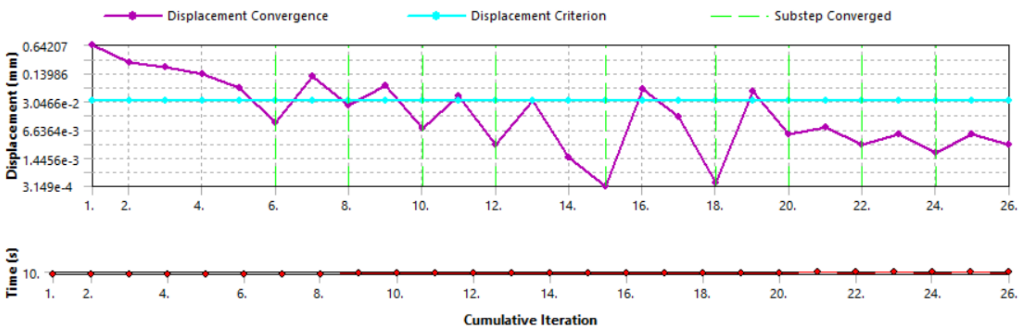

Figure APP-D.2 Example of Newton-Raphson displacement convergence for a nonlinear numerical solution

APPENDIX E: CALCULATIONS OF BENDING MOMENTS OF BEAMS AND COLUMNS

For specimens under concentric loading, bending moment is zero. But for column specimens under eccentric loading, the bending moment was calculated as follows:

<u>For column specimens</u>

$M_u = P_{ult}(e + \delta)$

For specimen 0UC-25e,

$e = 25mm$

$\delta_{EXP} = 2.62mm$

$\delta_{FEA} = 7.56mm$

$P_{ult-EXP} = 255.53kN$

$P_{ult-FEA} = 245.48kN$

$\therefore M_{u-EXP} = 255.53(25 + 2.62) = 7.06kN.m$

$\therefore M_{u-FEA} = 245.48(25 + 7.56) = 7.99kN.m$

For specimen 0UC-50e,

$e = 50mm$

$\delta_{EXP} = 1.98mm$

$\delta_{FEA} = 6.75mm$

$P_{ult-EXP} = 181.69kN$

$P_{ult-FEA} = 175.52kN$

$\therefore M_{u-EXP} = 181.69(50 + 1.98) = 9.44kN.m$

$\therefore M_{u-FEA} = 175.52(50 + 6.75) = 9.96kN.m$

For specimen 1FWC-25e

$e = 25mm$

$\delta_{EXP} = 3.26mm$

$\delta_{FEA} = 11.05mm$

$P_{ult-EXP} = 281.61kN$

$P_{ult-FEA} = 280.78kN$

$\therefore M_{u-EXP} = 281.61(25 + 3.26) = 7.96kN.m$

$\therefore M_{u-FEA} = 280.78(25 + 11.05) = 10.12kN.m$

For beam specimens

$M_{uf} = \frac{1}{2} P_{ult} L$

For beam 0UB

$L = 230mm$

$P_{ult-EXP} = 94.39kN$

$P_{ult-FEA} = 101kN$

$\therefore M_{uf-EXP} = \frac{1}{2} \times 230 \times 94.39 = 10.85kN.m$

$\therefore M_{uf-FEA} = \frac{1}{2} \times 230 \times 101 = 11.62kN.m$

For beam 1FWB,

$P_{ult-EXP} = 116.69kN$

$P_{ult-FEA} = 189kN$

$\therefore M_{uf-EXP} = \frac{1}{2} \times 230 \times 116.69 = 13.42kN.m$

$\therefore M_{uf-FEA} = \frac{1}{2} \times 230 \times 189 = 21.74kN.m$